EXPERIMENTAL AND NUMERICAL ANALYSIS OF A PIPE ARCH CULVERT SUBJECTED TO EXCEPTIONAL LIVE LOAD

A Thesis Presented to
The Faculty of the College of Engineering and Technology
Ohio University
Athens, Ohio

In Partial Fulfillment
of the Requirements for the Degree
Master of Science in Civil Engineering

by
Devarajan Chelliah
March, 1992

This thesis has been approved
for the Department of Civil Engineering
and the College of
Engineering and Technology

Russ Professor of Civil Engineering

Dean of the College of
Engineering and Technology

ABSTRACT

A full-scale field test was conducted to determine the response of a corrugated metal pipe arch culvert for the exceptional live load. The design span and rise of the culvert were 15 feet 8 inches and 9 feet 6 inches respectively. The cover for the first and second day of testing were approximately 7.5 feet and 3 feet respectively. Position transducer and strain gage techniques were used to measure the deflection and strains. Data was collected by using computer controlled data acquisition system. A tape extensometer was used to determine the shape of the culvert before and after the testing. Exceptional live load was applied through the two seven inch diameter piston rod hydraulic cylinders. They had a capacity of 230 tons and connected to a hydraulic control unit for simultaneous operation. A total of three loading sequences were applied, one on the first day and two on the second day.

The ultimate load carrying capacity of this type of culvert under 3 feet cover was determined to be 100 tons approximately. Maximum vertical deflection of 6.989 inches occured at the crown point during the third loading sequence. During the first sequence the magnitude of moment and thrust was insignificant. In the first loading sequence symmetric nature prevailed in the culvert response. No section exceeded its ultimate moment capacity of 3.745 kips-ft/ft. During the second and third loading sequences of only section four exceeded its plastic moment capacity and formed a plastic hinge. The formation of creases at both sides of the instrumented section were reported. The slip occured at a bolted connection near to the crown was also reported.

A numerical analysis was done using the CANDE finite element program. Parameters for Duncan's hyperbolic model were derived from the triaxial tests conducted using the undisturbed soil samples from the field. The numerical predictions were compared with the field response. Although the magnitude didn't agree well an identical trend was observed between the numerical simulations and the field results.

ACKNOWLEDGEMENTS

I would like to express my sincere appreciation and gratitude to Dr. Shad M. Sargand for his instructive guidance and supervision that made this research work possible. I would also like to thank him for supporting me during my entire stay in Athens.

I would like to thank Dr. Glenn A. Hazen for his helpful suggestions and constructive criticism. I am deeply indebted to Mr. Teruhisa Masada for the long hours of tireless work that he put in from the beginning to the end of this project.

I am also grateful to all the students and technicians who were responsible for the experimental set-up and data acquisition.

Funding for this project was provided through a research grant from the Ohio Department of Transportation.

TABLE OF CONTENTS

Chapter 3

MEASUREMENT OF CULVERT DEFORMATION

Chapter 4

MEASUREMENT OF PLATE FORCES

Chapter 5

FINITE ELEMENT ANALYSIS

LIST OF TABLES

LIST OF FIGURES

Chapter 2

Chapter 3

Chapter 4

Chapter 5

CHAPTER 1
INTRODUCTION

1.1 GENERAL STATEMENT

Corrugated metal buried conduits have been used as drainage structures for many years and, especially in the past two decades as short-span bridge substitutes. The reasons for this development are light weight, lower material cost, relatively easy handling and installation procedures. These structures other than the very smallest, are constructed by bolting together curved, corrugated metal plates. One of the most popular type of corrugated metal pipes (CMPs) has been the corrugated steel pipe arch culvert. The pipe arch culverts do not require concrete footings and are advantageous over some other CMPs where head room is limited and hydraulic capacity is demanded.

In the last two decades, there have been many investigations dealing with the analysis and design of corrugated steel culverts [2,5,7,8,17,18]. Laboratory testing, field testing, and analytical methods have been utilized. Most of these reported studies are related to the performance of culverts under various backfill and under normal live-load conditions. However, very few investigations have been focused on the maximum load carrying capacity and the failure mechanism of these soil-structure systems. This is because a full-scale field failure test of a culvert is generally costly, time consuming, and presents problems to the construction plan and/or local traffic conditions.

The strength of a culvert depends on properties of backfill material, plate and soil-structure interaction. There is limited Information on the amount of deflection, shape of deformation and live-load capacity of these culverts before full or partial failure occurs. For more rational design, it is very important to inquire into possible failure mechanisms.

1.2 OBJECTIVES

The objectives of the investigation were as follows:

a) To determine the maximum moment capacity of the pipe arch culvert.

b) To define the collapse mechanism.

c) To identify critical sections on the geometry of the pipe arch culvert.

d) To evaluate the load-deflection relation of the pipe arch culvert under exceptionally large live loads.

e) To compare the measured ultimate moment capacity with AASHTO design guidelines and with CANDE Finite Element Method predictions.

1.3 OUTLINE OF RESEARCH

In 1989, the Ohio Department of Transportation (ODOT) made a decision, after a careful hydrologic and hydraulic evaluation, to remove a large span pipe arch culvert structure identified as MER-707-1703, which had been existing under State Route 707, near the north limit of the village of Mendon in Mercer county, Ohio. This pipe was originally installed in 1953 as an overflow structure, for a nearby short span bridge structure, MER-707-1697, over St. Mary's river. On September 24 and 26, 1990, a research group from Ohio University took full advantage of this unique situation and conducted one of the first comprehensive full-scale field failure testing of the pipe arch culvert structure.

This thesis presents details of the findings of previous investigations on failure of culverts, descriptions of the pipe arch culvert structure tested, field instrumentation methods utilized, related background theory and design guidelines, experimental results, CANDE Finite Element Analysis and the conclusions drawn.

Chapter two describes in detail the information regarding the geometry of the

corrugated steel pipe arch culvert structure and its surrounding subsurface conditions in the field. This chapter also presents the concept and descriptions of the field instrumentation and live-load application methods used to fulfill the objectives of the investigation.

Chapter three presents necessary background information utilized in the analysis of the field data for deflection. It also provides the field measured data which were obtained before, during, and after the testing. Field measurements of initial and final geometry of the pipe arch culvert are presented.

Chapter four presents necessary theory utilized for analysis of strain gage data and the results obtained. Bending moments and thrusts are computed and presented for the corresponding loading conditions. Locations of plastic hinges and creases observed in the field are also reported here.

Chapter five gives details about the laboratory testing of backfill material. It also represents the calculated soil model parameters for the CANDE finite element analysis. It explains the numerical analysis of the pipe arch culvert/soil system using the CANDE computer program. Predictions of the CANDE program are presented, in terms of deformations, thrusts, and moments, in correlation with the measured field values.

And, finally Chapter six presents the summary of the results and conclusions drawn from this investigation.

1.4 LITERATURE REVIEW

The corrugated steel culvert has been increasingly subjected to investigation during the last two decades. Mayerhof and Baikie [16] as part of their study investigated the strength of corrugated metal culverts under fills.

From this investigation they concluded that for small values of the co-efficient of

soil reaction or modulus of deformation of the soil, and for small values of the flexural rigidity of the plates, the sheets would fail by buckling, but for larger values of these parameters the sheets would fail by yielding of the section. The observed ultimate loads and modes of failure of the sheets were in reasonable agreement with these estimates and also support the ring compression theory.

Buckling of culvert structures was studied by Ghobrial and Abdel-Sayed [12]. In their study of this phenomenon, they considered the formation of plastic hinges in the culvert walls. They observed sudden snap-through failure for large spans and shallow cover conditions. Short span culverts with deep soil cover did not exhibit this response but experienced increasing displacements after each load step. In addition, the first plastic hinge formed at the crown. The formation of the second plastic hinge was observed farther away from the crown.

Duncan [8] after an extensive study suggested controlling the factor of safety against formation of a plastic hinge as a design requirement for flexible culverts with shallow fill, and has given three reasons why structural collapse will not occur at this point:

1) Multiple plastic hinges are required to form a collapse mechanism.

2) The soil will restrain deformations after formation of a mechanism.

3) The design estimates are based on minimum values of yield stress.

Selig and Musser [18] rated the performance of a rib reinforced, long-span culvert by field tests and a limited finite element analysis. Results were compared with current design practice. They concluded that rib stiffeners decrease deflections, increase moments, and do not affect thrusts. Reinforcing ribs increase the factor of safety against plastic hinge formation.

Cary [4] examined the inelastic flexural stability of corrugations. He investigated the local stability of arc-and-tangent corrugated profiles when subjected to moments in the

inelastic range. Twenty four flexural tests were used to obtain empirical expressions. The expressions related design variables, corrugation dimensions, minimum curvature radius, maximum moment capacity, and critical buckling strain. Results show that as the radius of curvature to thickness ratio increases the strain at which buckling occurs reduces.

Seed and Rains [17] analyzed three full-scale field case studies involving failure of flexible long span culvert structures due to inadvertent application of exceptional live loads. Each case was simulated using nonlinear finite element analysis methods with a modified Duncan and Drawsky procedure to develop equivalent line loads. Their numerical results indicate that the nonlinear finite element analysis can provide excellent agreement with observed field behavior, in terms of not only failure conditions but also locations of plastic hinge formation.

Dessouki A.K. and Monforton G.R. [6] used a plane strain finite element analysis procedure to determine the effect of soil failure on soil-steel structures. They used hyperbolic soil model to represent the interface element and the soil elements far from the structure. An elasto-plastic model represented the soil behavior in the severely stressed regions. They reported good agreement between the model tests they conducted in the laboratory and the analytical results. Their investigation clearly indicated the significant effect on the load carrying capacity of the soil-steel structure due to soil failure.

In all of the above investigations, full-sized culverts were not instrumented and loaded to failure to determine their actual ultimate moment capacity, load-deflection relation, and influence of soil-structure interaction.

CHAPTER 2

PIPE ARCH CULVERT AND FIELD INSTRUMENTATION

2.1 GENERAL

The details of the history, general information and geometrical characteristics of the culvert, results of the subsurface boring work performed close to the culvert, methods of instrumentation, and live load application system for the pipe arch culvert tested for failure are presented in this chapter.

In order to meet the objectives outlined in chapter one, it was necessary to develop a system which could simulate exceptional vehicular live load to the culvert and to instrument the pipe to obtain deflection, moment and thrust measurements before and during the full scale field failure test. Two large-capacity hydraulic cylinders, connected in parallel, were set over the culvert and extended against a dead load, consisting of more than forty 2.2 ton concrete blocks placed on top of a steel I-beam frame, to achieve application of exceptional live load. In oder to obtain deflection data, position transducers were attached to a reference truss structure erected inside the culvert, and transducer's wires were connected to selected points on the inside perimeter of the culvert. Movement of the reference truss structure was monitored with the conventional level surveying technique to single out true deflections of the pipe. Measurements of moment and thrust were made using electric strain gages. An assumption was made that effects of exceptional live load would be significant mostly in a cross section under the loading points (plain stress). Therefore, a mid-length plane section along the longitudinal axis of the culvert was chosen to establish instrumentation and to apply live load. A tape extensometer was used to establish the initial and final cross-sectional shapes of the selected mid-section of the culvert.

To perform realistic CANDE numerical simulation of the culvert, a knowledge of the vertical profile of the surrounding subsurface conditions and the stress-strain relations

of backfill material is required. This information was obtained by performing subsurface exploration work at two locations next to the culvert structure on the day of testing.

2.2 DESCRIPTION OF PIPE ARCH CULVERT AND BACKFILL MATERIAL

The pipe arch culvert (MER-707-1703), the main subject of the investigation, was installed in 1953, parallel to St. Marys River at an appropriate distance of 400 feet, under state route 707, near the north limit of the village of mendon in Mercer County, Ohio. The culvert, situated in a flood plain, was designed as an overflow structure for a nearby short span bridge structure (MER-707-1697) and supposed to have a minimum safe load capacity of S-15.

The design span and rise dimensions for the culvert were 15 feet-8 inches and 9 feet-6 inches respectively. Figure 2.1 illustrates the geometry of the pipe arch culvert. The contract document stated that a maximum of 1 inch tolerance was permitted on nominal span and rise dimensions. The steel structural plates for the culvert had #7 gage thickness for the top section and #5 gage thickness for the corner and bottom sections. Corrugation pattern was defined by a pitch of 6 inches and a depth of 2 inches. Table 2.1 summarizes the geometrical characteristics of the pipe arch culvert. Backfill material used during construction was a typical cohesive earth material available locally. According to a record dated 1955, the vertical profile surrounding the culvert included a 2 inch asphalt concrete layer and 33.5 foot wide, 7.4 foot thick fill above the culvert crown. The culvert was installed perpendicular to the centerline of the road, and it had a total length of 86 feet and a grade of 0.0%. No stiffeners were attached to the culvert structure during its construction.

On September 24,1990 just before the first loading, a drilling rig equipped with a rotary auger was utilized to obtain detailed subsurface soil data at two locations within the shoulder section of the roadway one on each side, near the west end of the culvert.

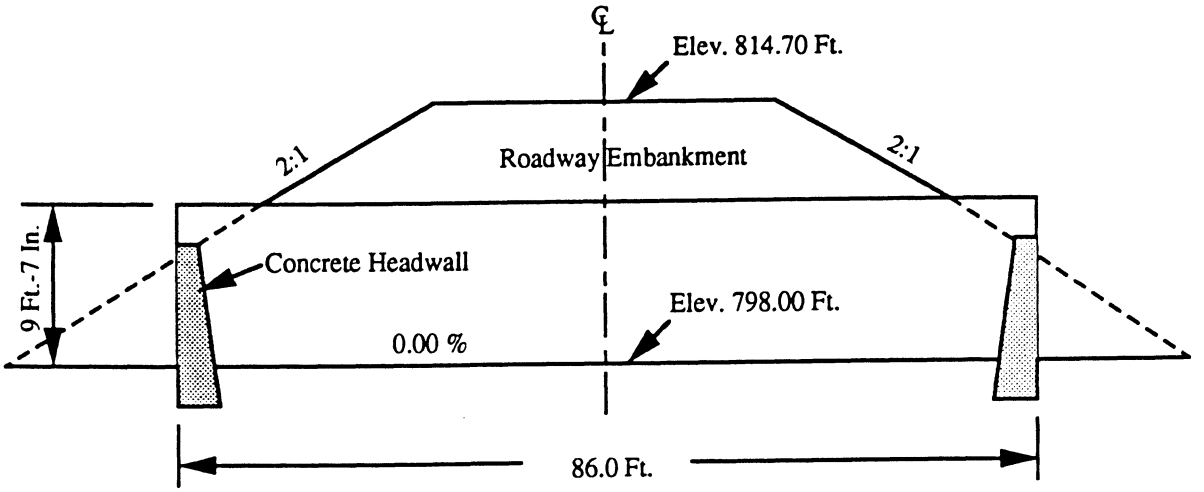

(a) General Side View

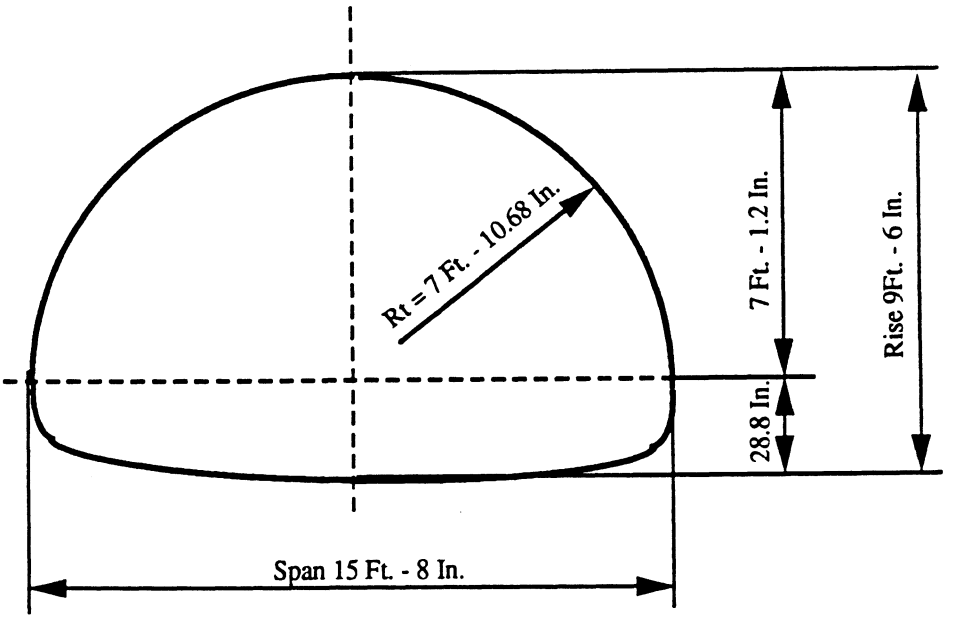

(b) General Cross-Sectional View

Figure 2.1 Geometry of Pipe Arch Culvert

Table 2.1 Characteristics of Pipe Arch Culvert

Type	Corrugated Steel
Design Span	15 feet - 8 inches
Design Rise	9 feet - 6 inches
Length	86 feet
Height of Cover Over Crown	7 feet - 5 inches
Corrugation Pitch	6 inches
Corrugation Depth	2 inches
Plate Thickness: Above Springline	0.188 inch (Galvanized)
Plate Thickness: Below Springline	0.218 inch (Galvanized)
Section Area of Plate	2.739 $in.^2/ft.$
Moment of Inertia	1.296 $in.^4/ft.$
Section Modulus	1.187 $in.^3/ft.$
Radius of Gyration	0.688 inch

Locations of the boreholes with respect to the culvert structure are shown in fig 2.2. These borings were extended down to a depth of approximately 3 feet below the bottom invert of the culvert. A 18 inch length split spoon sampler was used and the SPT values were recorded. Soil samples were placed in seal-tight containers and transported to the Ohio DOT soil laboratory for analysis. Tables 2.2 and 2.3 provide a summery of the data obtained from the two test borings and results of the laboratory soil tests. The backfill material encountered in the bore holes are regarded as a stiff to very stiff silty clay with varying amounts of sand and gravel. In addition to the soil boring work, the thickness of the asphalt concrete layer was measured after the first sequence of loading, and it was determined to be 16 inches. It is apparent that the Ohio DOT bridge maintenance has placed several layers of asphalt concrete, since the culvert has been developing a moderate amount of sagging which results in a minor dip/cracking on the asphalt pavement surface.

2.3 LIVE LOAD APPLICATION SYSTEM

In this investigation, it was necessary to apply exceptional live load, simulating the rear axle of a heavy vehicle. The traditional concept of pressing against a large dead load, often used in the pile load test procedure, was chosen to achieve this goal. Figures 2.3 and 2.4 illustrate the overall setting, and figure 2.5 presents actual pictures of the loading system taken in the field. First, two 4 feet by 8 feet pedestals, made up with concrete blocks and guard rail posts, were set on the roadway surface at a 36 foot spacing from center to center, across the culvert structure. A 6 to 8 inch thick well compacted sandy material layer was placed under the pedestals to smooth out the roadway surface slopes and to keep the pedestals vertical. A steel I-beam frame was constructed by welding eight 5 foot long 12 x 65 H piles at a 5 foot spacing between two 40 foot long W36 x 182 beams. Web stiffeners 1/2 inch thick were attached to these I beams at the mid-span. This frame was laid atop across the pedestals. Concrete blocks (or jersey barriers), each weighing about 2.2 tons, were lifted by a crane and placed over the I-beams. On the first day of testing (sept 24, 1990), a total of 45 jersey barriers were piled in three layers-20 in the first layer, 15 in the second layer, and 10 in the third layer. On the second day of testing (Sept

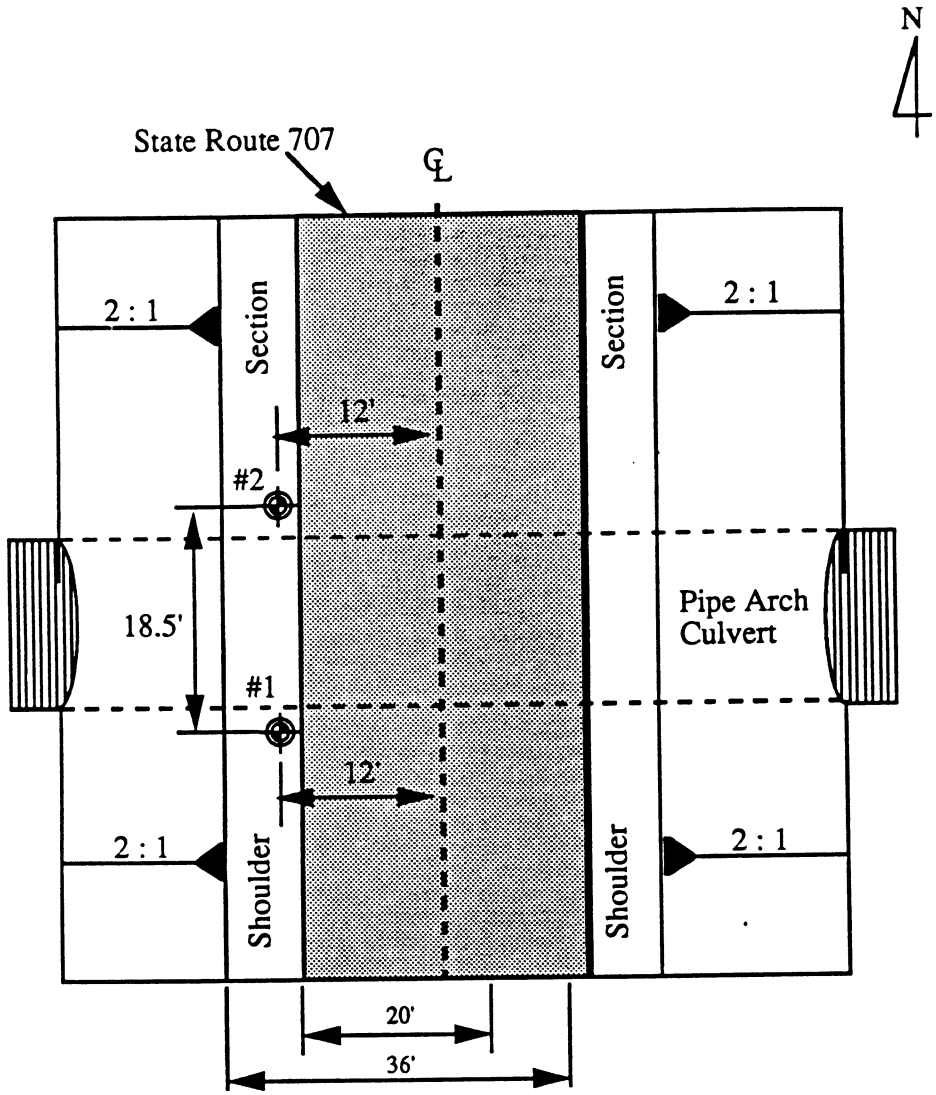

Figure 2.2 Locations of Test Soil Borings

Table 2.2 Soil Boring Data For Test Hole #1

Elev. (Ft.)	Depth (Ft.)	SPT Value	Material Description	Physical Characteristics					L.L	P.I.	W.C.	SHTL Class
				% Agg	% C.S.	%F.S.	% Silt	% Clay				
814.2	0.0	—	Top of Berm Shoulder Section	—	—	—	—	—	—	—	—	—
812.2	2.0											
811.7	2.5	4/8/8	Brown Sandy Clay	0	7	13	37	43	31	12	16	A-6A
809.2	5.0	2/4/5	Brown And Gray Sandy Clay	12	6	11	31	40	33	12	19	A-6A
806.7	7.5	3/5/8	Brown And Gray Sandy Clay	0	8	14	36	42	33	14	18	A-6A
804.2	10.0	4/5/9	Brown And Gray Sandy Gravelly Clay	18	5	10	27	40	33	12	20	A-6A
801.7	12.5	4/7/12	Brown And Gray Sandy Clay	8	5	11	30	46	34	13	19	A-6A
799.2	15.0	5/8/15	Gray Silty Clay	5	2	10	49	34	45	18	26	A-7-6
796.7	17.5	4/9/13	Gray Gravelly Clay	17	3	7	31	42	46	16	27	A-7-5
795.2	19.0		Bottom of Boring									

Table 2.3 Soil Boring Data For Test Hole #2

Elev. (Ft.)	Depth (Ft.)	SPT Value	Material Description	Physical Characteristics					L.L	P.I.	W.C.	SHTL Class
				% Agg.	% C.S.	%F.S.	% Silt	% Clay				
813.8	0.0		Top of Berm Shoulder Section	—	—	—	—	—	—	—	—	—
812.8	1.0	—										
811.3	2.5	3/4/5	Brown Sandy Clay	8	6	12	34	40	31	11	17	A-6A
808.8	5.0	3/4/5	Brown And Gray Sandy Clay	9	6	12	34	39	31	11	18	A-6A
806.3	7.5	3/6/9	Brown Sandy Clay	7	5	12	33	43	33	13	17	A-6A
803.8	10.0	3/5/7	Gray Silty Clay	4	4	11	32	49	38	17	20	A-6B
801.3	12.5	3/6/9	Gray Silt And Clay	0	5	12	35	48	35	15	21	A-6A
798.8	15.0	5/15/7	Gray Silty Gravelly Sand	22	31	13	19	15	NP	NP	24	A-2-4
796.3	17.5	5/7/9	Brown And Gray Silty Clay	0	0	15	43	42	40	20	22	A-7-6
794.8	19.0		Bottom of Boring									

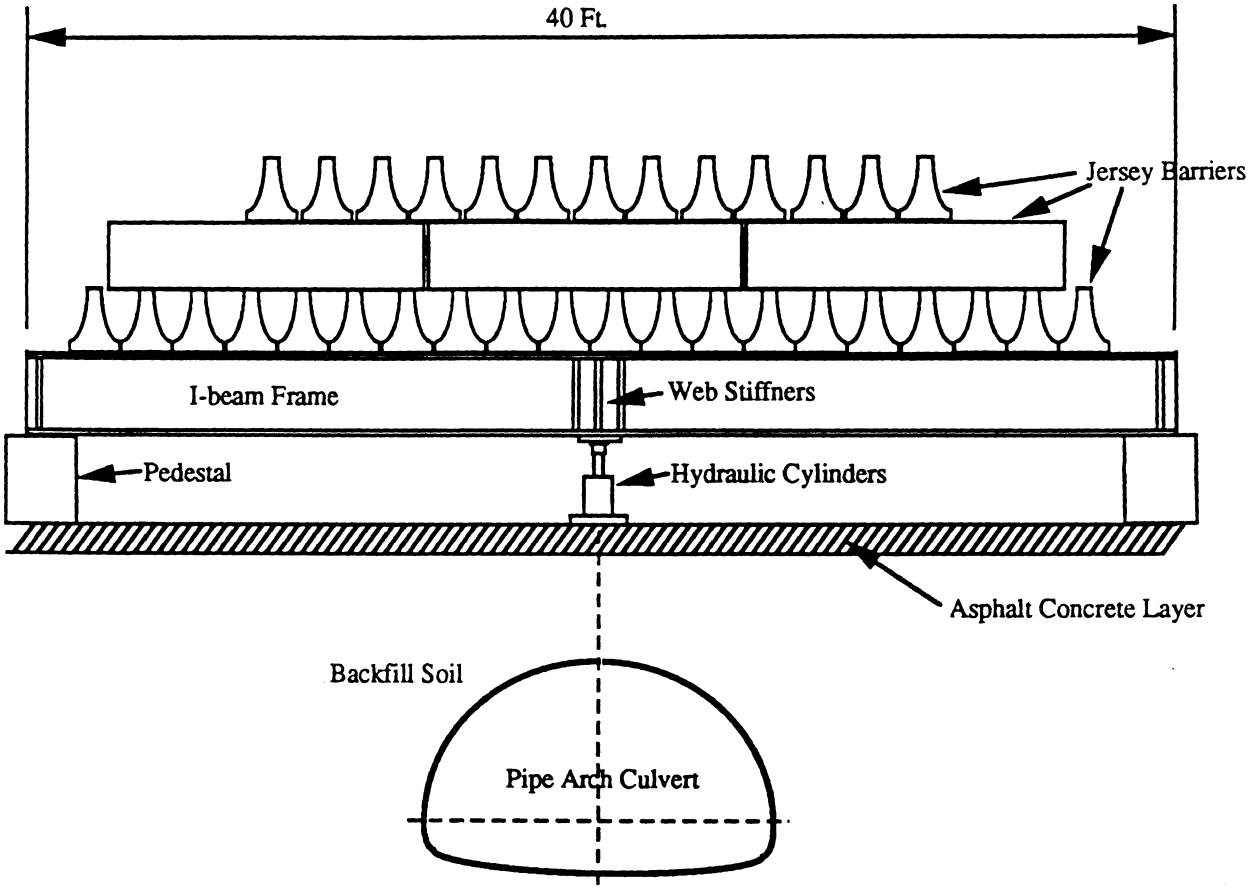

FIGURE 2.3 LIVE LOAD APPLICATION SYSTEM
(VIEW PARALELL TO ROADWAY)

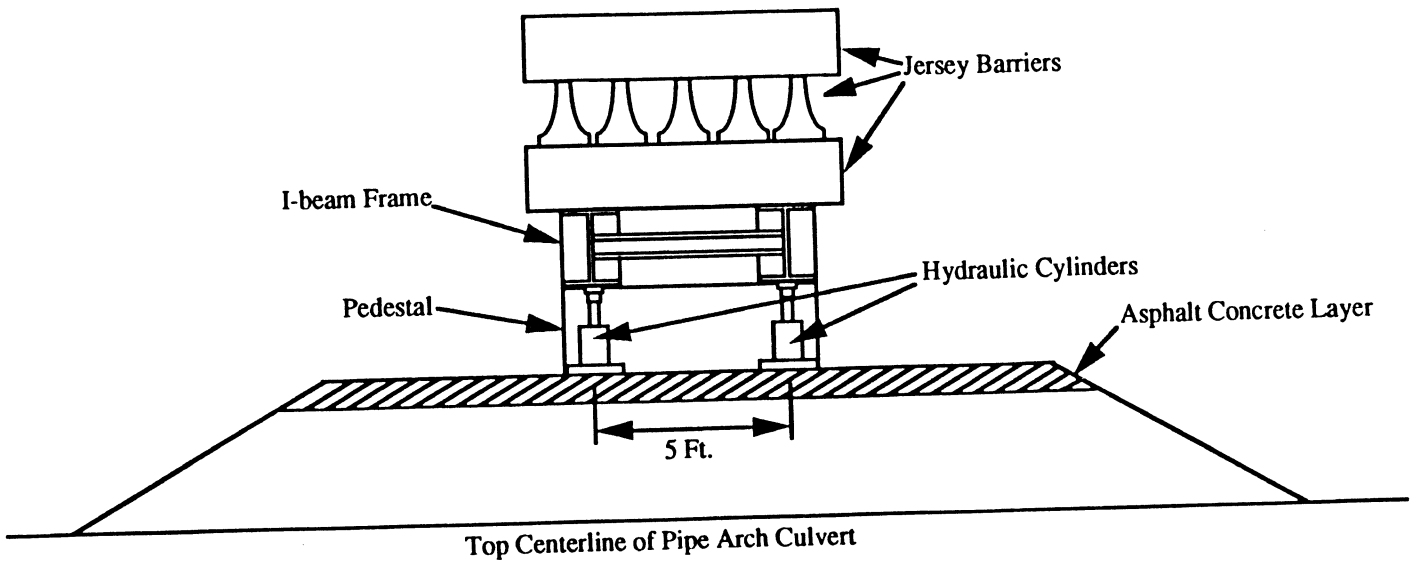

FIGURE 2.4 LIVE LOAD APPLICATION SYSTEM
(VIEW PERPENDICULAR TO ROADWAY)

FIGURE 2.5 FIELD PICTURE OF LIVE LOAD APPLICATION SYSTEM

26, 1990), the number was increased to 53, placed in four layers. Under the web-stiffened I-beam sections, two 14 inch bore, 24 inch stroke, 7 inch diameter piston rod hydraulic cylinders were set 5 feet apart to simulate the rear axle load. Both cylinders had a capacity of 230 tons, and they were connected to a hydraulic control unit for simultaneous operation.

The testing was conducted in the field under two different subsurface conditions. On the first day of testing (Sept. 24, 1990), the hydraulic cylinders were placed on top of the existing asphalt pavement layer, and pressure of up to 800 psi was developed in each cylinder. On the second day of testing (Sept. 26, 1990), the asphalt material layer was completely removed as well as some portion of the cohesive backfill material, so that there would be only 3 feet of soil cover between the crown point and the bottom of the hydraulic cylinders. Two cycles of monotonically increasing large live load was applied on the second day, since the total stroke was almost used up during the first cycle. Tables 2.4 and 2.5 summarize the actual sequence of load application which took place on these two testing days. Each load increment was maintained approximately 15 to 20 minutes before the next load was applied, since the data acquisition system required that amount of time to sweep through all the (forty two) strain gage channels, readout outputs from the nine position transducers, and to print out hard copies of the data.

2.4 FIELD INSTRUMENTATION OF PIPE ARCH CULVERT

Cross-sectional Shape Measurement

The initial and final shapes of the culvert's cross section at the center location are determined by the technique called the "triangulation method". Details of the concept of this method is provided in section 3.2. In this method, two ground reference points are established at known locations inside the pipe, and distances are measured from these reference points to each of the monitoring points installed on the inside culvert periphery. The x, y coordinate values for each of the monitoring points are computed applying simple

TABLE 2.4 LIVE LOAD APPLICATION - FIRST DAY
(FIRST SEQUENCE OF LOADING)

Load Increment	Total Live Load Applied (Tons)
1	69.27 (= 450 psi in Each Cylinder)
2	86.59 (= 562.5 psi in Each Cylinder)
3	100.06 (= 650 psi in Each Cylinder)
4	107.76 (= 700 psi in Each Cylinder)
5	115.45 (= 750 psi in Each Cylinder)
6	123.15 (= 800 psi in Each Cylinder)
7	107.76 (= 700 psi in Each Cylinder)
8	123.15 (= 800 psi in Each Cylinder)
9	123.15 (= 800 psi in Each Cylinder)
10	123.15 (= 800 psi in Each Cylinder)
11	123.15 (= 800 psi in Each Cylinder)
12	123.15 (= 800 psi in Each Cylinder)
13	123.15 (= 800 psi in Each Cylinder)
14	123.15 (= 800 psi in Each Cylinder)
15	123.15 (= 800 psi in Each Cylinder)

First Sequence of Loading

TABLE 2.5 LIVE LOAD APPLICATION - SECOND DAY
(SECOND AND THIRD SEQUENCES OF LOADING)

Load Increment		Total Live Load Applied (Tons)
1	Second Sequence of Loading	30.79 (= 200 psi in Each Cylinder)
2		38.48 (= 250 psi in Each Cylinder)
3		50.03 (= 325 psi in Each Cylinder)
4		65.43 (= 425 psi in Each Cylinder)
5		78.89 (= 512.5 psi in Each Cylinder)
6		88.51 (= 575 psi in Each Cylinder)
7		101.6 (= 660 psi in Each Cylinder)
8		103.91 (= 675 psi in Each Cylinder)
9		111.6 (= 725 psi in Each Cylinder)
10		101.6 (= 660 psi in Each Cylinder)
11		111.6 (= 725 psi in Each Cylinder)
12		113.9 (= 740 psi in Each Cylinder)
1	Third Sequence of Loading	46.18 (= 300 psi in Each Cylinder)
2		57.73 (= 375 psi in Each Cylinder)
3		80.81 (= 525 psi in Each Cylinder)
4		100.06 (= 650 psi in Each Cylinder)
5		107.76 (= 700 psi in Each Cylinder)
6		115.46 (= 750 psi in Each Cylinder)
7		115.46 (= 750 psi in Each Cylinder)

principles of geometry. For the pipe arch culvert of concern, a total of nine monitoring points were established by installing eyebolts directly onto the corrugated plates, within the arc above the springline. The two ground reference points were established by installing larger size eyebolts on the top surface of a concrete support constructed for the reference truss structure (which was used to attach position transducers for deflection measurements during the tests). The distances were then measured with an accuracy of plus or minus 0.005 inch, using a tape extensometer. Figure 2.6 presents a clear picture of the set-up. The possible movements of the reference points were observed with the conventional level surveying method. Independent of the above triangulation measurements, the Ohio DOT engineers took detailed dimensions of the pipe arch, such as rise, span, top mid-ordinate, top left and right chords and mid-ordinates, by stretching a cloth tape and/or a nylon string at several sections along the longitudinal axis of the pipe.

Deflection Measurement

In this investigation, response of the culvert structure under the application of exceptional live load was entirely unknown before the test. There was a need to develop a deflection measurement system which would not require presence of any field personnel inside the culvert and which could achieve a relatively rapid collection and storage of deflection readings. After considering various options, it was decided to use constant-tension wire type position transducers. Nine units of the 10 inch range position transducers manufactured were utilized along with the data acquisition system. A minimum of nine units were required since the deflection measurement would have to be obtained for the nine monitoring points used for the cross-sectional shape measurement. It was assumed that deflection of the pipe due to the live load would be primarily in the direction normal to the surface of the plate, confined within the two dimensional cross-sectional plane.

These position transducers were attached to a reference truss structure erected at the mid-length section inside the culvert. The transducer wires were then extended carefully and hooked to each of the nine monitoring eyebolts installed on the pipe. Figure 2.6 shows

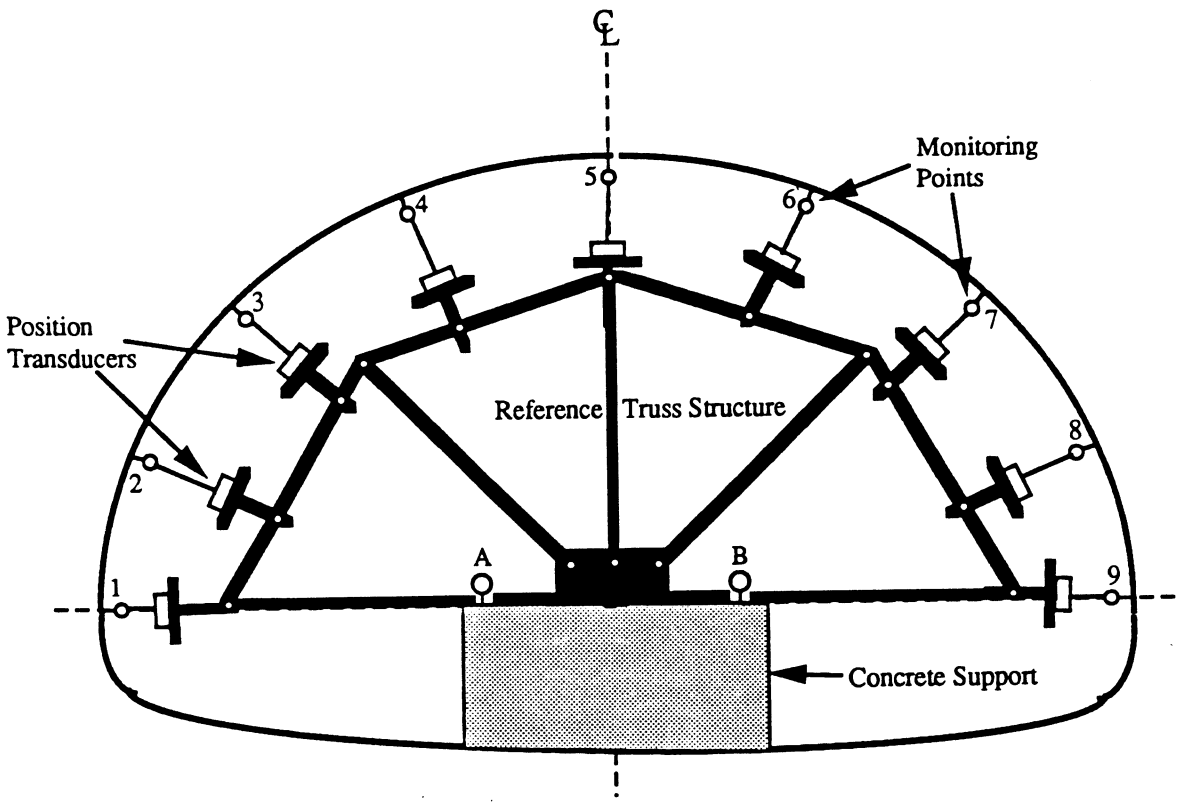

A, B = Ground Reference Points

FIGURE 2.6 SYSTEM USED FOR CROSS-SECTIONAL SHAPE AND DEFLECTION MEASUREMENTS

the installation of the position transducers with respect to the culvert pipe geometry.

Biaxial Strain Measurement

The nine locations across the center section of the culvert, where both cross-sectional shape and deflection measurements were to be obtained, were also chosen to measure biaxial strains. Two biaxial electrical strain gages were mounted on the inside corrugated plate at each location, except for the crown, and the two shoulder locations where the third strain gage was added. The first gage was installed at the peak of the inside corrugation, and the second gage was installed, half a corrugation away from the first, in the valley of the inside corrugation, as shown in Figure 2.7. Each strain gage was positioned so that its two axes would be oriented parallel and perpendicular to the direction of the plate corrugation and therefore strains could be read in the circumferential and the longitudinal directions. Computations of moment and thrust values based on the strain readings are explained in chapter four. A computer data acquisition system was loaded on the back of the CGGR research vehicle and utilized in the field to obtain the strain gage readings and the position transducer outputs during the loading steps.

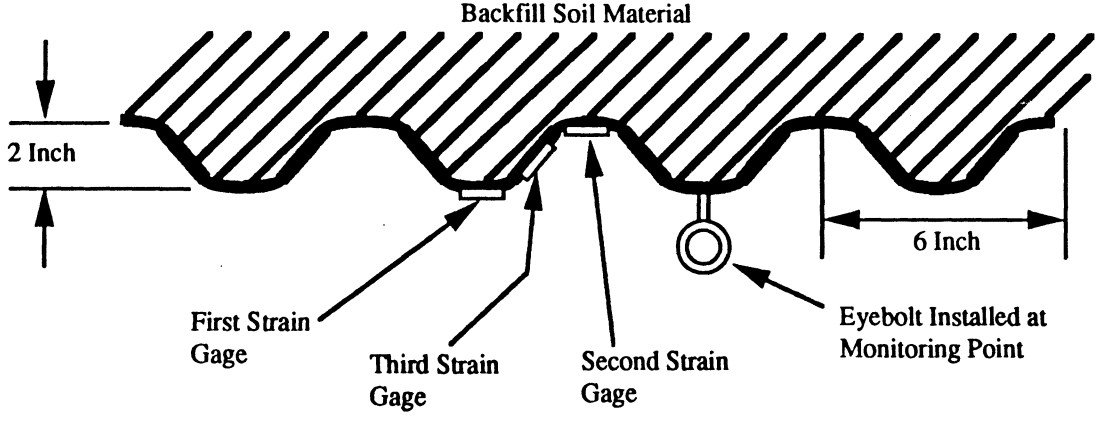

FIGURE 2.7 TYPICAL INSTALLATION OF BIAXIAL STRAIN GAGES

CHAPTER 3

MEASUREMENT OF CULVERT DEFORMATION

3.1 OVERVIEW OF DEFORMATION MEASUREMENT

Culvert deformations were monitored after each increment of monotonically applied live load. Deformation measurements were made by position transducers. A tape extensometer was used to take readings to determine the shape of the culvert before and after the test. This chapter explains the instruments used to collect the deformation data, principles used for data reduction and the results obtained from the analysis. Movement of the control hooks A and B were monitored by the ODOT personnel.

3.2 TAPE EXTENSOMETER MEASUREMENTS

The tape extensometer, used to determine the shape of the culvert, does not read out the true length between two points. Instead, a calibration constant of 17.458 inches must be applied to obtain the true length. The principle of this equipment and probable error in any reading have been studied and well documented by Allan Rauch.(1990)

The tape extensometer measurements were taken between two control hooks A, B and the nine reference hooks distributed along the culvert periphery. Hooks A and B were permanently installed into the four foot square concrete pedestal. It is reported that only negligible movement occured in concrete pedestal. Therefore, throughout this chapter it is assumed that there was no movement of control hooks.

DATA REDUCTION:

The readings a_i and b_i were taken from control hooks to all nine reference points as shown in Fig.3.1. As shown in Fig.3.1, control hooks A and B were not on the same plane as the nine reference hooks. Control hooks A and B were off by 1.5 inches and 2.25

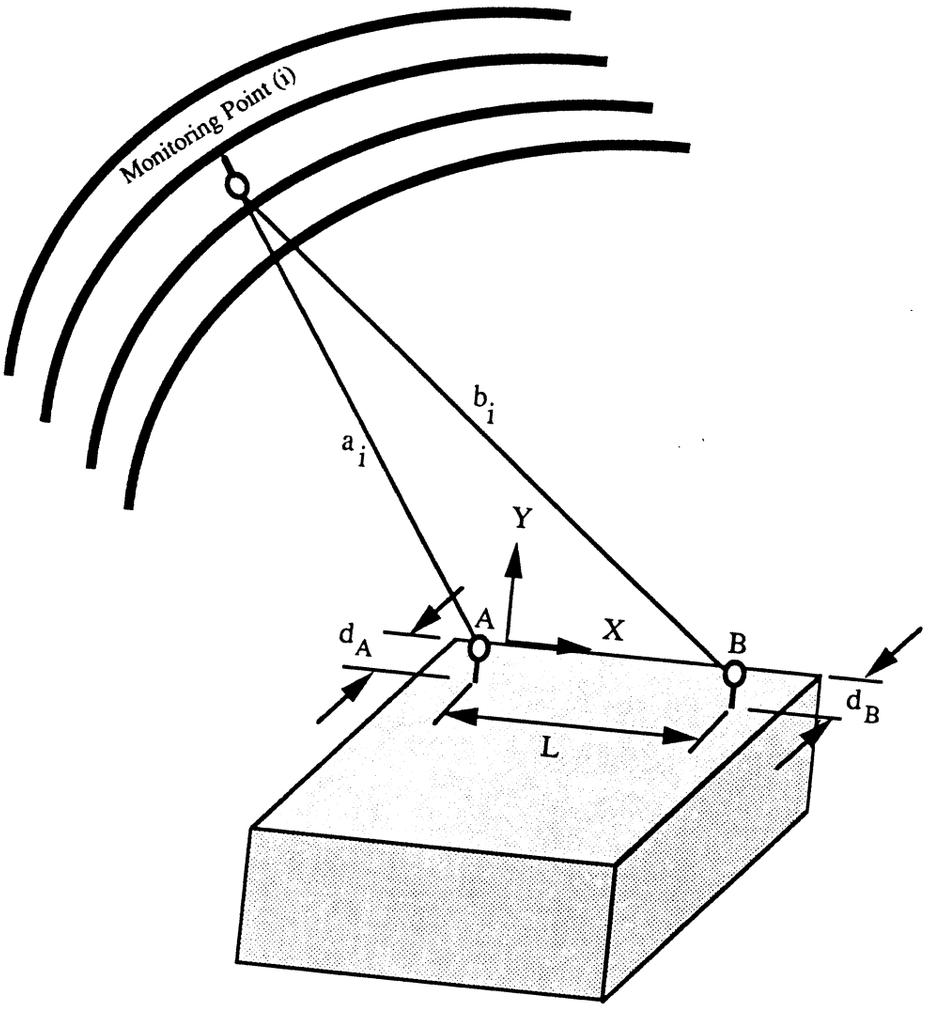

A, B = Ground Reference Points

FIGURE 3.1 MEASUREMENTS FOR CROSS-SECTIONAL SHAPE DETERMINATION

inches respectively. Therefore, the actual readings of the tape extensometer, after adding the tape constant :

$$a_i = \sqrt{\left(a_i^2 - 1.5^2\right)} + 17.458 \qquad \text{Eqn. (3.1)}$$

$$b_i = \sqrt{(b_i^2 - 2.25^2)} + 17.458 \qquad \text{Eqn. (3.2)}$$

Coordinates of all nine reference points were calculated using the triangularization method. By establishing the origin of a two dimensional x,y coordinate system at a point where reference point A is projected onto the cross-sectional plane and applying simple geometry principles, the x and y coordinate values for the monitoring point i can be expressed as:

$$x_i = \frac{1}{2L}\left[L^2 + a_i^2 - b_i^2\right] \qquad \text{Eqn. (3.3)}$$

$$y_i = \sqrt{a_i^2 - x_i^2} \qquad \text{Eqn. (3.4)}$$

It is assumed that there is no elevation difference between control hooks A and B. Initial co-ordinates and final co-ordinates of all nine reference points were tabulated in Tables 3.1 and 3.2, respectively. Initial and final shapes of the culvert are given in Fig 3.2. Initial shape of the pipe is superpositioned over the final shape curve, with a magnification factor of five applied to the vertical movements, to clearly indicate the overall deformation pattern.

The establishment and the evaluation of the initial and the final cross-section of the pipe arch was accomplished using two approaches. The first approach using tape extensometer is more accurate than the second method. The second method, which

TABLE 3.1 RESULTS OF INITIAL TRIANGULATION MEASUREMENTS

Monitoring Point	X_i	Y_i
1	- 78.4764	7.283646
2	- 67.7104	32.82528
3	- 45.8207	56.49094
4	- 16.0193	70.90557
5	16.62255	74.56251
6	48.06325	69.91524
7	78.06078	55.16796
8	100.6137	31.77941
9	111.4759	6.716778

(Note) The Above Data Reflects The Cross-Sectional Condition Of The Pipe Arch Culvert Before The Test On Sept. 24, 1990.

TABLE 3.2 RESULTS OF FINAL TRIANGULATION MEASUREMENTS

Monitoring Point	X_i	Y_i	ΔX_i	ΔY_i
1	- 78.4588	7.502599	0.017615	0.218953
2	- 67.9353	32.71373	-0.22499	-0.11156
3	- 46.2760	56.84925	-0.45531	0.358302
4	- 16.6364	70.05201	-0.61708	-0.85356
5	15.88784	67.24892	-0.73471	-7.31359
6	48.12747	66.56939	0.064227	-3.34586
7	78.61048	55.45415	0.549698	0.286184
8	100.8489	31.78826	0.235275	0.008845
9	111.5824	6.04567	0.106518	-0.67111

(Note) The Above Data Reflects The Cross-Sectional Condition Of The Pipe Arch Culvert After The Test On Sept. 26, 1990.

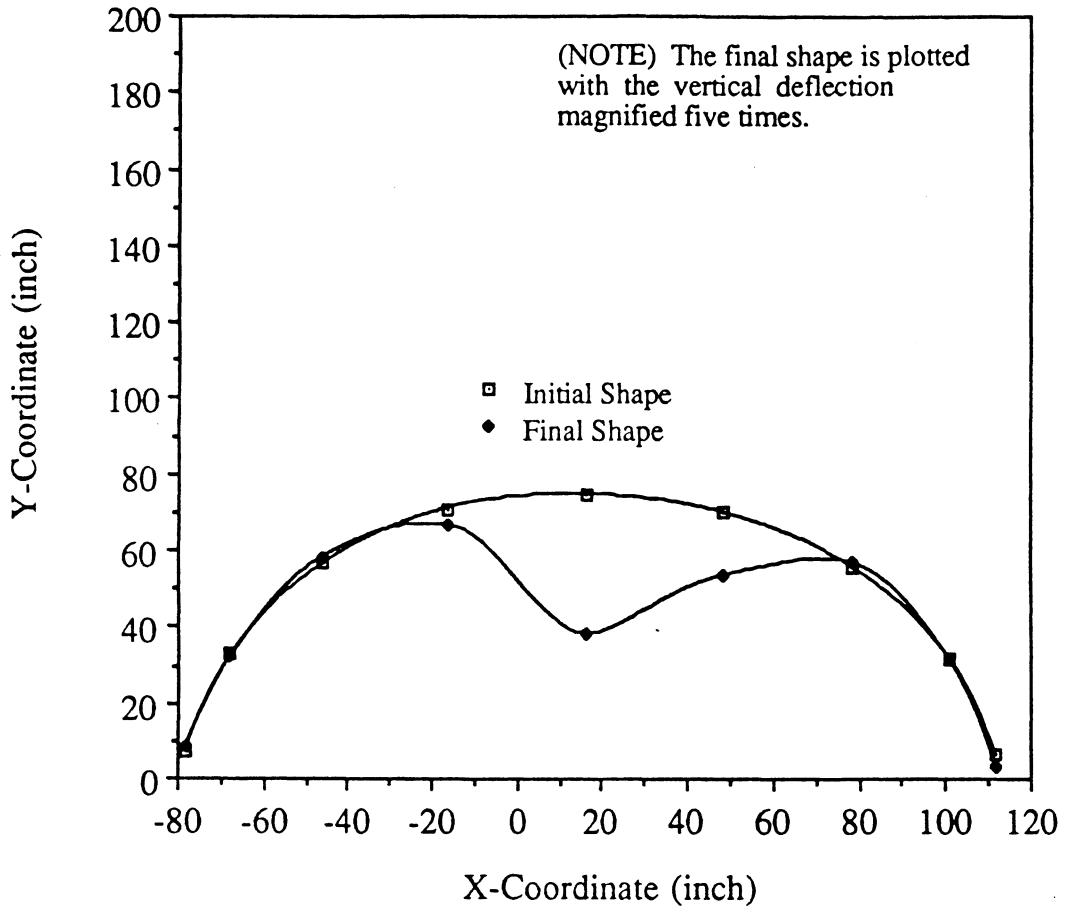

FIGURE 3.2 FINAL CROSS-SECTIONAL SHAPE AT CENTER LOCATION

consisted of taking tape measurements of rise, span, skew span, chords and mid ordinates, was applied through out almost the entire length of the pipe. Figure 3.3 presents the different tape measurements taken by the Ohio DOT engineers and Tables 3.3 and 3.4 presents the various measurements recorded inside the pipe along its length before and after the test respectively

Reduction in the rise was initially detected due to sagging of the pipe arch in the middle. Measurements in the rise varied from 4.74% to 10.0%, with the maximum reduction was observed at the center. Span is increased by 1.15% near the west end to 2.94% at the center location. No significant leaning of the pipe to one side was detected.

Final tape measurements taken after the experiment indicate that there was very small outward movement at the monitoring points one and nine, agreeing well with the position transducer measurements. Both the rise and the top center mid-ordinate dimensions experienced more than 10% reduction from their initial values, while the top left and right mid-ordinates increased by 16% to 17% and the top left and right chords decreased by about 4%.

.

3.3 POSITION TRANSDUCER MEASUREMENTS

Position transducers were utilized to measure the deformation because of their simple and remote ability to obtain highly accurate measurement. Since taking readings with the tape extensometer is a time consuming process and requires persons to be inside the culvert it was done only before and after the testing to find out the shape of the culvert.

An excitation voltage was applied to the position transducer and the resulting electrical outputs were set proportional to the linear position of the extension of a stainless steel cable. Measurements were made by attaching the cable clip to a moving element and mounting the position transducer to a fixed surface. Extension of the cable rotates the shaft

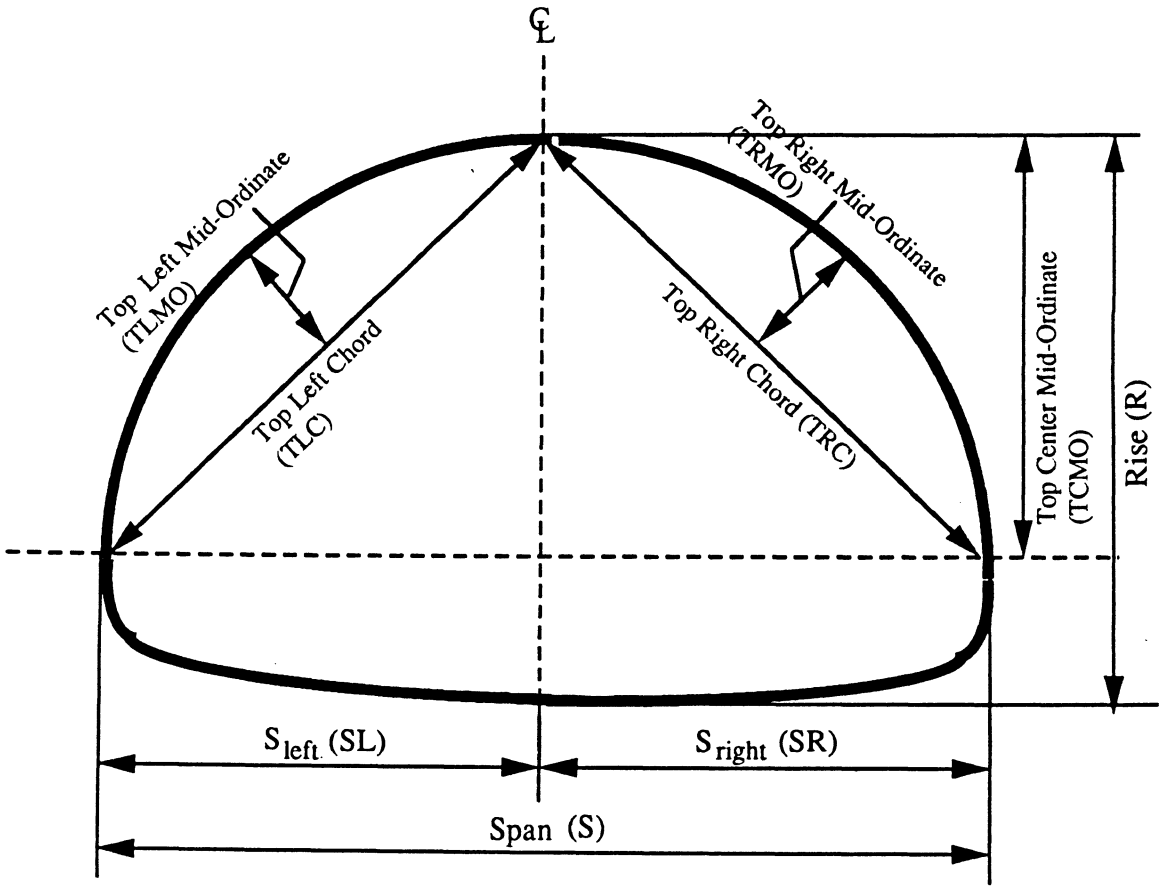

FIGURE 3.3 TYPES OF TAPE MEASUREMENTS TAKEN

TABLE 3.3 INITIAL TAPE MEASUREMENT DATA

Station	Distance From West Pipe End (ft.)	Various Dimensions Taken (in ft.)								
		S	SL	SR	R	TCMO	TLMO	TRMO	TLC	TRC
1	24.0	15.85	7.90	7.95	9.05	6.86	2.14	2.00	10.40	10.42
2	32.0	15.98	NT	NT	8.77	6.69	2.02	2.01	10.38	10.38
3	40.0	16.13	NT	NT	8.55	6.60	2.13	2.05	10.36	10.39

TABLE 3.4 FINAL TAPE MEASUREMENT DATA

Station	Distance From West Pipe End (ft.)	Various Dimensions Taken (in ft.)								
		S	SL	SR	R	TCMO	TLMO	TRMO	TLC	TRC
1	24.0	15.85	7.90	7.95	9.05	6.84	2.17	1.97	10.44	10.43
2	32.0	15.98	NT	NT	8.81	6.69	2.16	2.02	10.37	10.38
3	40.0	16.13	NT	NT	7.81	5.90	2.50	2.39	9.90	9.99
4	48.0	16.06	NT	NT	8.49	6.54	2.23	2.11	10.35	10.28
5	56.0	16.08	NT	NT	8.66	6.65	2.09	2.08	10.41	10.32

of the internal electromechanisms.

A constant-tension spring maintains the tension on the cable during extension from the base and provides torque for rewinding the cable during retraction. The cable may accelarate in retraction until the terminal velocity is reached.

The model used had a range of zero to ten inches. During the test, a total of nine position transducers were used. These transducers were calibrated in the laboratory. Instrumentation of these transducers were explained in Chapter 2. Data was collected using the HP3497A data aquisition system.

In order to calculate the deflection of the reference points the coordinates of the base of the wire needed to be determined. These coordinates are tabulated in Table 3.5. During the course of the experiment, the angle of the position transducer wire from the horizontal changed considerably for the reference points #4, #5, and #6. The change in the angle of all nine reference points are tabulated in Table 3.6.

During the analysis of transducer data, a decision was made to distribute the change in angle proportional to the change in the lenth of the wire during the application of the live load. At each step of loading, readings were taken from all nine units. For each step of the loading, the deflection was presented in both the x and the y direction. These deflections are presented in Figs. 3.4 through 3.12 for the first cycle of loading, Figs. 3.13 through 3.21 for the second cycle of loading and Figs.3.22 through 3.30 for the third cycle of loading.

3.4 DISCUSSION

Section one which was located at the west springline, had hardly moved during the

TABLE: 3.5 Co-ordinates of position transducer wire at its base

Position transducer no	X_j	Y_j
1	-74.78	2.00
2	-58.04	29.03
3	-36.06	48.56
4	-7.02	58.57
5	16.46	63.25
6	42.64	62.22
7	71.85	49.57
8	94.87	29.39
9	93.33	0.97

TABLE: 3.6 Change of angle on position transducer wire during the experiment

Position transducer no.	Angle on wire α		$\Delta\alpha$
	Initial	Final	
1	55.02	56.24	1.22
2	21.43	20.42	-1.01
3	39.1	39.06	-0.04
4	54.11	50.3	-3.81
5	89.18	81.86	-7.32
6	54.83	38.53	-16.3
7	42.03	41.04	-0.99
8	22.59	21.86	-0.73
9	17.57	15.54	-2.03

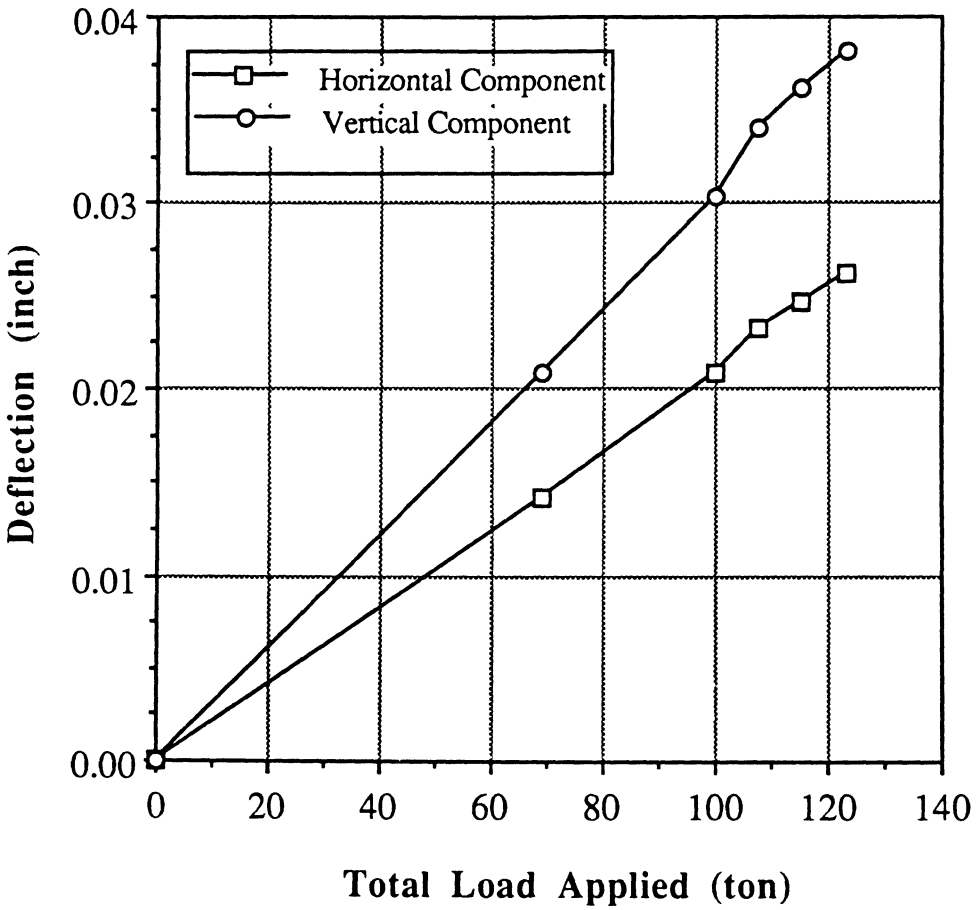

FIGURE 3.4 DEFLECTION OF MONITORING POINT#1 (SPRINGLINE) DURING FIRST LOAD SEQUENCE

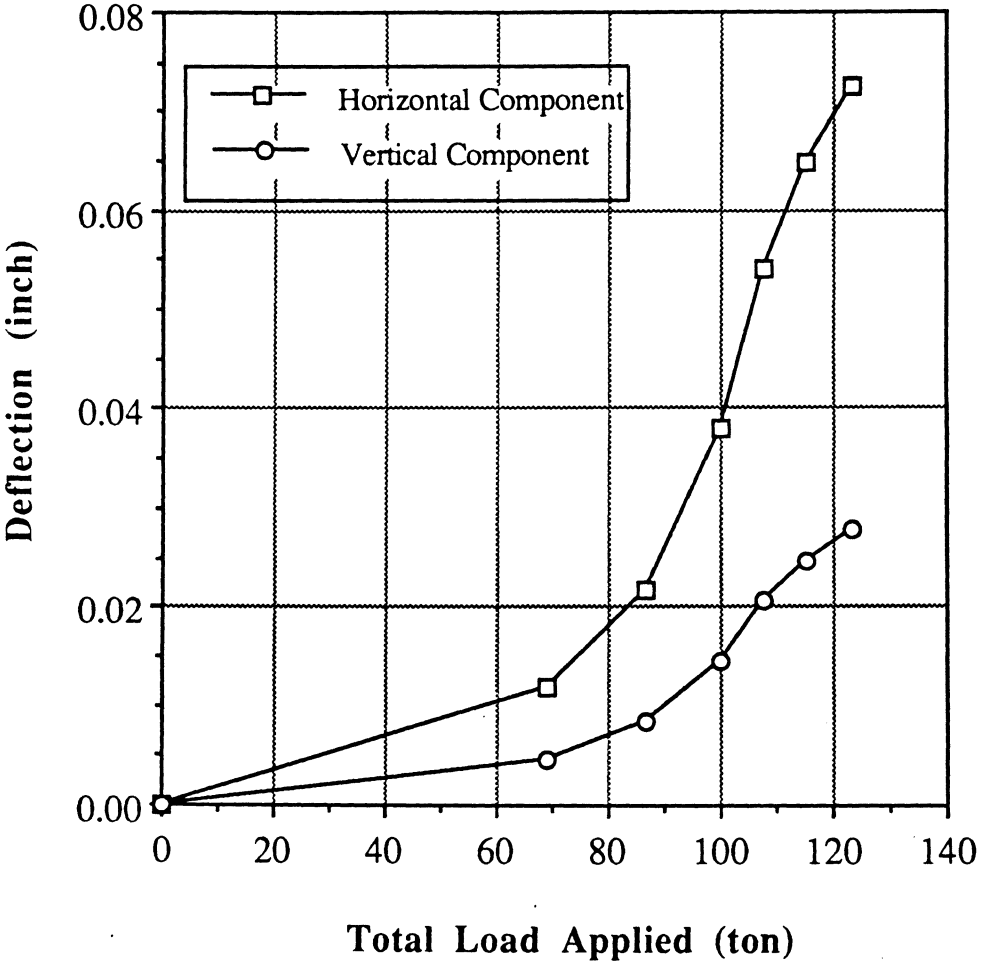

FIGURE 3.5 DEFLECTION OF MONITORING POINT #2 DURING FIRST LOAD SEQUENCE

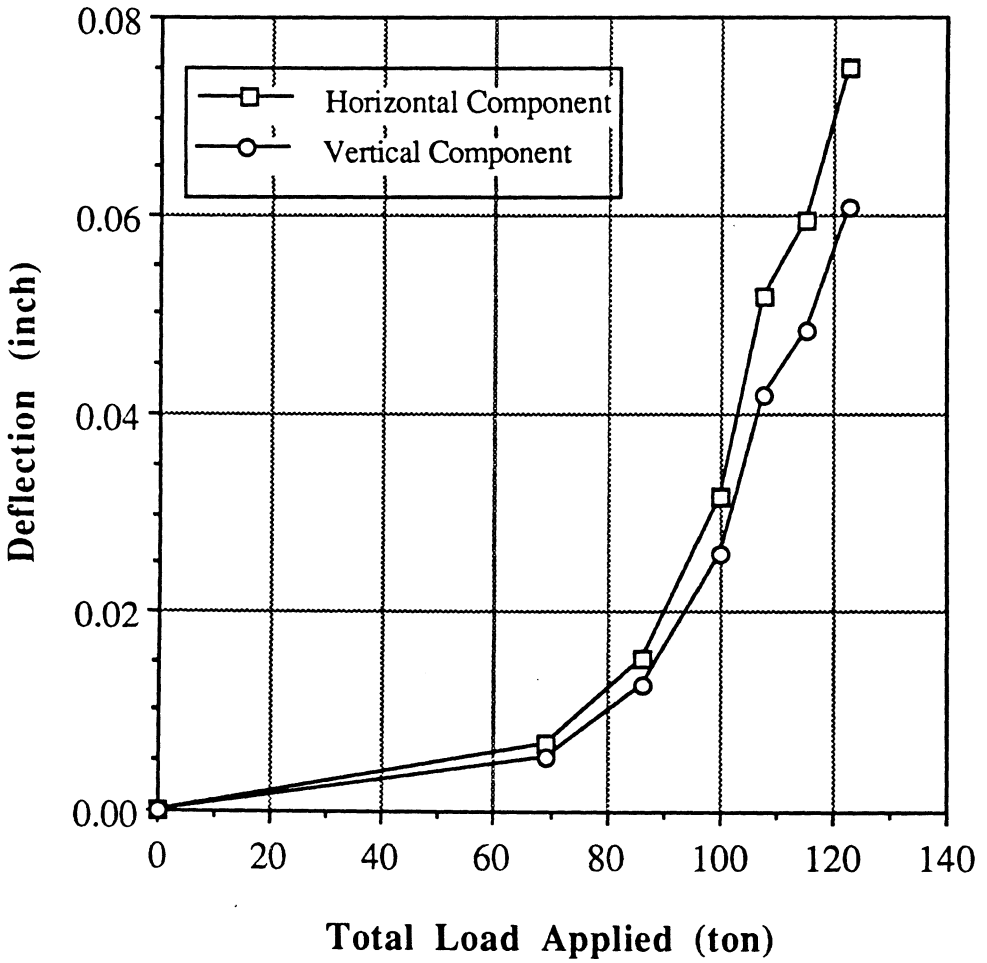

FIGURE 3.6 DEFLECTION OF MONITORING POINT#3 (SHOULDER) DURING FIRST LOAD SEQUENCE

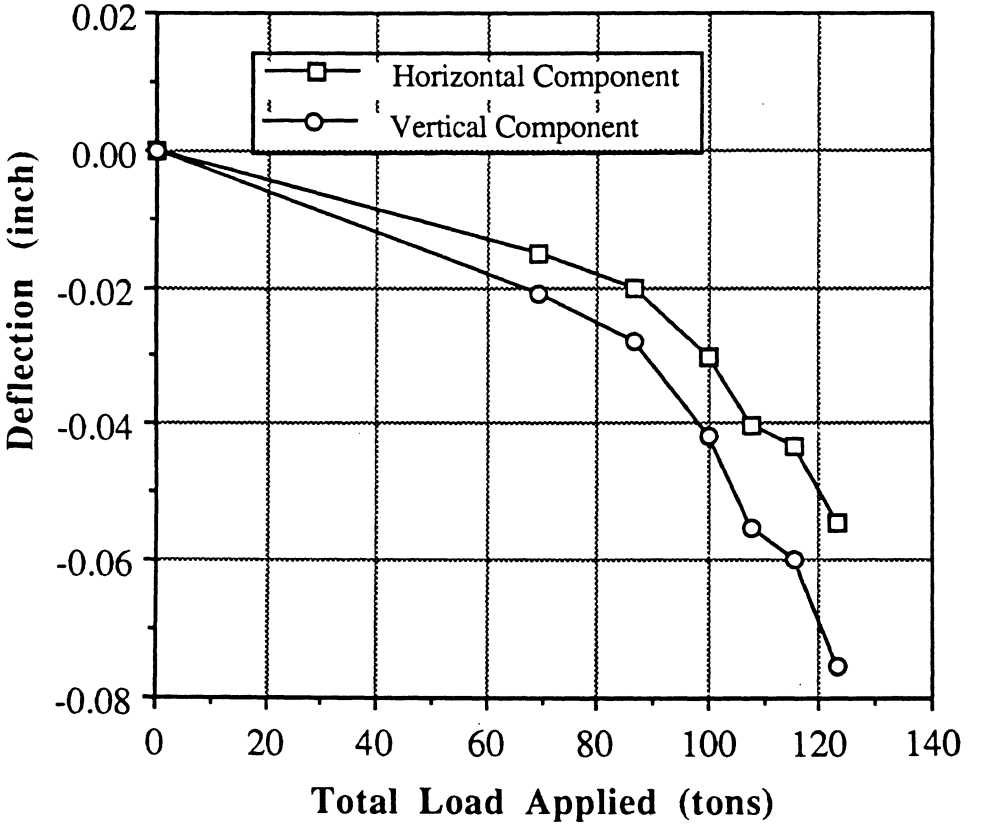

FIGURE 3.7 DEFLECTION OF MONITORING POINT #4 DURING THE FIRST LOAD SEQUENCE

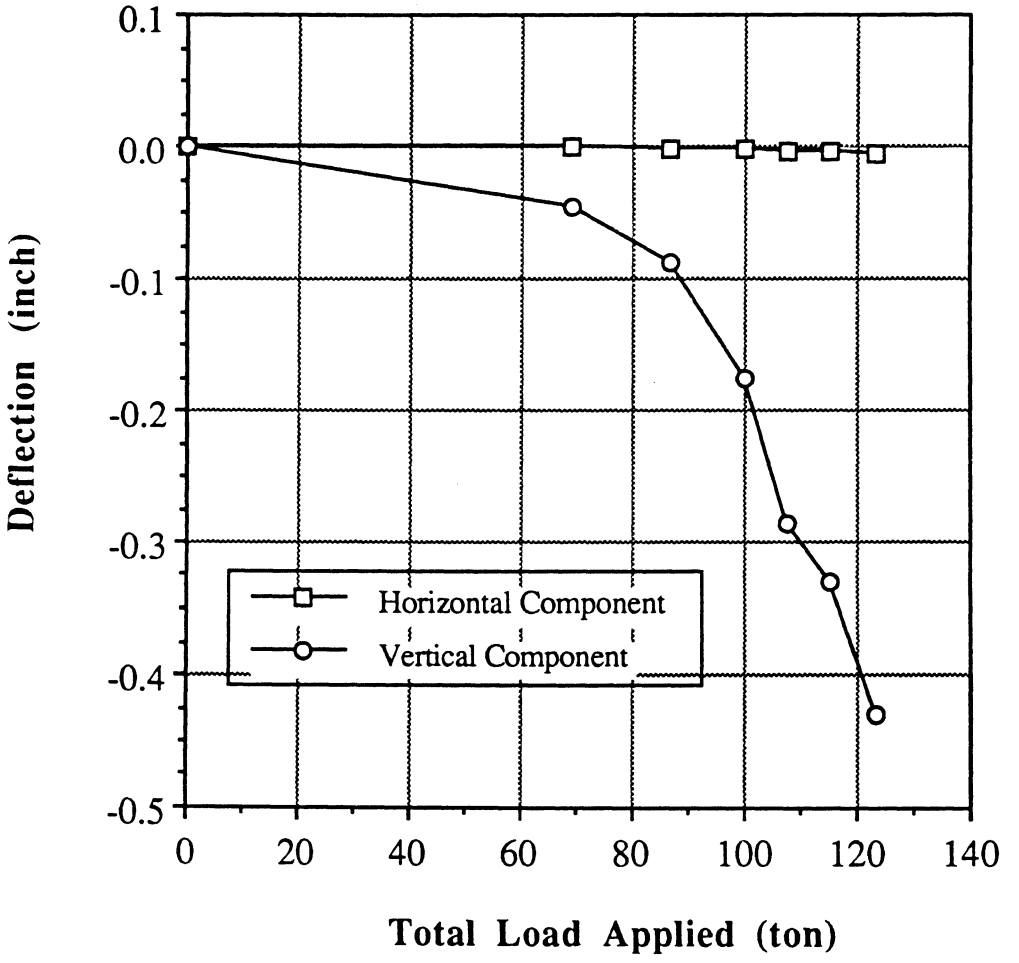

FIGURE 3.8 DEFLECTION OF MONITORING POINT #5 (CROWN) DURING FIRST LOAD SEQUENCE

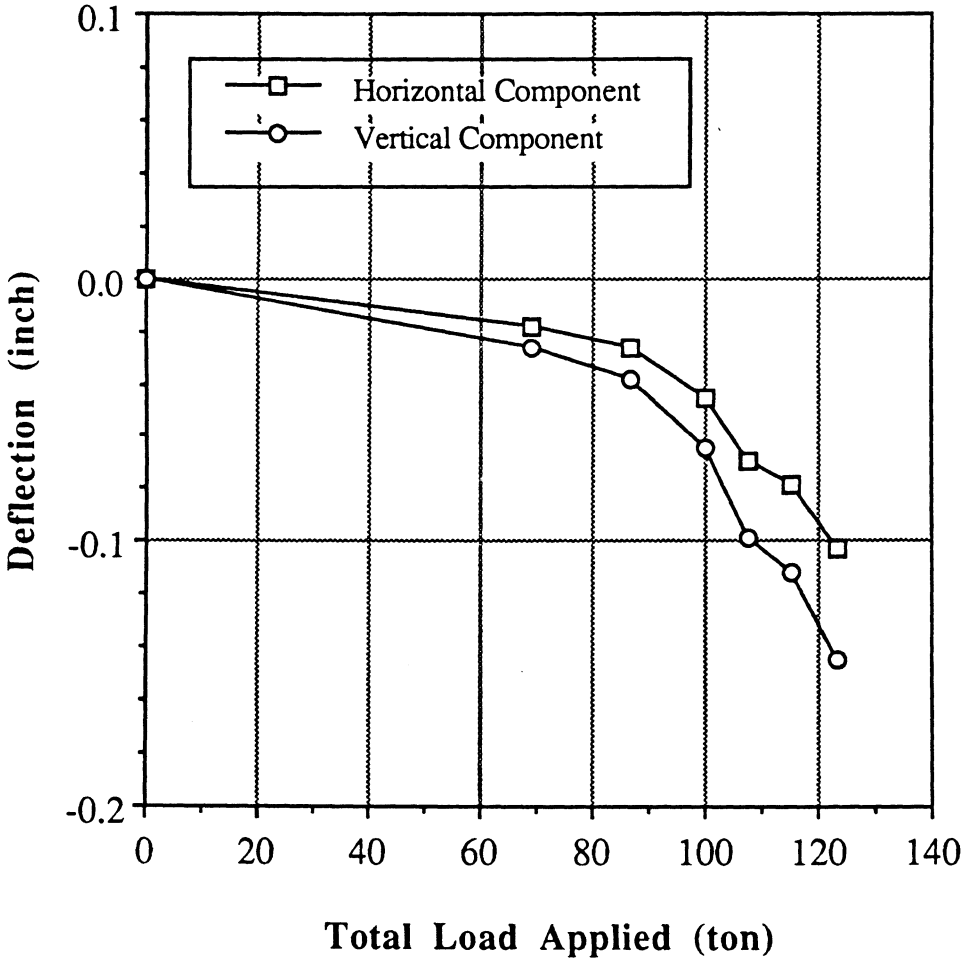

FIGURE 3.9 DEFLECTION OF MONITORING POINT #6 DURING FIRST LOAD SEQUENCE

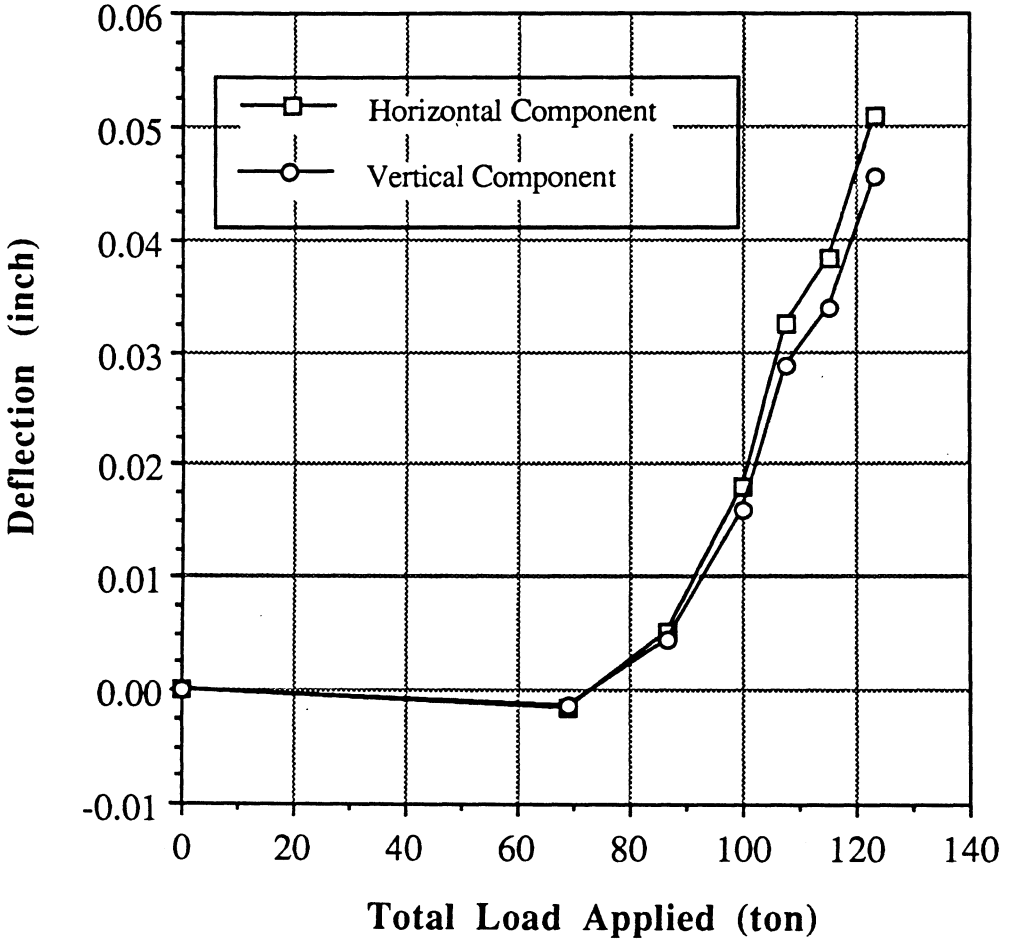

FIGURE 3.10 DEFLECTION OF MONITORING POINT #7 (SHOULDER) DURING FIRST LOAD SEQUENCE

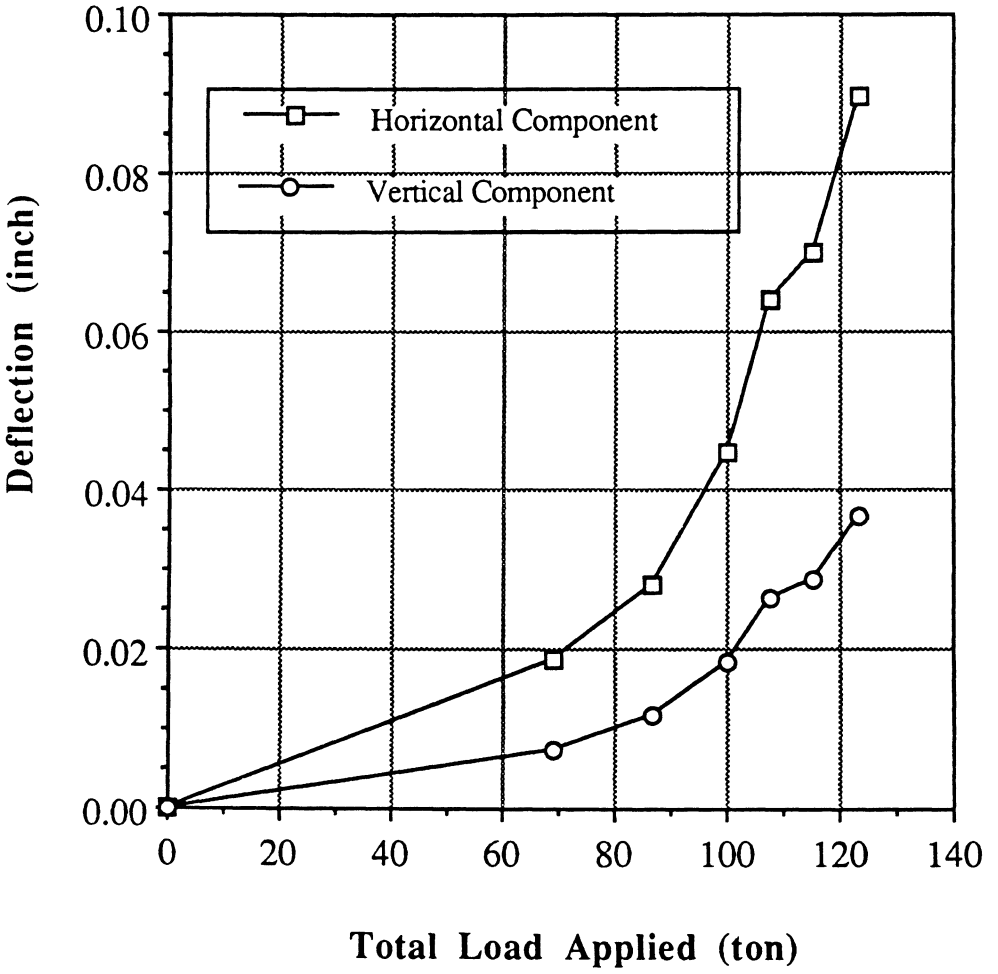

FIGURE 3.11 DEFLECTION OF MONITORING POINT #8 DURING FIRST LOAD SEQUENCE

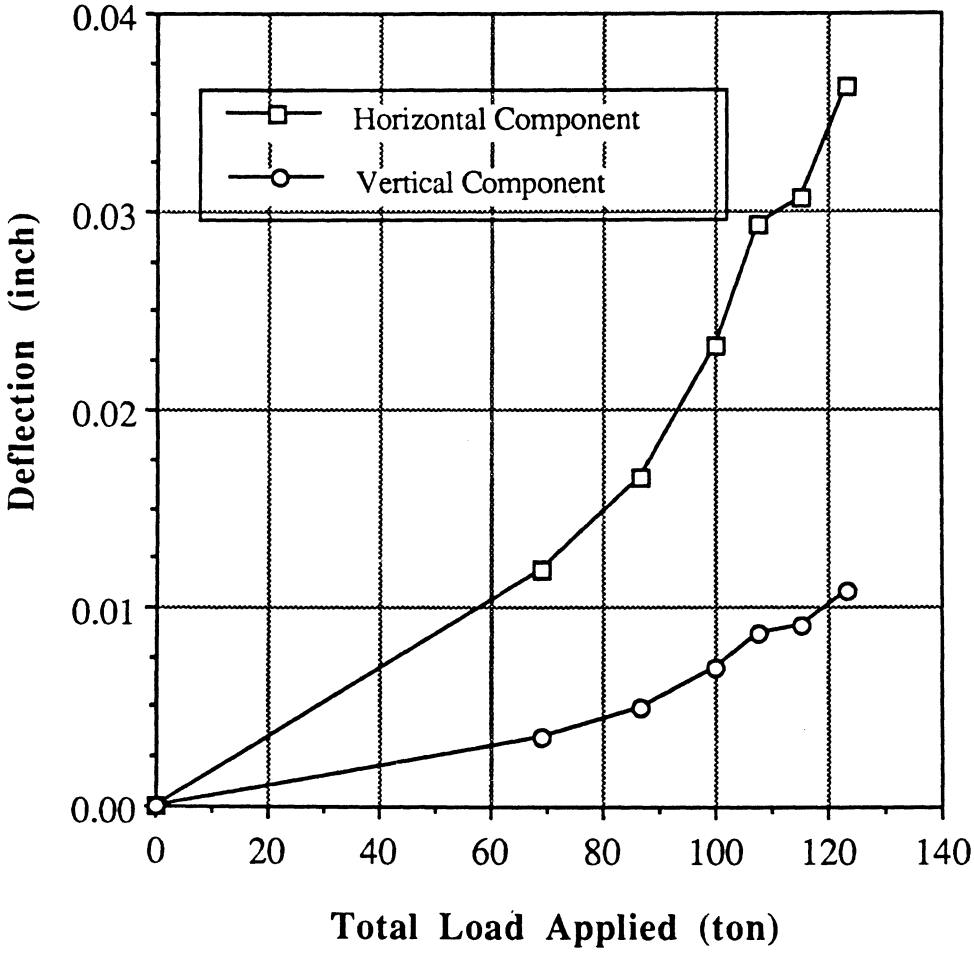

FIGURE 3.12 DEFLECTION OF MONITORING POINT #9 (SPRINGLINE) DURING FIRST LOAD SEQUENCE

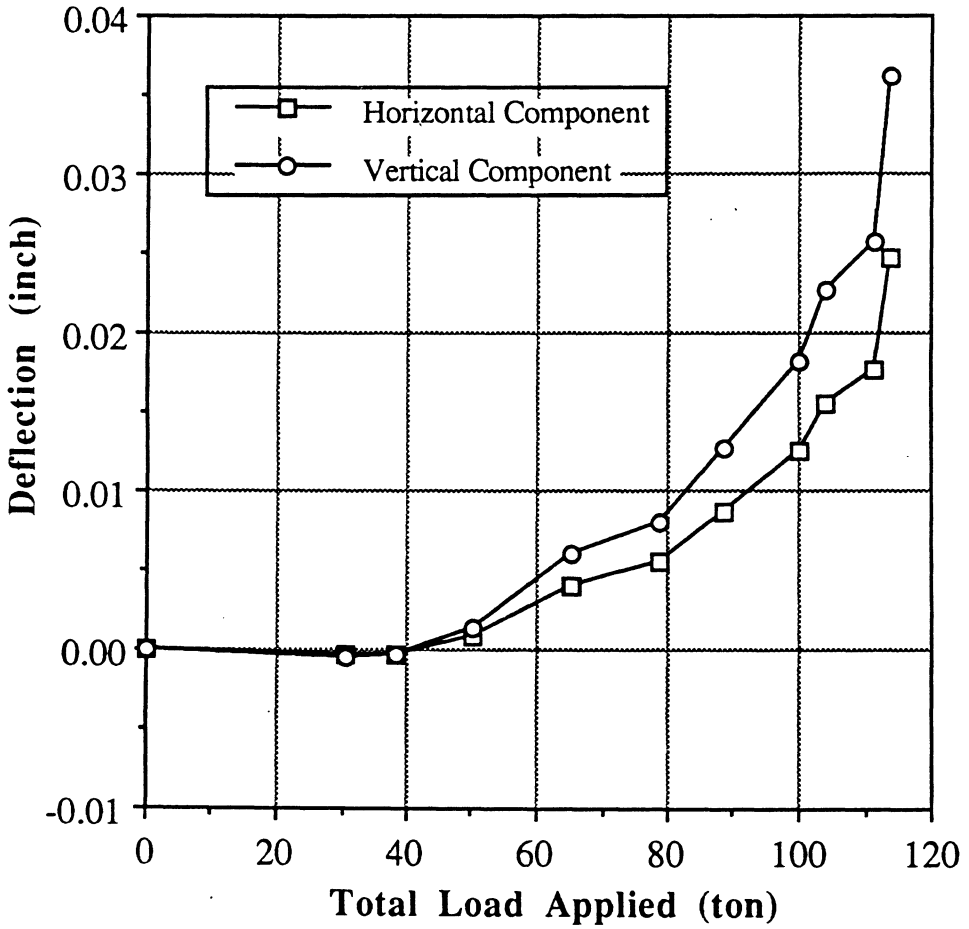

FIGURE 3.13 DEFLECTION OF MONITORING POINT #1 (SPRINGLINE) DURING SECOND LOAD SEQUENCE

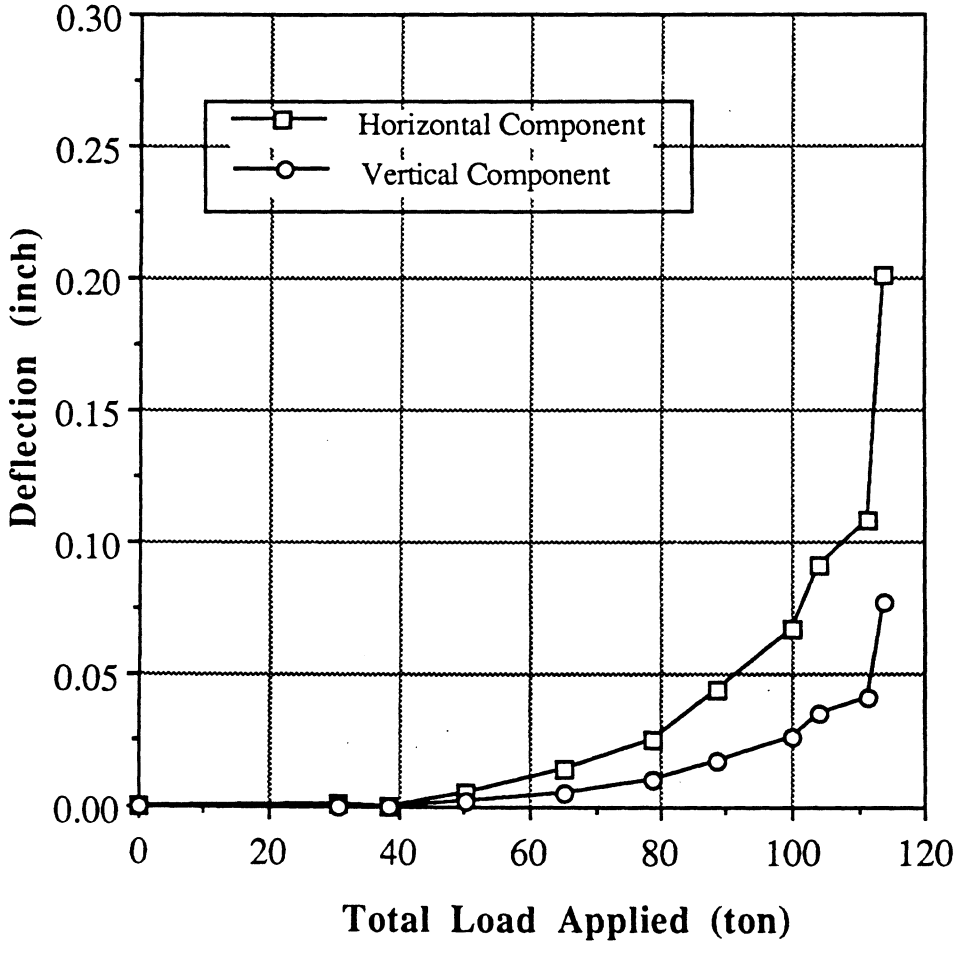

FIGURE 3.14 DEFLECTION OF MONITORING POINT #2 DURING SECOND LOAD SEQUENCE

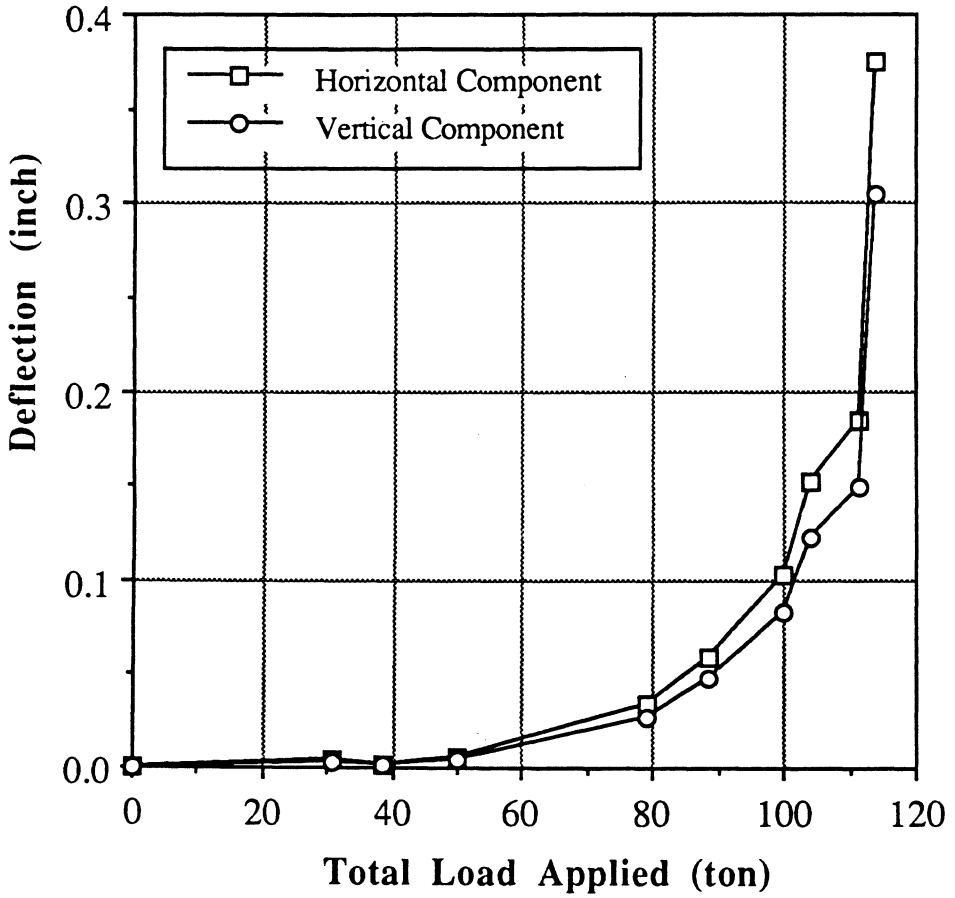

FIGURE 3.15 DEFLECTION OF MONITORING POINT #3 (SHOULDER) DURING SECOND LOAD SEQUENCE

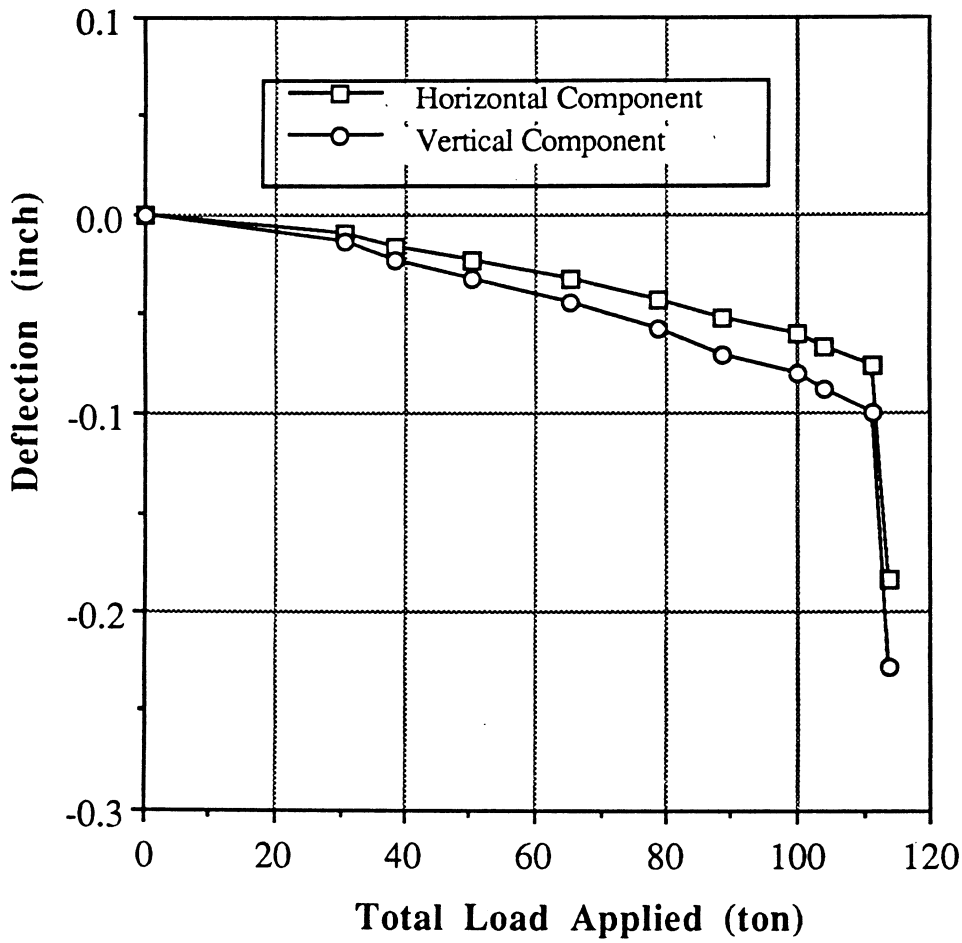

FIGURE 3.16 DEFLECTION OF MONITORING POINT #4 DURING SECOND LOAD SEQUENCE

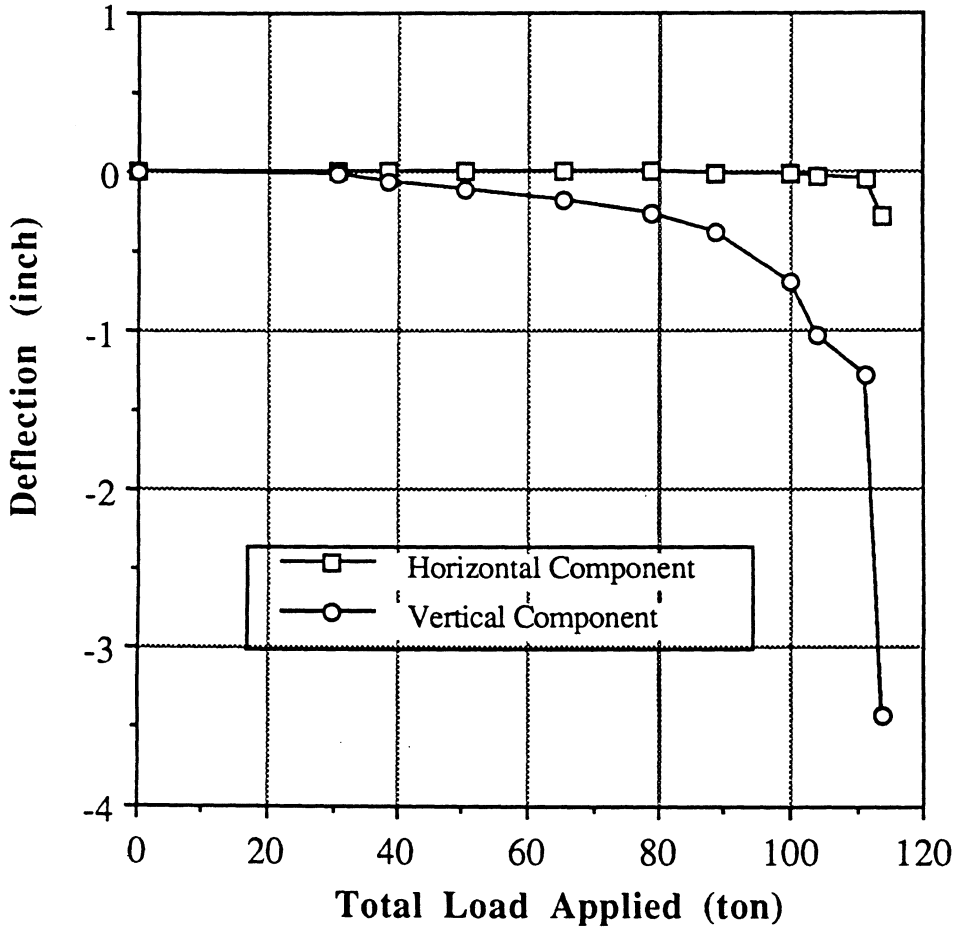

FIGURE 3.17 DEFLECTION OF MONITORING POINT #5 (CROWN) DURING SECOND LOAD SEQUENCE

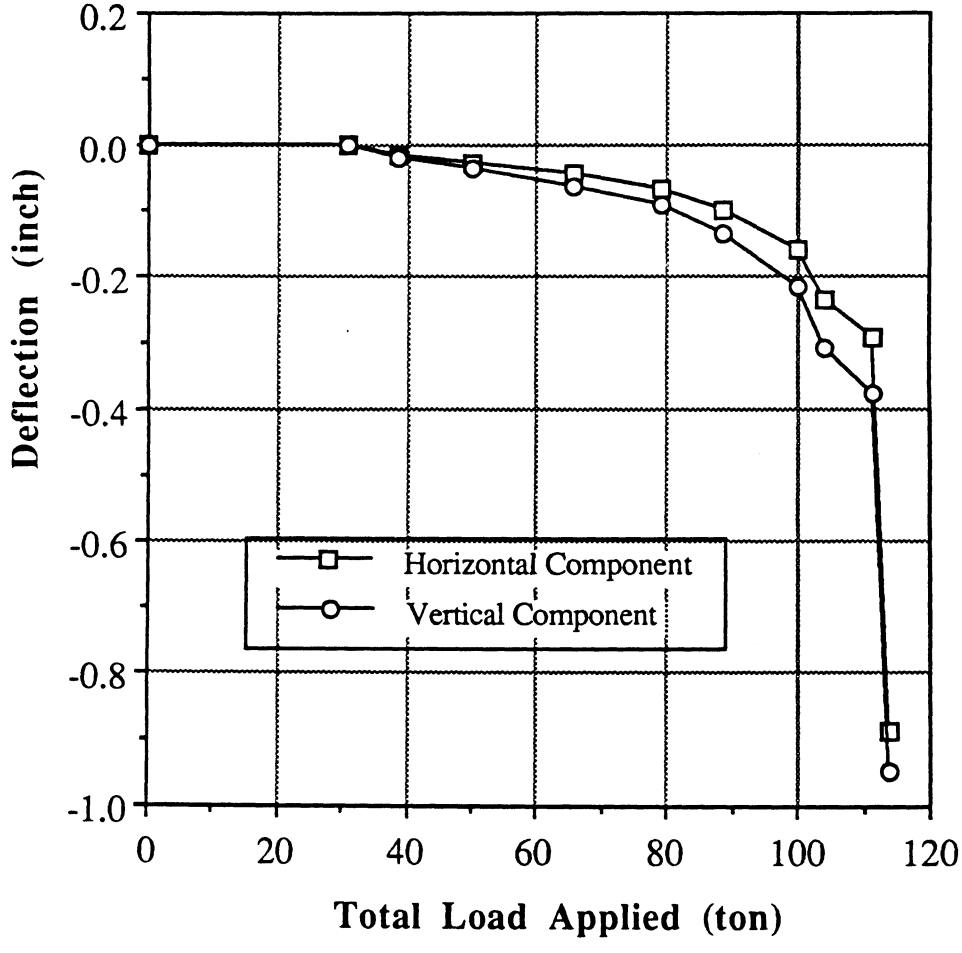

FIGURE 3.18 DEFLECTION OF MONITORING POINT #6 DURING SECOND LOAD SEQUENCE

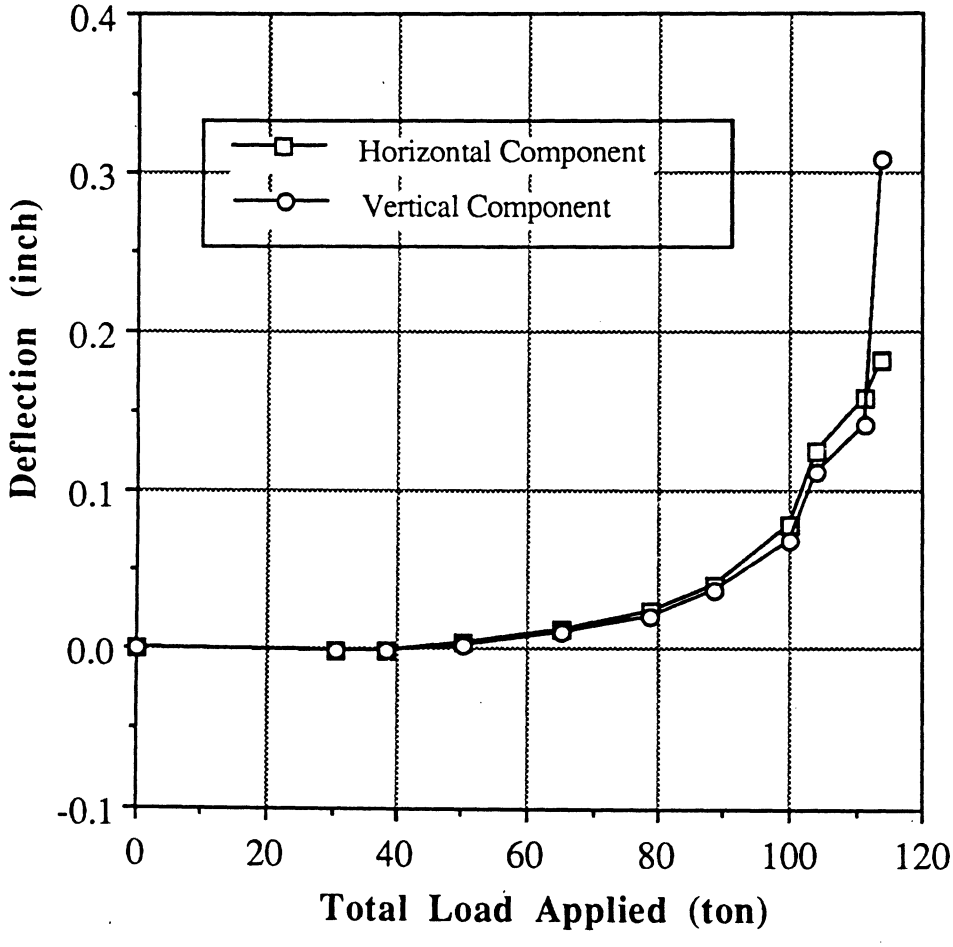

FIGURE 3.19 DEFLECTION OF MONITORING POINT #7 (SHOULDER) DURING SECOND LOAD SEQUENCE

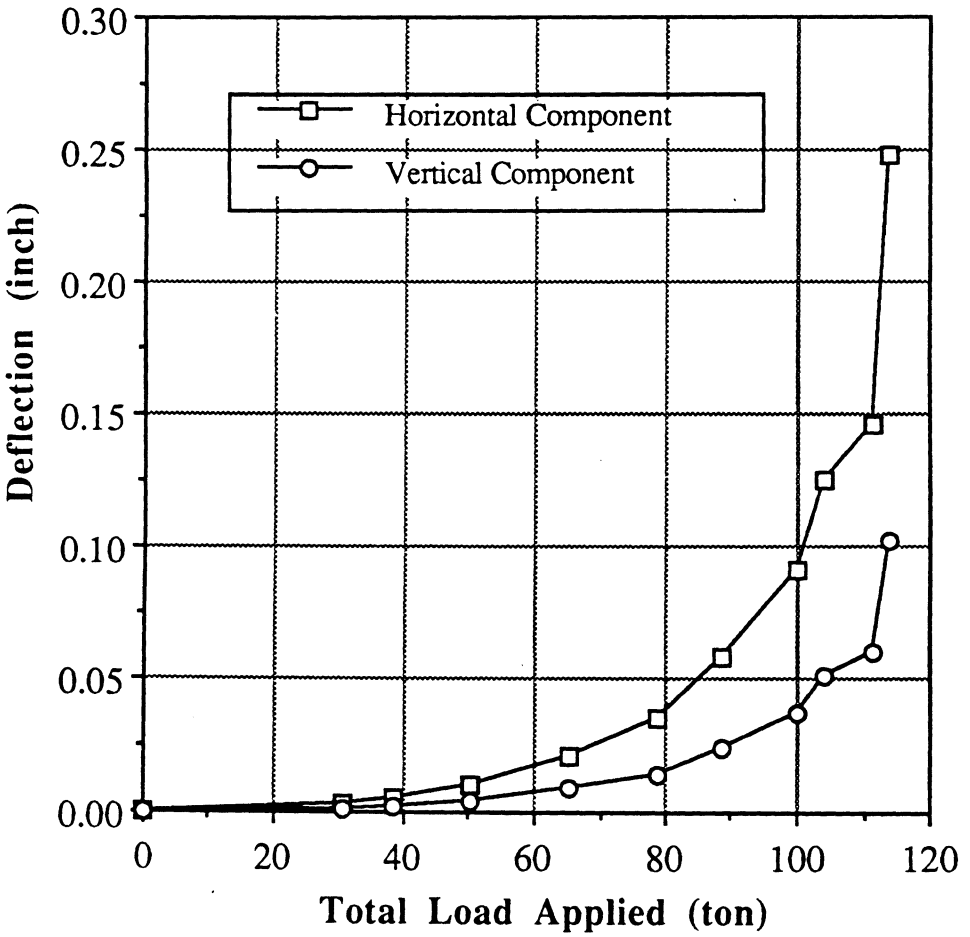

FIGURE 3.20 DEFLECTION OF MONITORING POINT #8 DURING SECOND LOAD SEQUENCE

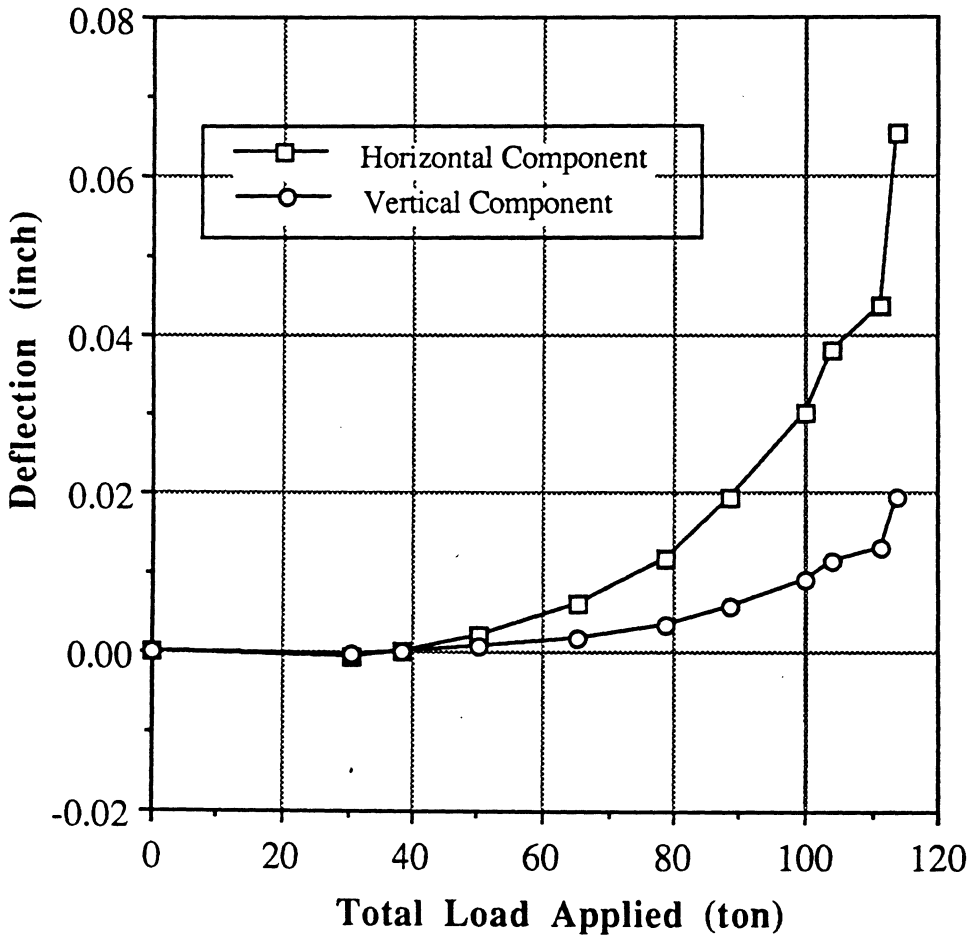

FIGURE 3.21 DEFLECTION OF MONITORING POINT #9 (SPRINGLINE) DURING SECOND LOAD SEQUENCE

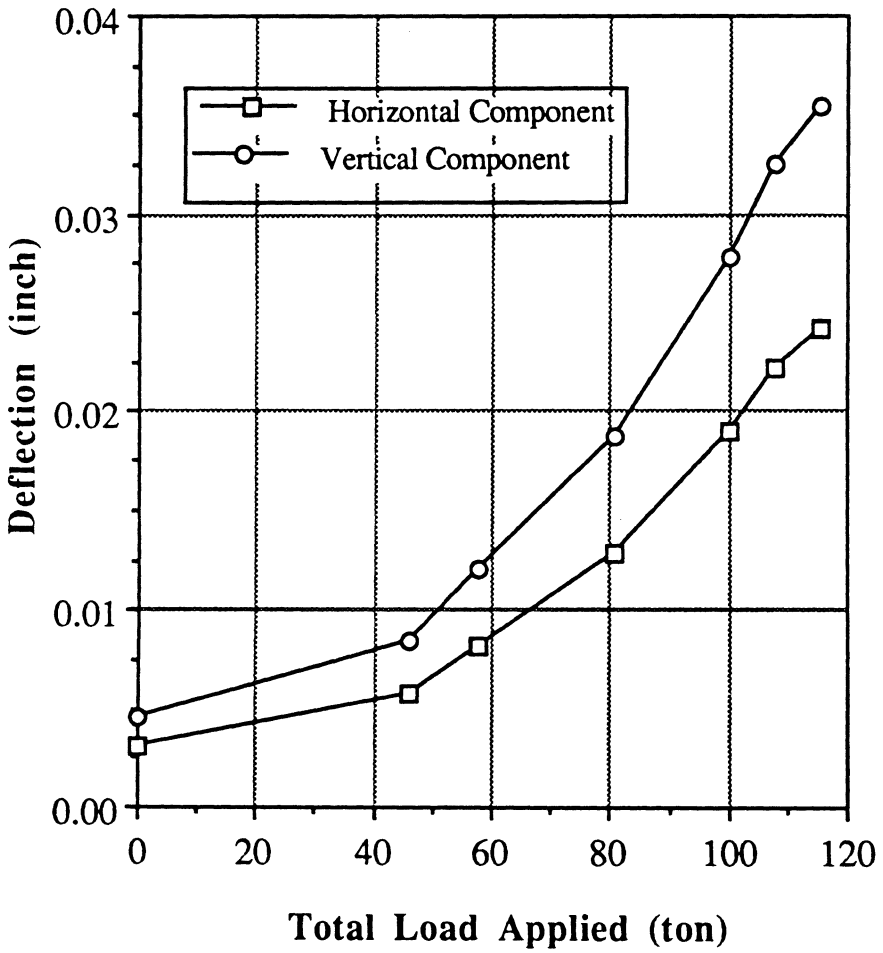

FIGURE 3.22 DEFLECTION OF MONITORING POINT #1 (SPRINGLINE) DURING THIRD LOAD SEQUENCE

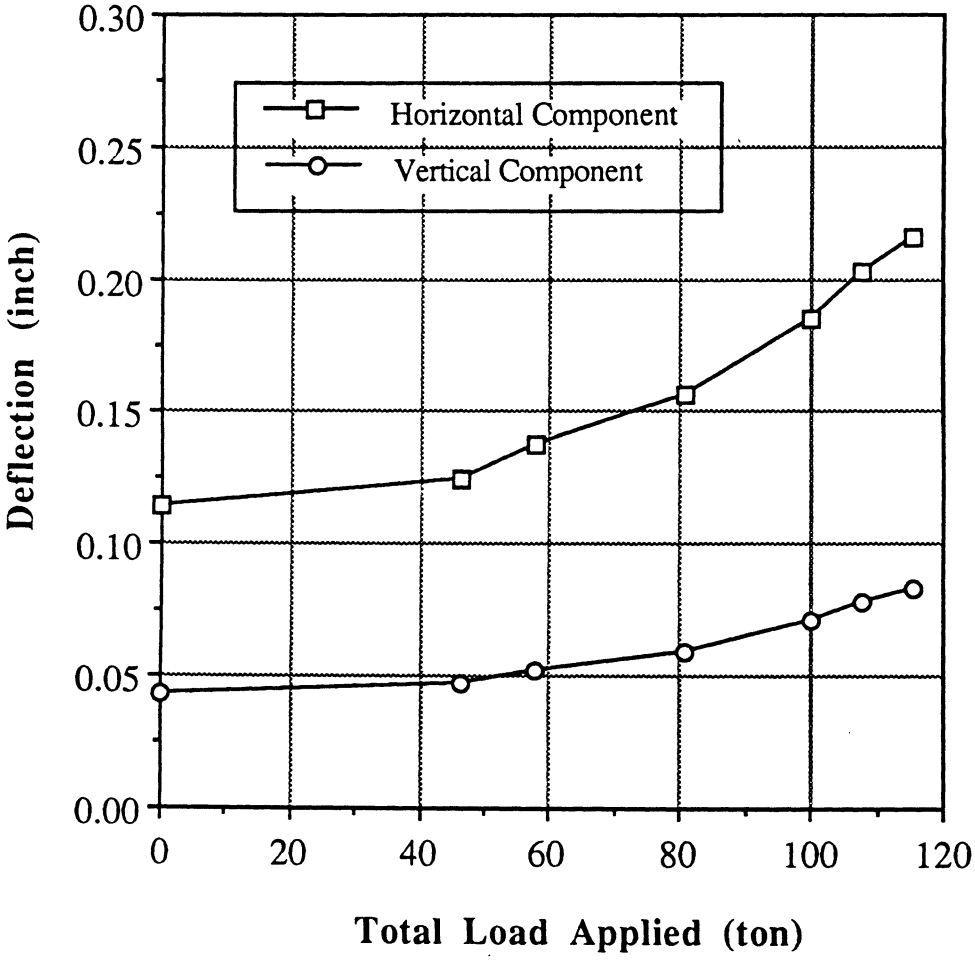

FIGURE 3.23 DEFLECTION OF MONITORING POINT #2 DURING THIRD LOAD SEQUENCE

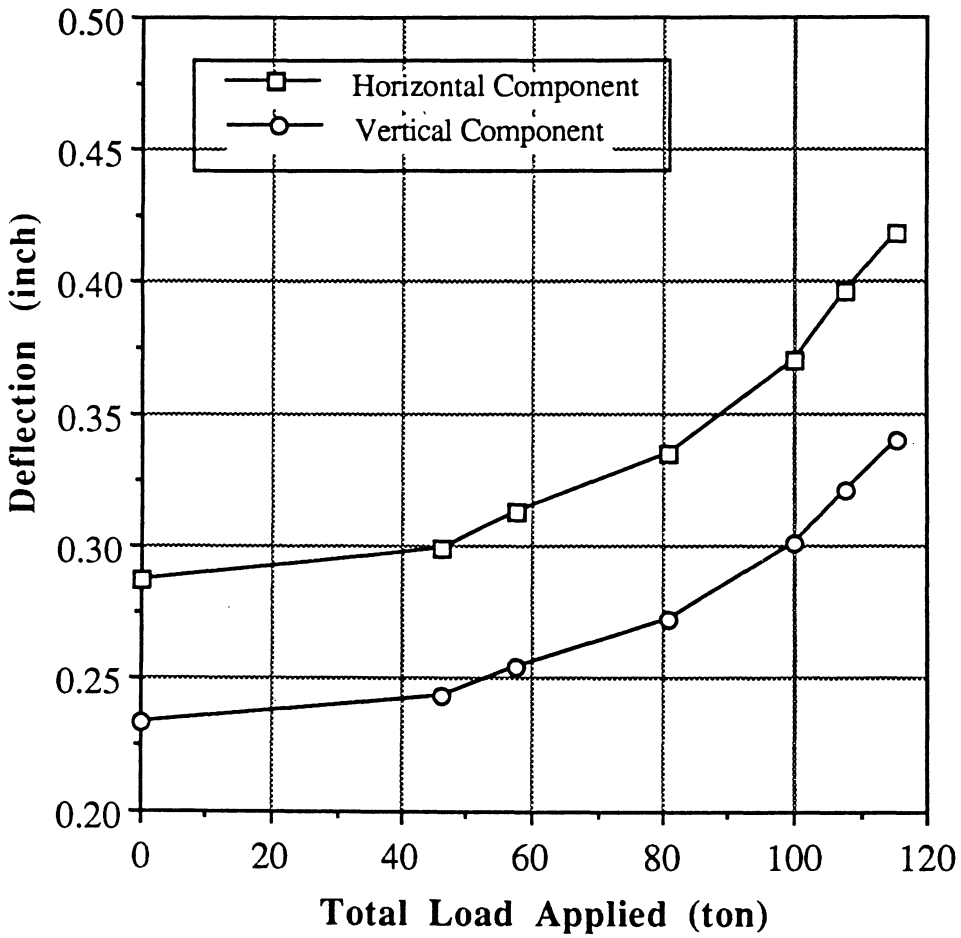

FIGURE 3.24 DEFLECTION OF MONITORING POINT #3 (SHOULDER) DURING THIRD LOAD SEOUENCE

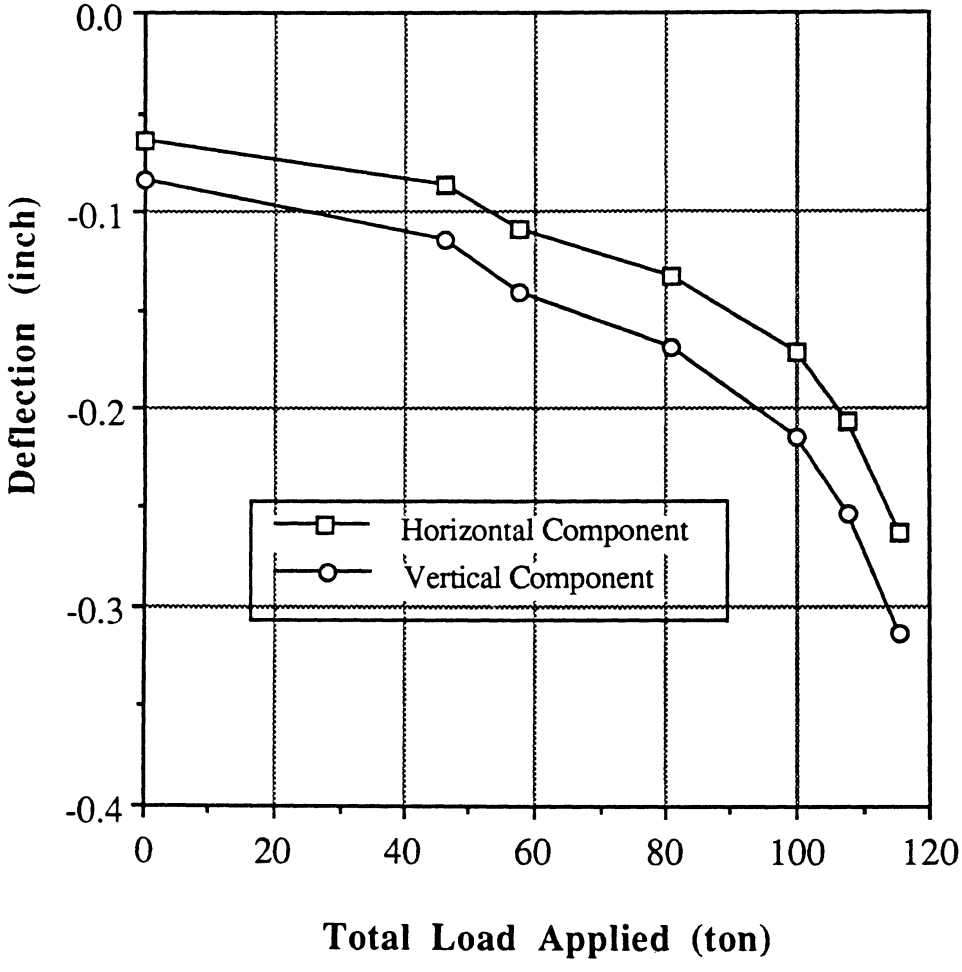

FIGURE 3.25 DEFLECTION OF MONITORING POINT #4 DURING THIRD LOAD SEQUENCE

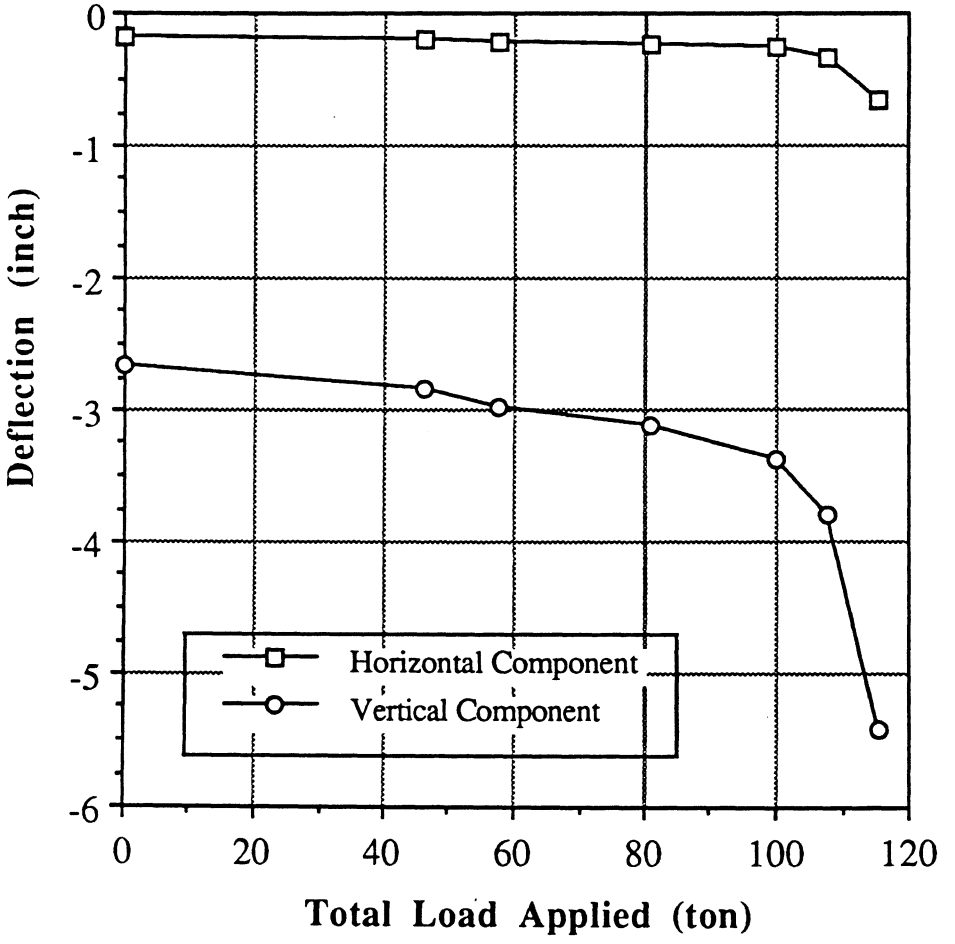

FIGURE 3.26 DEFLECTION OF MONITORING POINT #5 (CROWN) DURING THIRD LOAD SEQUENCE

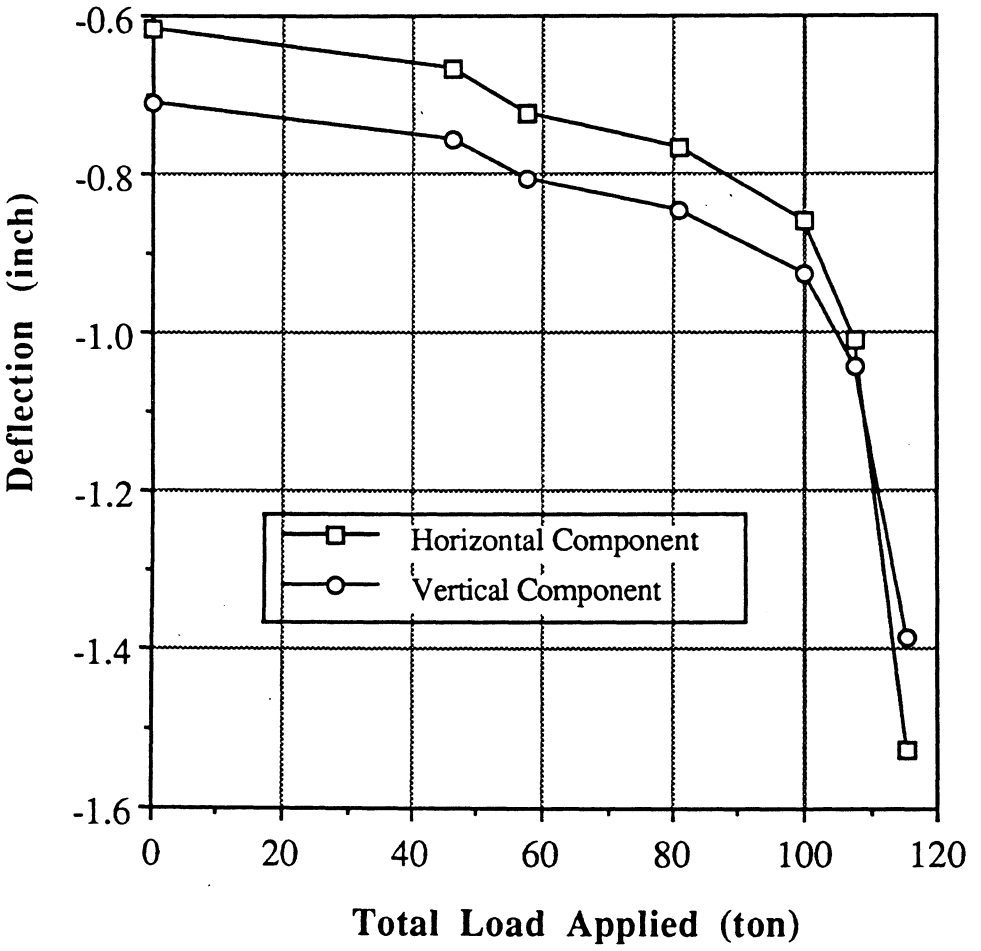

FIGURE 3.27 DEFLECTION OF MONITORING POINT #6 DURING THIRD LOAD SEQUENCE

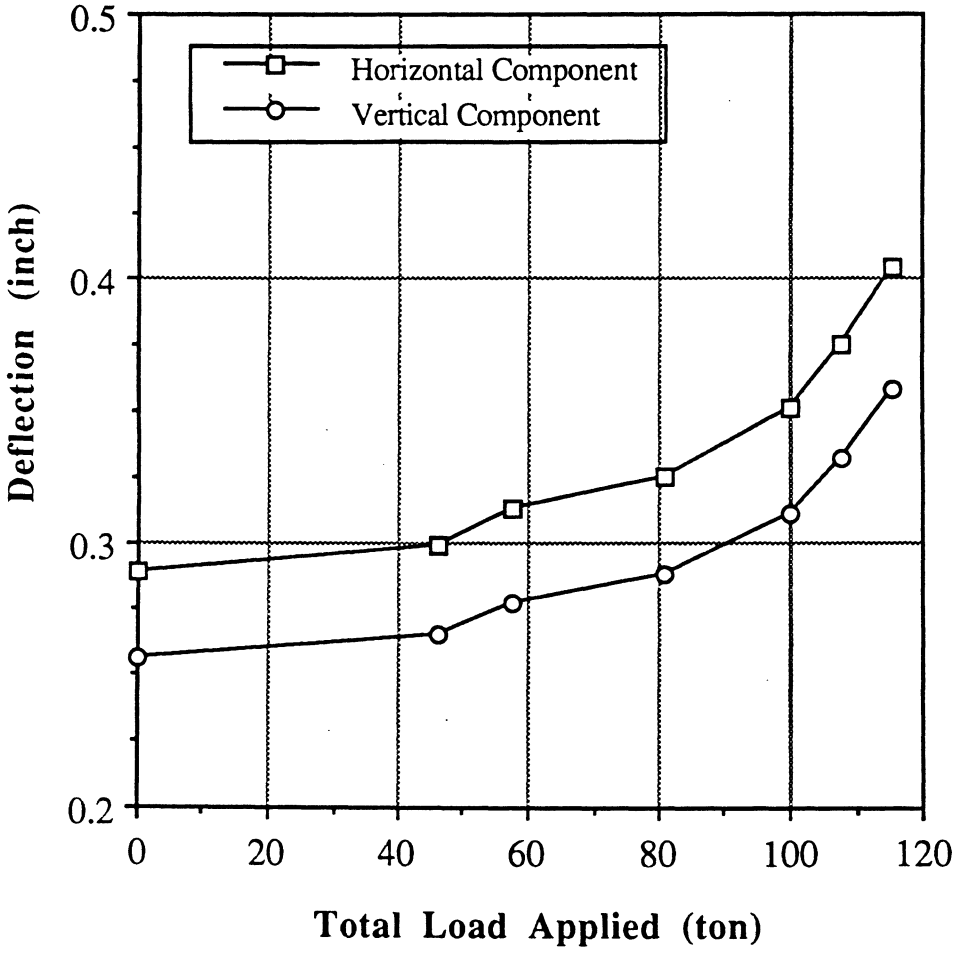

FIGURE 3.28 DEFLECTION OF MONITORING POINT #7 (SHOULDER) DURING THIRD LOAD SEQUENCE

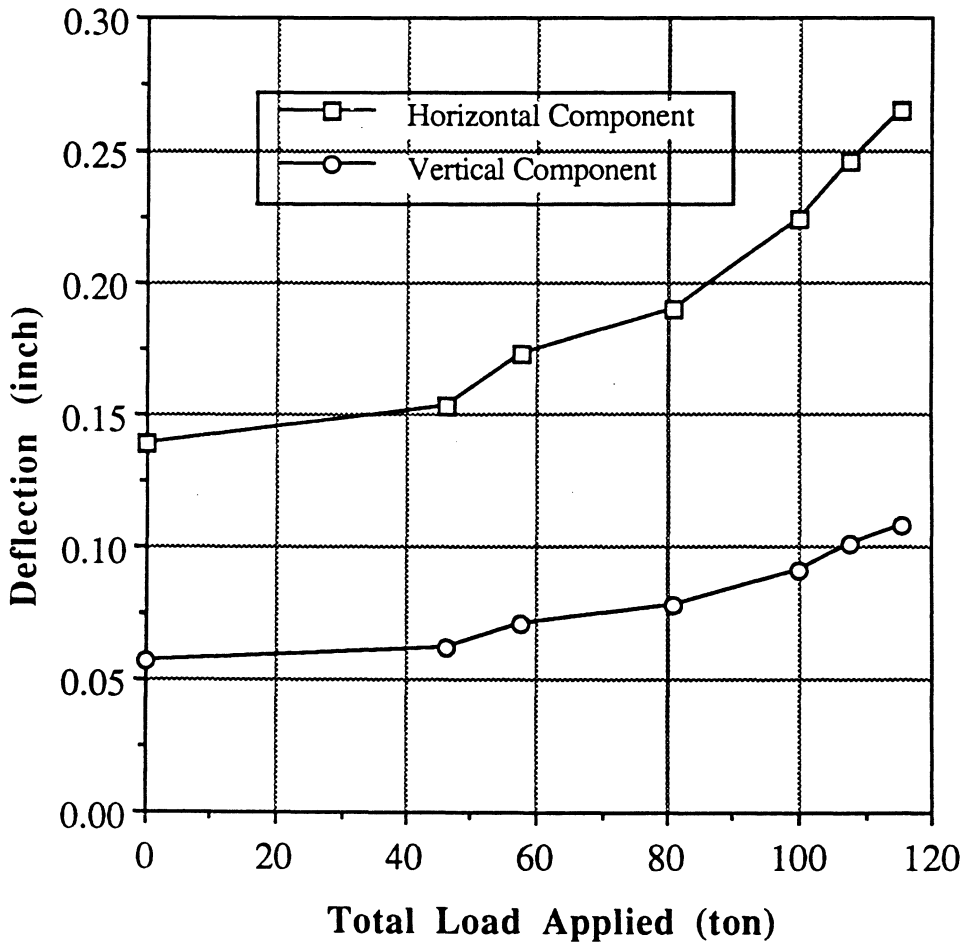

FIGURE 3.29 DEFLECTION OF MONITORING POINT#8 DURING THIRD LOAD SEQUENCE

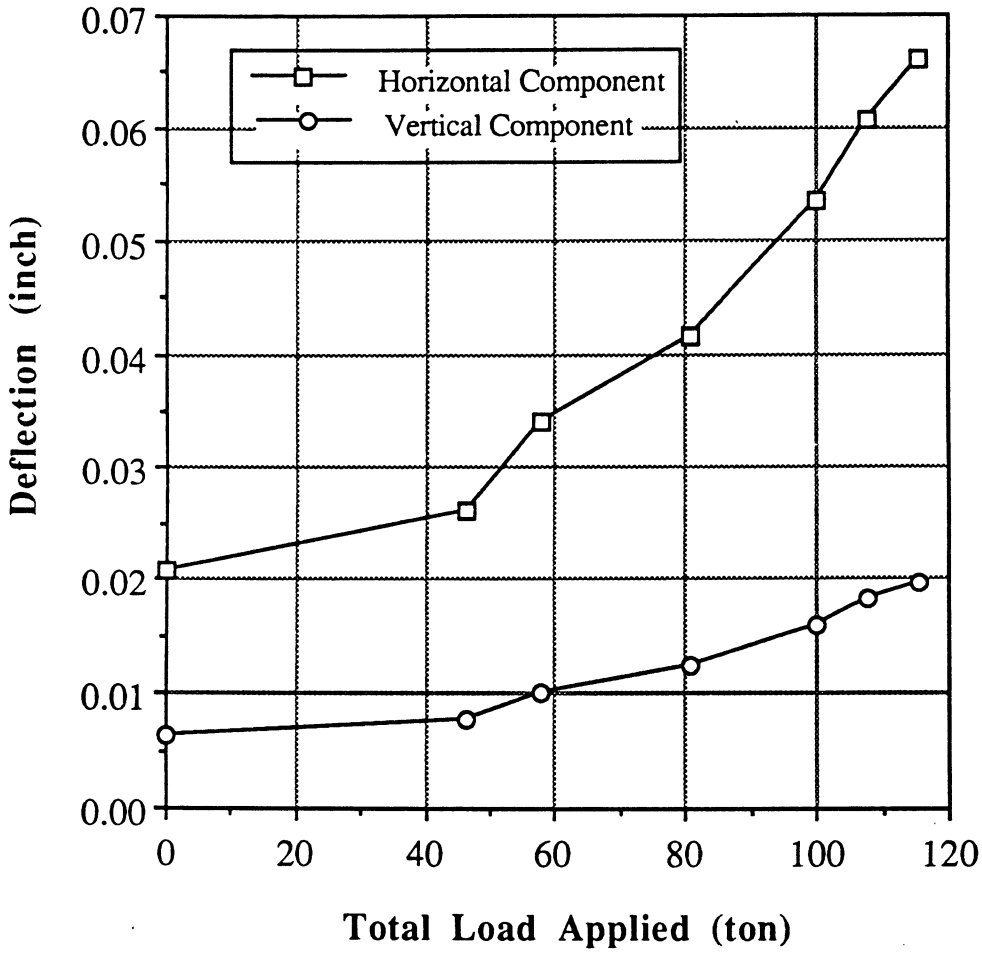

FIGURE 3.30 DEFLECTION OF MONITORING POINT #9 (SPRINGLINE) DURING THIRD LOAD SEQUENCE

test, with the total maximum vertical movement being 0.0376 inches. The first two loading steps of the second loading cycle resulted in an inward movement. Afterwards, that it always moved outward.

Section two constantly moved outward. The magnitute of the movement was similar during the second and third cycles. The maximum vertical movement at this section was 0.084 inches.

Section three which was located at the west shoulder also constantly moved outward. There was a slight variation in movement between the second and the third loading. Careful consideration of the data revealed a permanent deformation of 0.05 inches during the second cycle at this section.

Section four, located close to the crown, continuously moved inward. There was a considerable difference in total vertical deflection during the second and third cycles under the same load of 115 tons. The reason for this is that the stress level in this region exceeded the yield limit of the corrugated steel material during the second cycle of loading. Maximum vertical deflections at this section for the second and third loading cycle were 0.2282 inches and 0.5977 inches respectively.

Section five, located at the crown, experienced the maximum vertical deflection. This is understandable since the load application point was over this section. The maximum vertical deflections at the crown for the second and third cycles of loading were 3.435 and 6.989 inches respectively.

In section six, during the first step of second cycle loading, the hook moved upward, and afterwards it always moved downwards. The maximum deflections were 0.9487 inches and 1.8047 inches for the second and third cycles respectively. A maximum horizontal deflection of 2.4752 inches occured at this section during the third loading cycle.

The magnitude of the deflection did not coincide with that of section four.

Sections 7, 8, and 9 behaved in a similar manner to sections 3, 2, and 1, respectively. The maximum vertical deflection was 0.3625 inches at section 7, 0.1082 inches at section eight and 0.197 inches at section nine. All the maximum deflections occured during the third sequence of loading.

The positive x axis for #1 through #5 was towards west and for points #6 through #9 towards east. The positive y axis was always upwards. Deflection of all nine points started from the non-zero value for the third sequence of loading. Total maximum vertical deflection of 6.989 inches was recorded at the crown point. when the total load reached approximately 100 tons, rapid increase in the rate of deflection was monitored. The points at the crown moved downwards and the points at the haunch and springline moved outwards.

CHAPTER 4

MEASUREMENT OF PLATE FORCES

4.1 INTRODUCTION

This chapter presents the bending moment and axial thrust obtained from the field testing. In order to determine the axial force and bending moment due to monotonically applied live load, biaxial gages were installed at nine sections along the periphery of the culvert plate as described in Chapter 2. The bonded-foil electrical resistance strain gages were read using a computerized data acquisition system. Biaxial plane stress assumptions were used to compute circumferential stresses in the culvert plate. The data from the strain gages were reduced to moment and thrust as described in this chapter. The strain gages and the data acquisition system have been described in detail by Alan Rauch.(1990)

4.2 REDUCTION OF STRAINS TO AXIAL THRUST AND BENDING MOMENTS

The data acquisition system reads the two voltages, V_{in} and V_{out}, and returns the ratio, V_{out} / V_{in} . The computer program,"RATIO"stores this data in the diskettes for future analysis. Computer program "NEW" is used to calculate the strains from the stored ratios. Strains were computed using first set of readings, the readings taken before the load was applied, as an initial value.

As discussed earlier we had at least two biaxial gages at each section, one at the peak and the other at the crust. Assuming plane strain theory, we can calculate the circumferential stresses as follows:

$$\sigma_c = \frac{E}{(1 - \upsilon^2)}\{\varepsilon_c + \upsilon\varepsilon_l\} \qquad \text{Eqn. 4.1}$$

E = Young's modulus $30x10^6$ psi

ϑ = Poisson's ratio 0.3

ε_c= circumferential strain

ε_l= longitudinal strain

Stresses were assumed to be due to bending moment and axial forces. Superposition of these results gives the expression shown in Eqn. 4.2

$$\sigma_C = \frac{P}{A} \pm \frac{MC}{I} \qquad \text{Eqn. 4.2}$$

P = axial thrust

A = area of cross section

M = bending moment

I = moment of inertia

C = distance from the neutral axis

At each monitoring location, two circumferential stress values were obtained, one from the biaxial strain gage installed at the peak and the other is from the gage placed in the valley of the corrugation. From Eqn. 4.2, moment and thrust can be obtained by simple calculation. The equations obtained for moment and thrust are given in Eqns. 4.3 and 4.4 respectively.

$$M = \frac{(\sigma_1 - \sigma_2) I}{(C_1 + C_2)}$$ Eqn.4.3

C_1 = distance from neutral axis to interested point in tension zone (1.094 inches)

C_2 = distance from neutral axis to interested point in compression zone (0.906 inches)

$$P = \frac{(\sigma_1 C_2 + \sigma_2 C_1) A}{(C_2 + C_1)}$$ Eqn. 4.4

Figure. 4.1 presents the calculation details of C_1 and C_2. Calculated thrust and moment are presented in Tables 4.1 and 4.2. Figures. 4.2 through 4.7 presents moment and thrust graphically for the first sequence of loading. Figures 4.8 through 4.17 presents moment and thrust for the second sequence of loading and the Figures 4.18 through 4.23 presents the moment and thrust for the third sequence of loading. Figures 4.24 through 4.33 presents how the culvert responded at selected sections for the applied live load for the last two cycles of loading.. A consistent sign convention is employed throughout this study. Positive bending moments imply a concave-up bending in the crown region and for thrusts tensile forces are positive.

4.3 ANALYSIS OF RESULTS

Initial stages of the loading resulted in the negative moment at sections #1and #9 at the spring line indicating the outward movement of the culvert at those locations. During the second cycle of loading after load step 6 moment at these locations were changed to

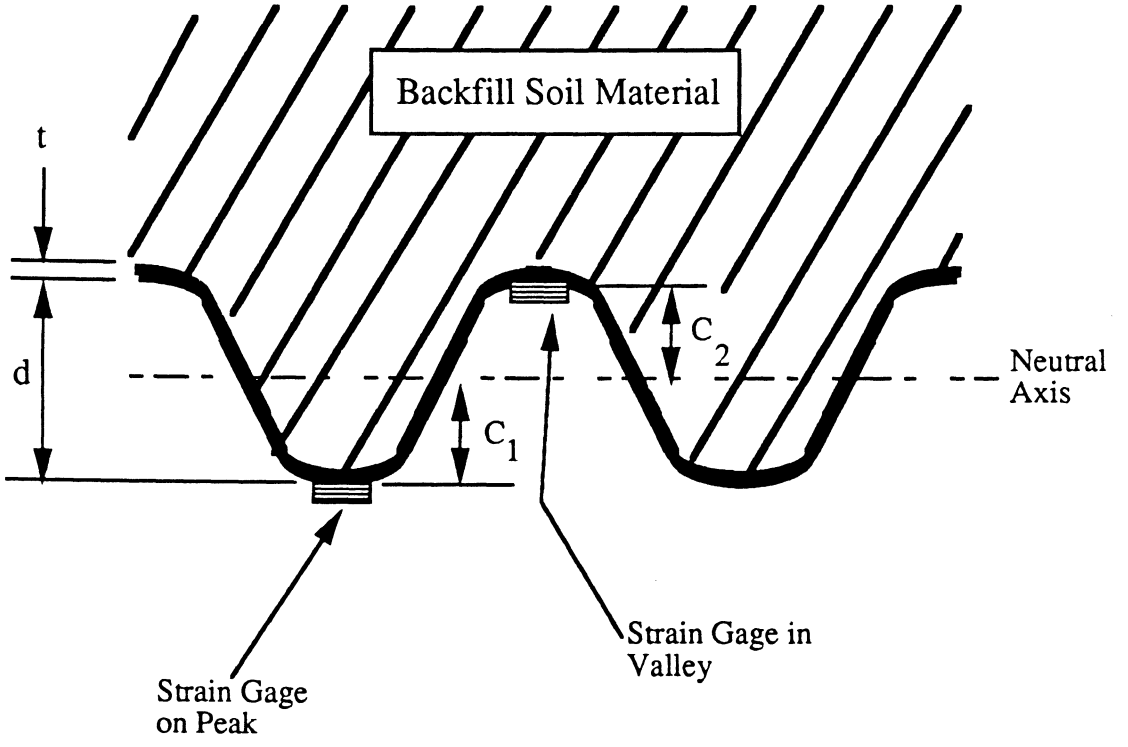

FIGURE 4.1 DEFINITION OF DISTANCES C1 AND C2 TAKEN FROM NEUTRAL AXIS

TABLE 4.1 COMPUTED AXIAL THRUST

Load Cycle No.	Load Step No.	Total Load (ton)	Thrust (kips/ft) @ Monitoring Point:								
			#1	#2	#3	#4	#5	#6	#7	#8	#9
2	0	0.000	0.000	0.000	0.000	0.000	0.000	0.000	0.000	0.000	0.000
	1	30.80	-0.366	-0.667	-1.329	-1.360	0.468	-1.129	-1.558	-0.900	-0.141
	2	38.48	-0.459	0.818	-1.848	-1.913	-0.826	-1.660	-2.312	-1.374	1.171
	3	50.03	-0.674	-1.603	-2.864	-3.076	-1.324	-2.597	-3.245	-2.221	0.876
	4	65.43	-0.899	-2.307	-3.856	-4.286	-2.292	-3.885	-5.430	-3.421	0.427
	5	78.89	-1.097	-2.954	-4.972	-5.675	-2.947	-4.814	-6.256	-4.345	0.271
	6	88.51	-1.235	-3.632	-6.305	-7.849	-5.157	-6.508	-8.151	-5.596	-0.017
	7	101.6	-1.337	-4.622	-7.863	-11.11	-5.226	-9.103	-10.16	-4.622	-0.245
	8	103.9	-1.329	-5.967	-8.645	-10.82	-3.714	-9.984	-9.380	-5.967	-0.292
	9	111.6	-1.394	-6.900	-9.215	NC	-1.706	-8.814	-8.121	-6.900	0.197
	10	102.0	-1.330	-7.230	-9.357	NC	-0.600	-7.150	-6.973	-7.230	0.059
	11	111.6	-	-	-	-	-	-	-	-	-
	12	113.9	-0.991	-9.977	-10.55	NC	11.29	3.844	-6.818	-9.977	0.168
3	0	0.00	0.000	0.000	0.000	0.000	0.000	0.000	0.000	0.000	0.000
	1	50.03	-0.630	-1.687	-2.574	-2.540	0.746	-1.318	-3.300	-6.743	-0.424
	2	57.73	-1.216	-3.404	-4.956	-4.634	1.885	-1.948	-6.690	-8.288	-0.829
	3	80.81	-1.573	-4.476	-6.657	-5.909	2.998	-2.141	-9.129	-10.04	-0.979
	4	100.1	-2.147	-6.102	-9.151	-6.214	5.108	-0.982	-11.46	-12.20	-1.347
	5	107.8	-2.359	-6.483	-9.861	-2.104	7.552	0.674	-11.70	-12.86	-1.580
	6	115.5	-2.293	-5.951	-10.66	12.57	14.15	7.881	-10.44	-13.40	-1.567

(Note) "NC"= Not Computed Since the Yield Stress was Reached.

TABLE 4.2 COMPUTED BENDING MOMENT

Load Cycle No.	Load Step No.	Total Load (ton)	Moment (kips-ft/ft) @ Monitoring Point:								
			#1	#2	#3	#4	#5	#6	#7	#8	#9
2	0	0.000	0.000	0.000	0.000	0.000	0.000	0.000	0.000	0.000	0.000
	1	30.80	-0.015	-0.004	-0.048	-0.081	0.195	-0.036	-0.051	-0.014	-0.022
	2	38.48	-0.022	-0.069	-0.079	-0.124	0.291	-0.050	-0.081	-0.015	-0.080
	3	50.03	-0.028	0.014	-0.142	-0.225	0.519	-0.081	-0.150	-0.013	-0.079
	4	65.43	-0.030	0.032	-0.255	-0.361	0.842	-0.092	-0.286	-0.010	-0.071
	5	78.89	-0.025	0.052	-0.390	-0.489	1.200	-0.073	-0.451	-0.009	-0.059
	6	88.51	-0.012	0.082	-0.582	-0.740	1.494	-0.198	-0.700	0.003	-0.029
	7	101.6	0.017	0.160	-0.808	-1.375	1.416	-0.871	-1.101	0.160	0.031
	8	103.9	0.063	0.249	-1.055	-2.113	1.302	-1.469	-1.417	0.249	0.090
	9	111.6	0.096	0.309	-1.238	NC	1.189	-1.782	-1.565	0.309	0.130
	10	102.0	0.126	0.346	-1.353	NC	1.094	-1.879	-1.633	0.346	0.159
	11	111.6	-	-	-	-	-	-	-	-	-
	12	113.9	0.313	0.636	-2.157	NC	-0.226	-2.154	-1.559	0.636	0.344
3	0	0.00	0.000	0.000	0.000	0.000	0.000	0.000	0.000	0.000	0.000
	1	50.03	-0.012	0.018	-0.147	-0.400	0.719	-0.114	-0.252	-0.202	-0.006
	2	57.73	-0.016	0.032	-0.343	-0.759	1.417	-0.079	-0.603	-0.180	-0.007
	3	80.81	-0.015	0.043	-0.518	-1.021	1.952	-0.032	-0.915	-0.200	0.002
	4	100.1	0.001	0.061	-0.847	-1.501	2.545	0.094	-1.235	-0.204	0.022
	5	107.8	0.013	0.081	-0.979	-1.671	2.313	0.081	-1.261	-0.196	0.032
	6	115.5	0.034	0.125	-1.140	-2.056	1.483	-0.130	-1.204	-0.199	0.057

(Note) "NC"= Not Computed Since the Yield Stress was Reached.

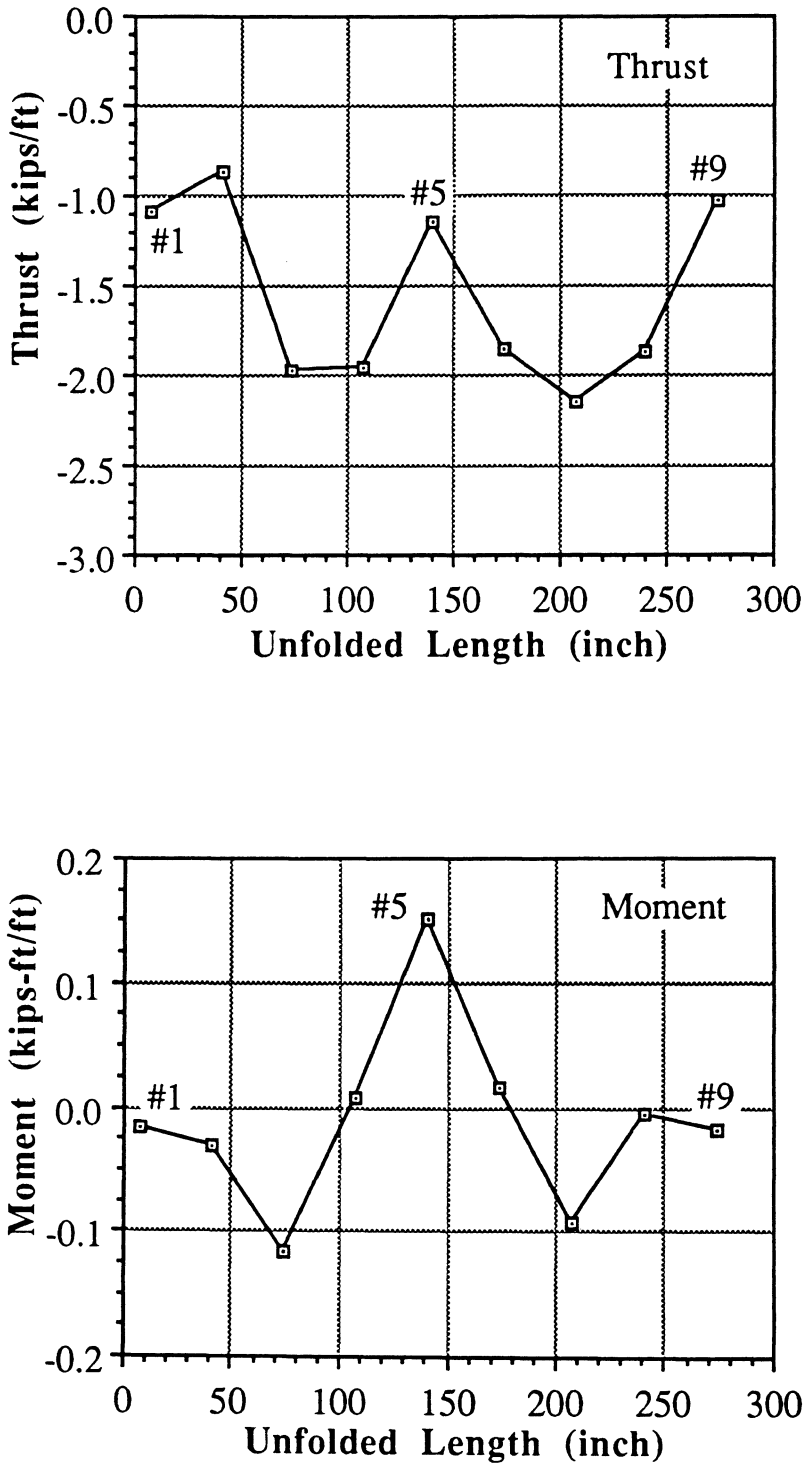

FIGURE 4.2 DISTRIBUTIONS OF THRUST AND MOMENT UNDER LOAD OF 69.27 TONS DURING FIRST LOADING SEQUENCE

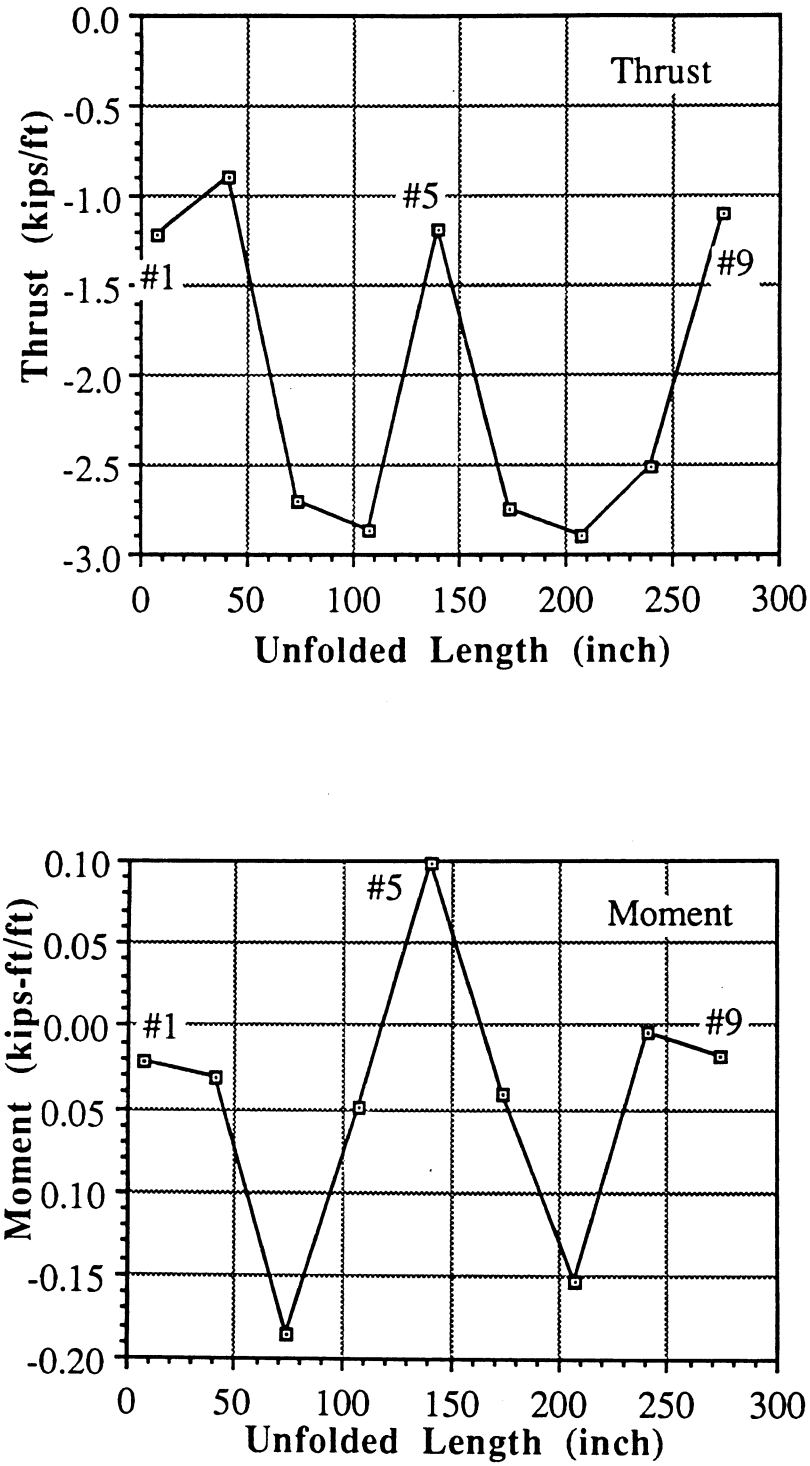

FIGURE 4.3 DISTRIBUTIONS OF THRUST AND MOMENT UNDER LOAD OF 86.59 TONS DURING FIRST LOADING SEQUENCE

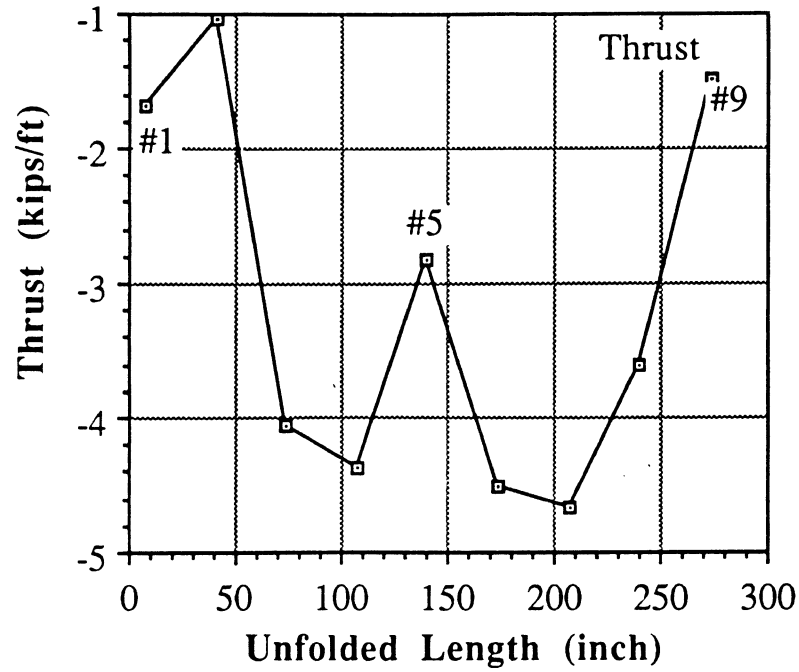

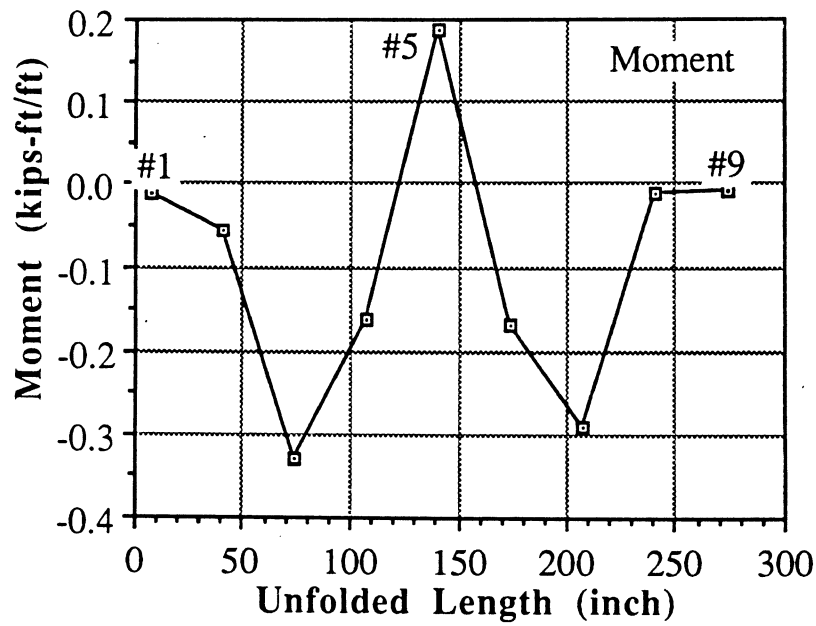

FIGURE 4.4 DISTRIBUTIONS OF THRUST AND MOMENT UNDER LOAD OF 100.06 TONS DURING FIRST LOADING SEQUENCE

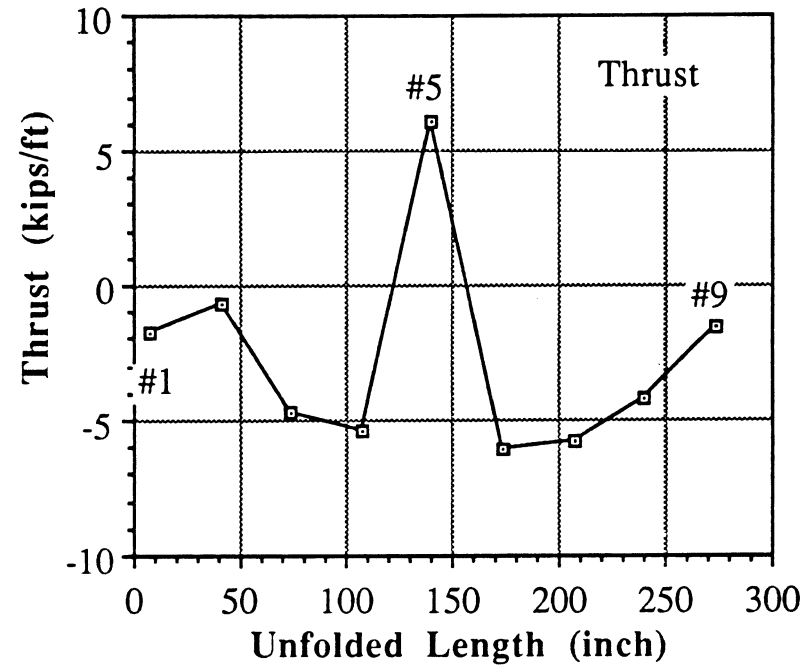

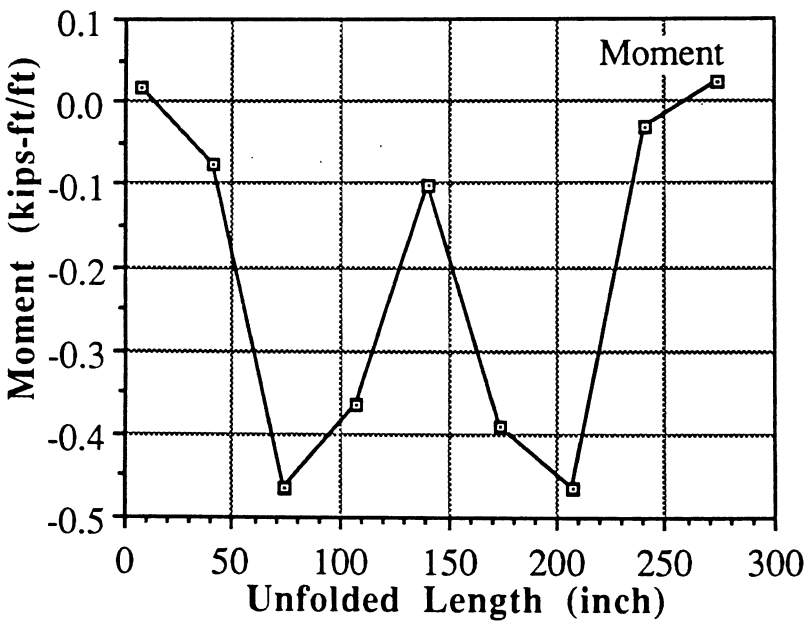

FIGURE 4.5 DISTRIBUTIONS OF THRUST AND MOMENT UNDER LOAD OF 107.76 TONS DURING FIRST LOADING SEQUENCE

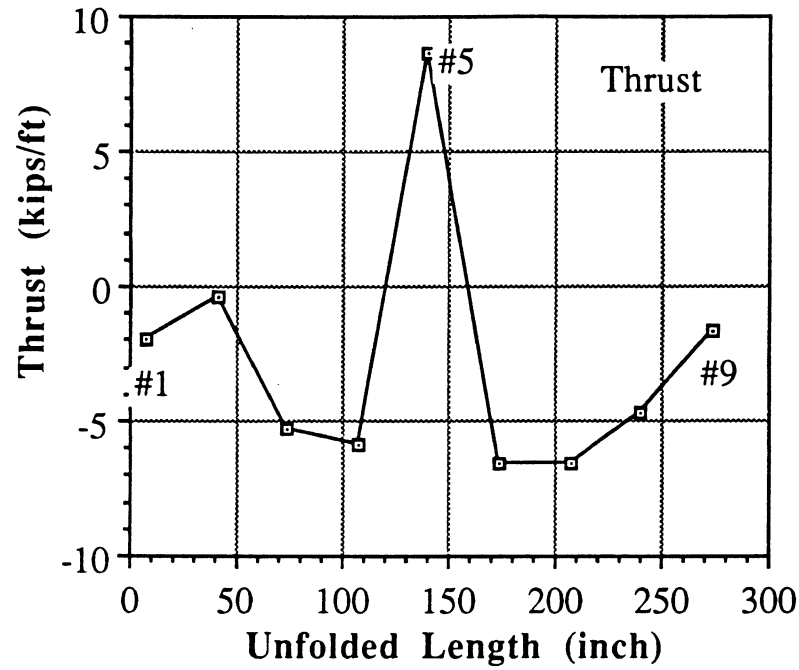

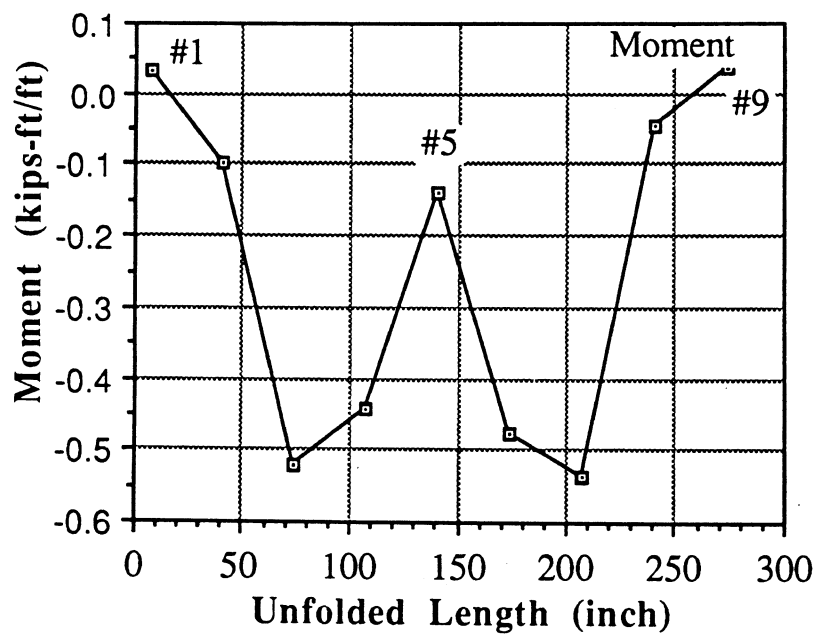

FIGURE 4.6 DISTRIBUTIONS OF THRUST AND MOMENT UNDER LOAD OF 115.45 TONS DURING FIRST LOADING SEQUENCE

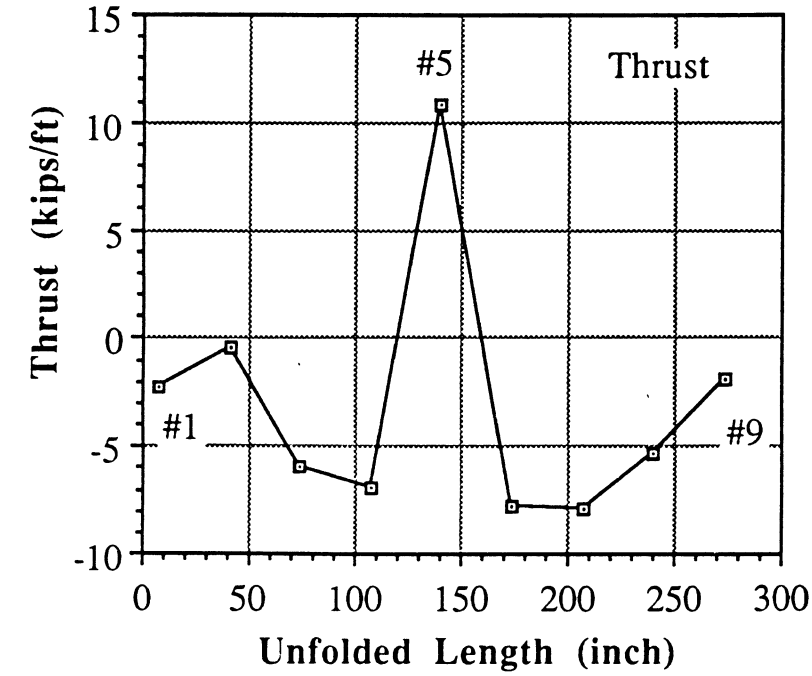

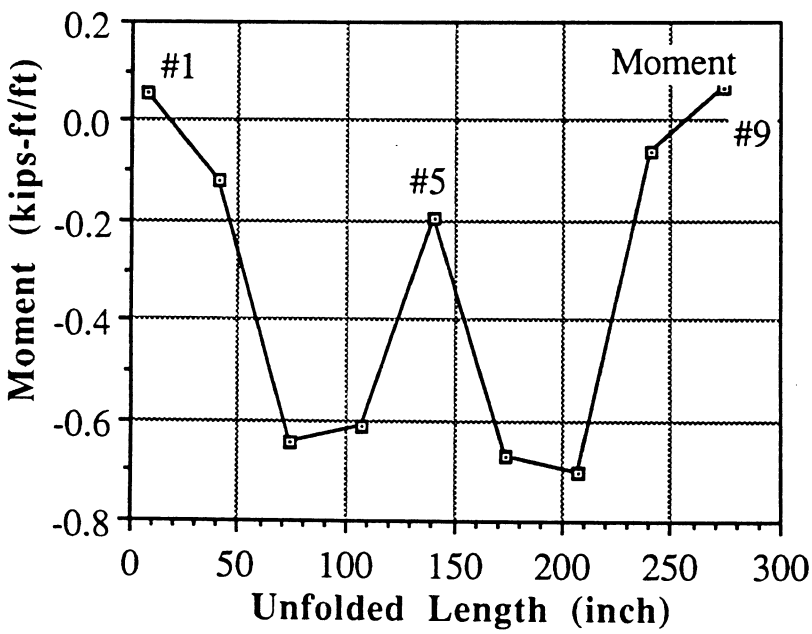

FIGURE 4.7 DISTRIBUTIONS OF THRUST AND MOMENT UNDER LOAD OF 123.15 TONS DURING FIRST LOADING SEQUENCE

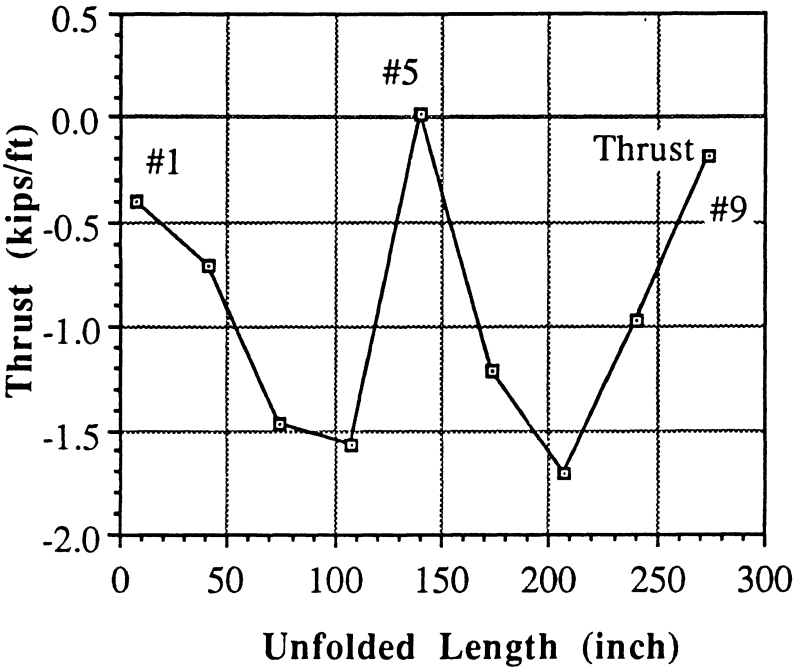

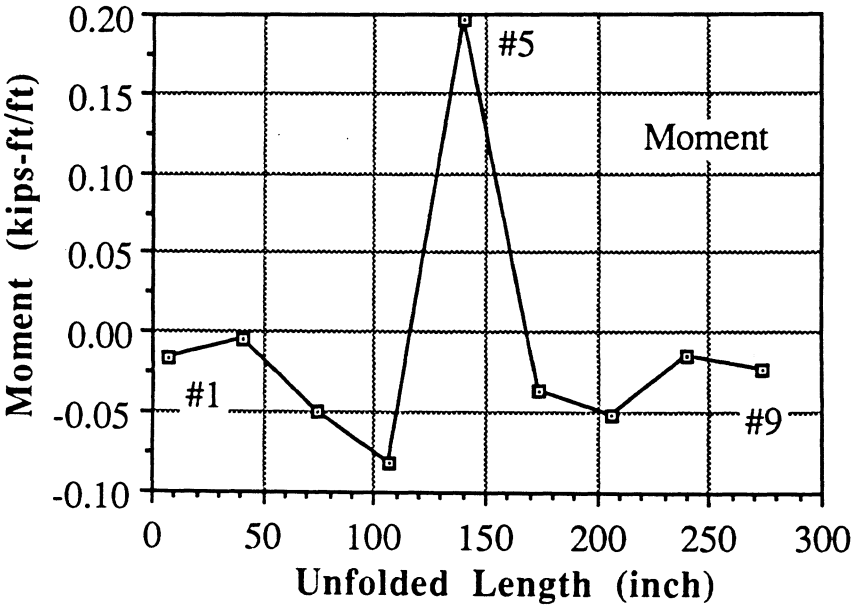

FIGURE 4.8 DISTRIBUTIONS OF THRUST AND MOMENT UNDER LOAD OF 30.79 TONS DURING SECOND LOADING SEQUENCE

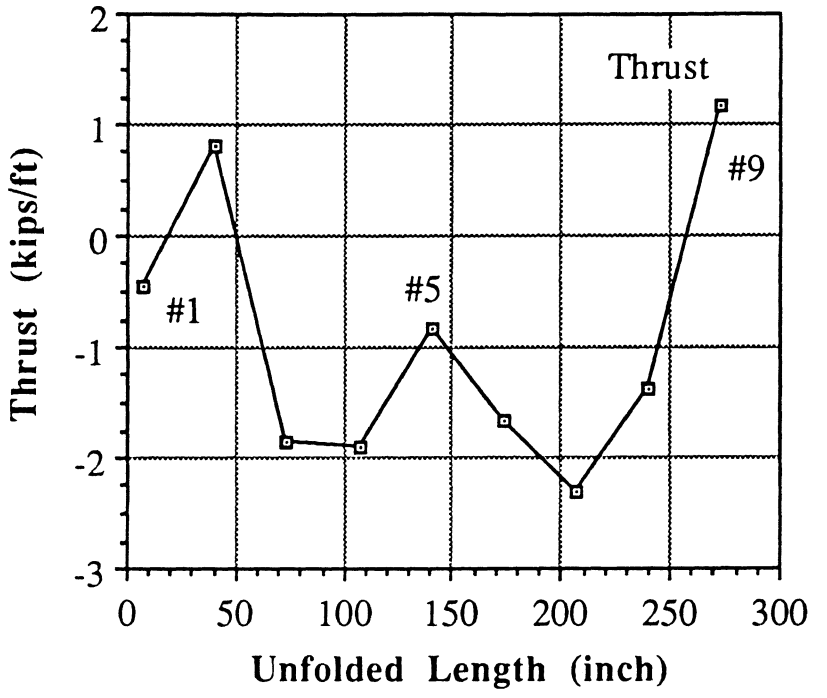

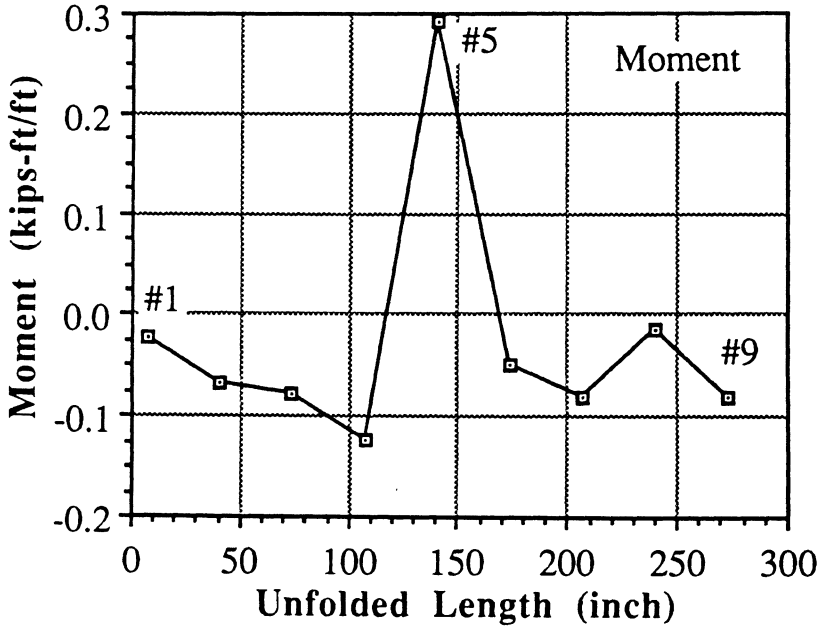

FIGURE 4.9 DISTRIBUTIONS OF THRUST AND MOMENT UNDER LOAD OF 38.48 TONS DURING SECOND LOADING SEQUENCE

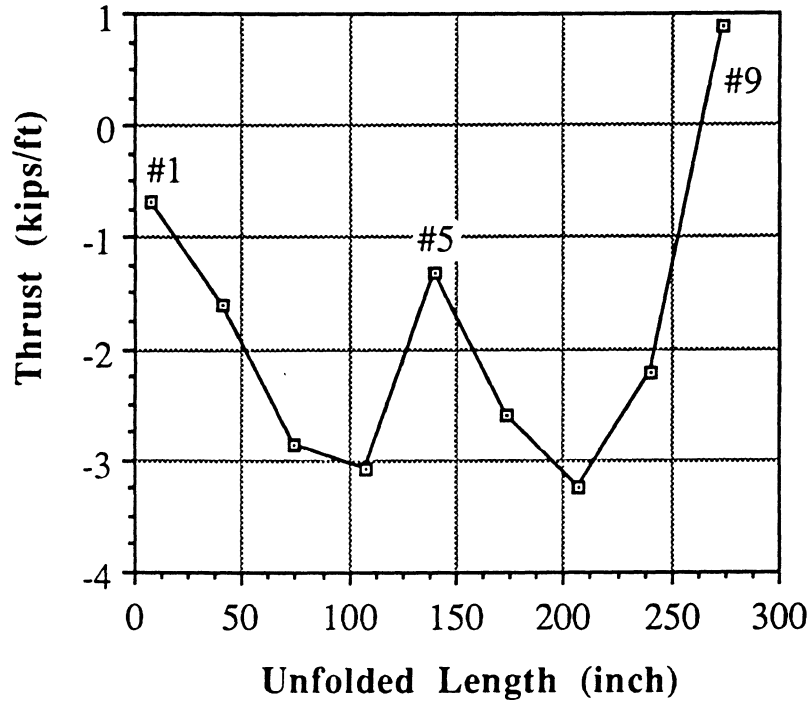

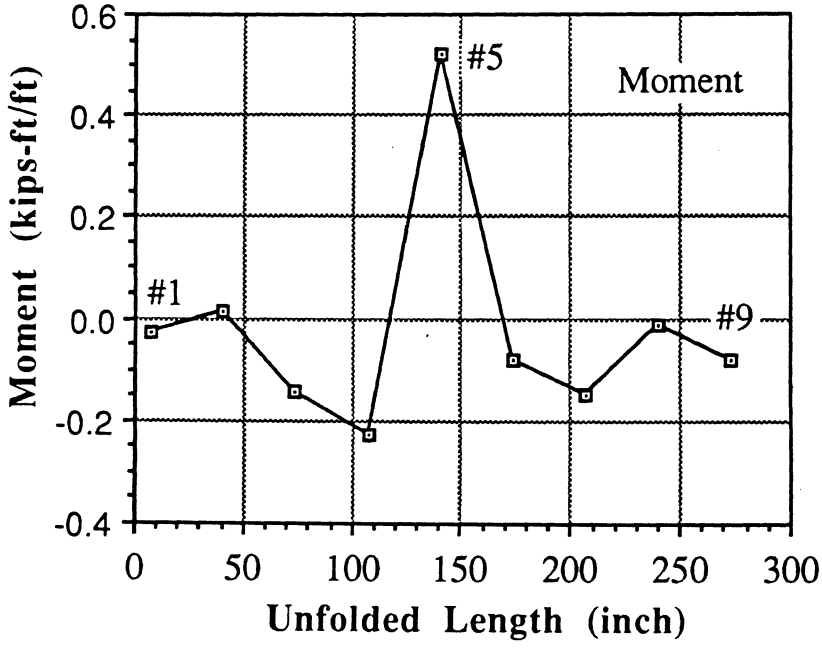

FIGURE 4.10 DISTRIBUTIONS OF THRUST AND MOMENT UNDER LOAD OF 50.03 TONS DURING SECOND LOADING SEQUENCE

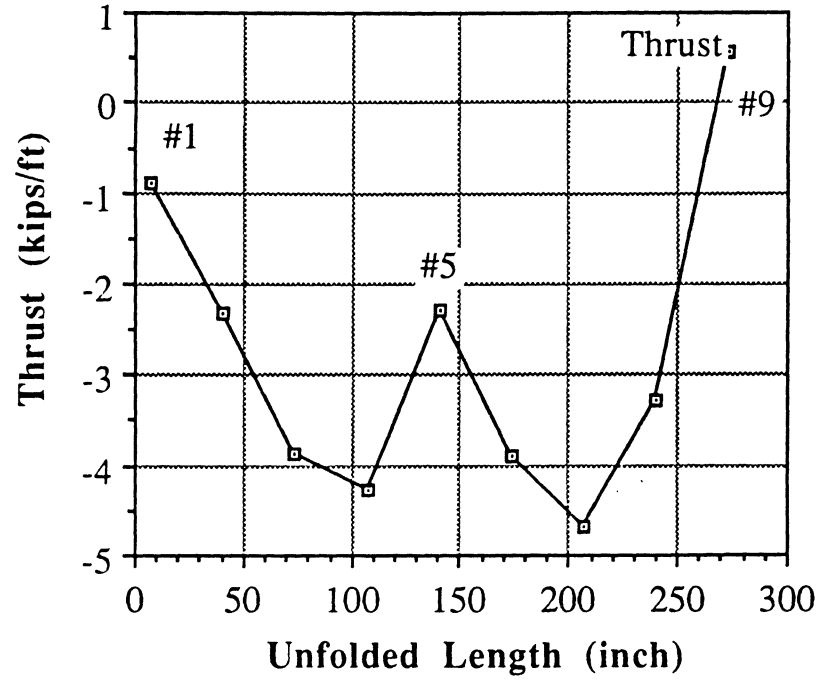

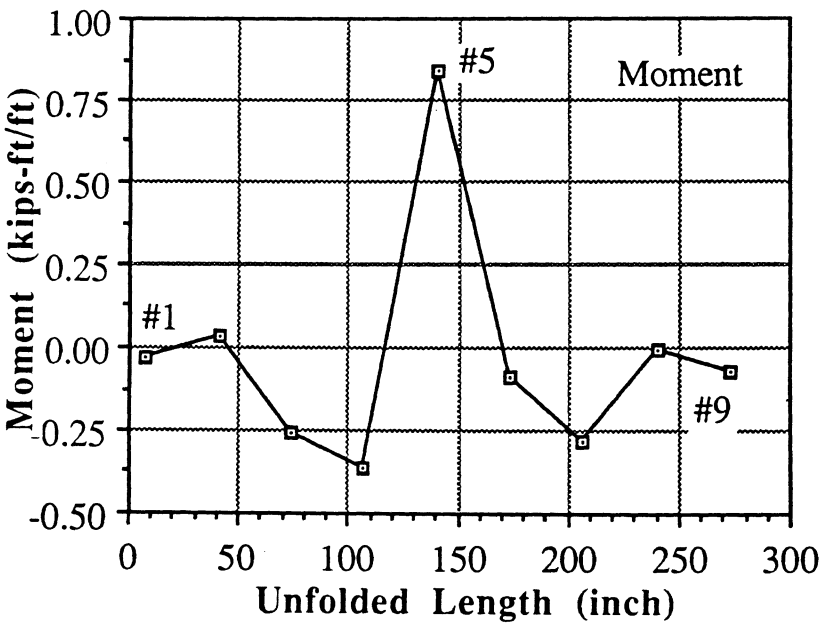

FIGURE 4.11 DISTRIBUTION OF THRUST AND MOMENT UNDER LOAD OF 65.43 TONS DURING SECOND LOADING SEQUENCE

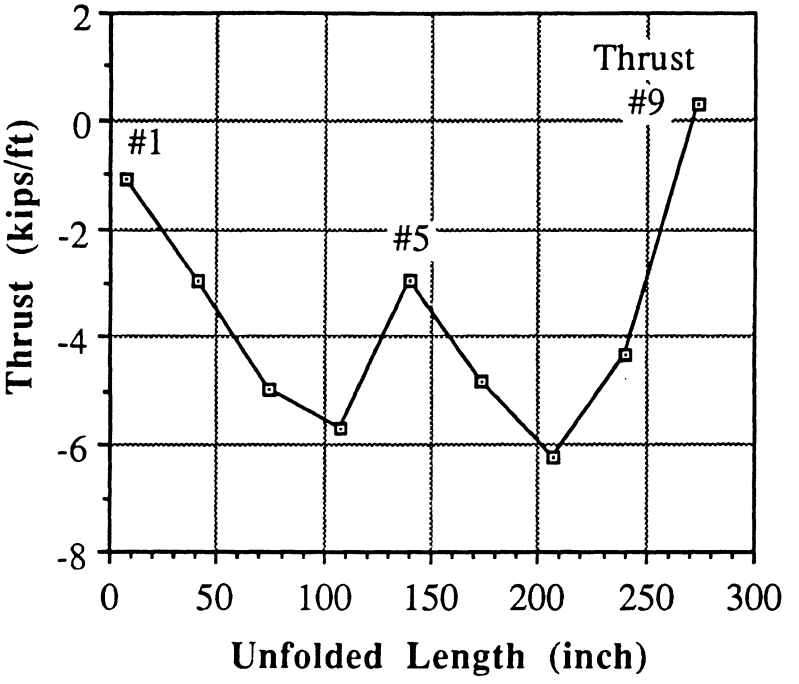

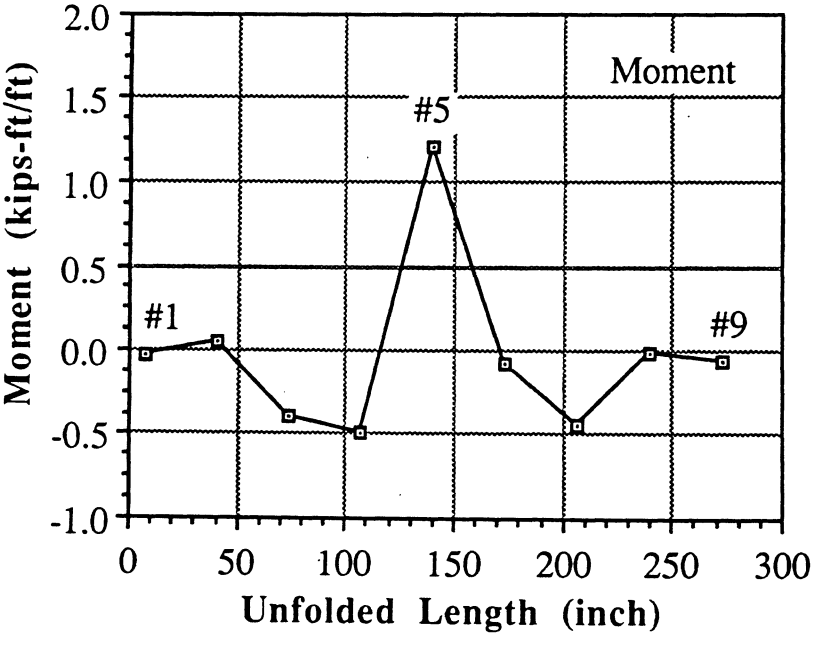

FIGURE 4.12 DISTRIBUTIONS OF THRUST AND MOMENT UNDER LOAD OF 78.89 TONS DURING SECOND LOADING SEQUENCE

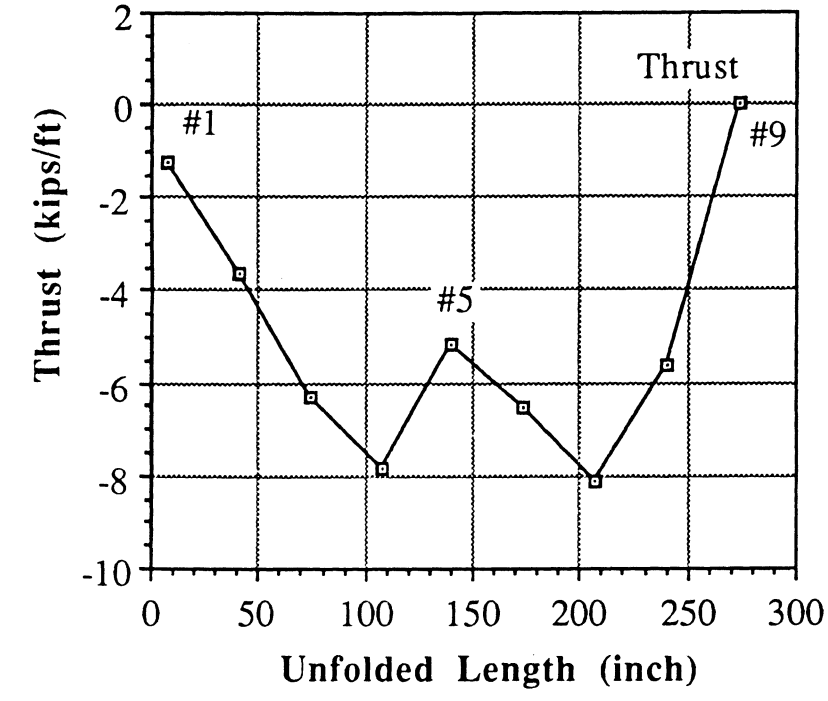

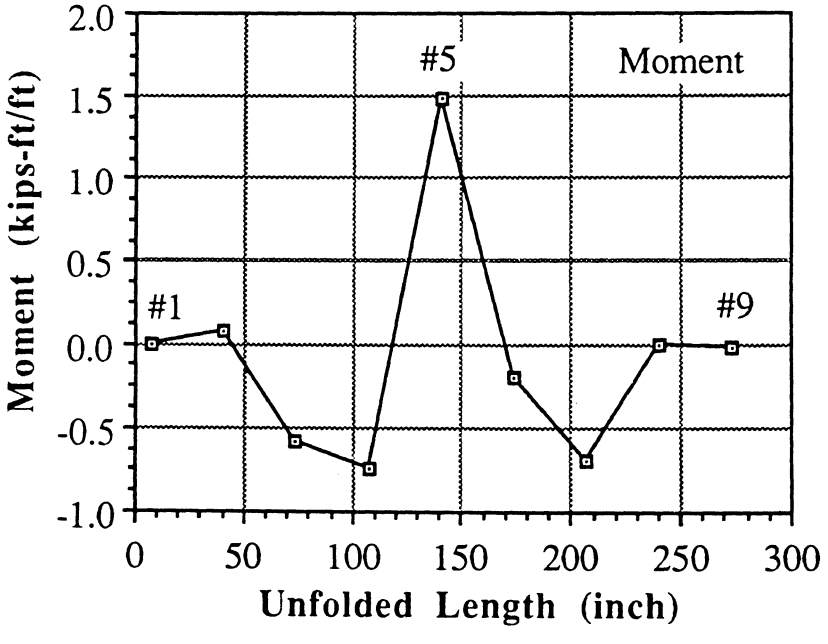

FIGURE 4.13 DISTRIBUTIONS OF THRUST AND MOMENT UNDER LOAD OF 88.51 TONS DURING SECOND LOADING SEQUENCE

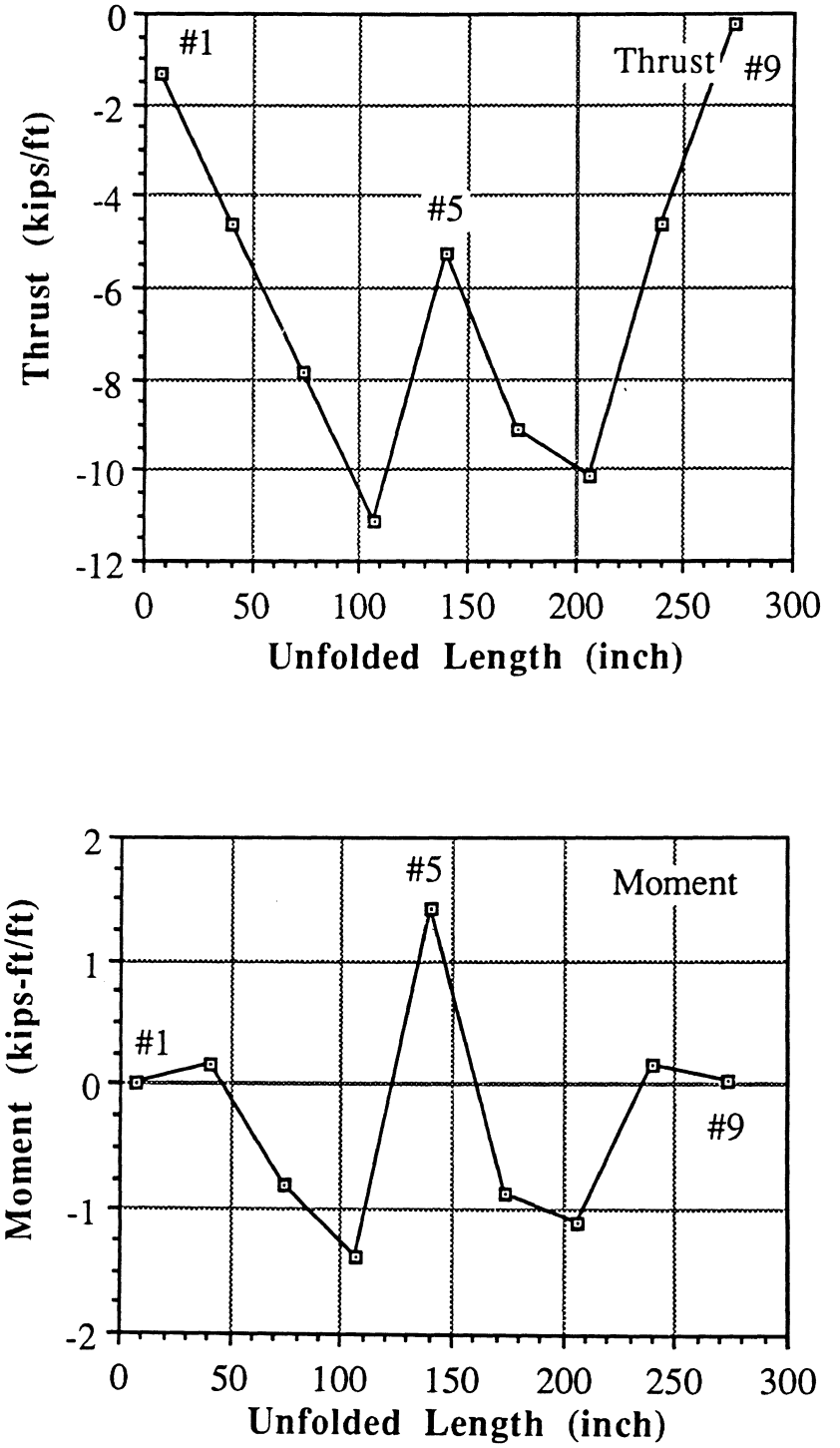

FIGURE 4.14 DISTRIBUTIONS OF THRUST AND MOMENT UNDER LOAD OF 101.6 TONS DURING SECOND LOADING SEQUENCE

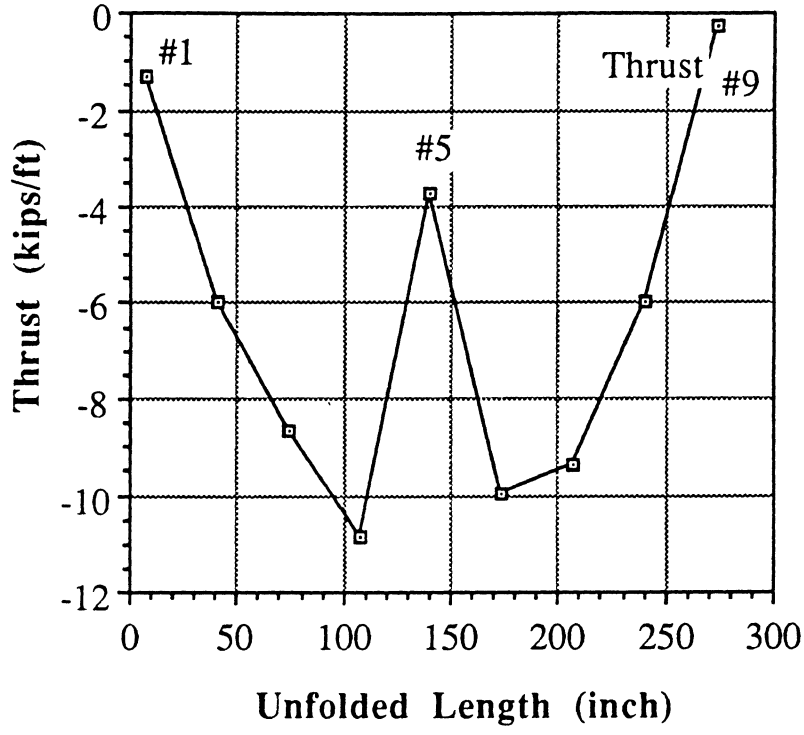

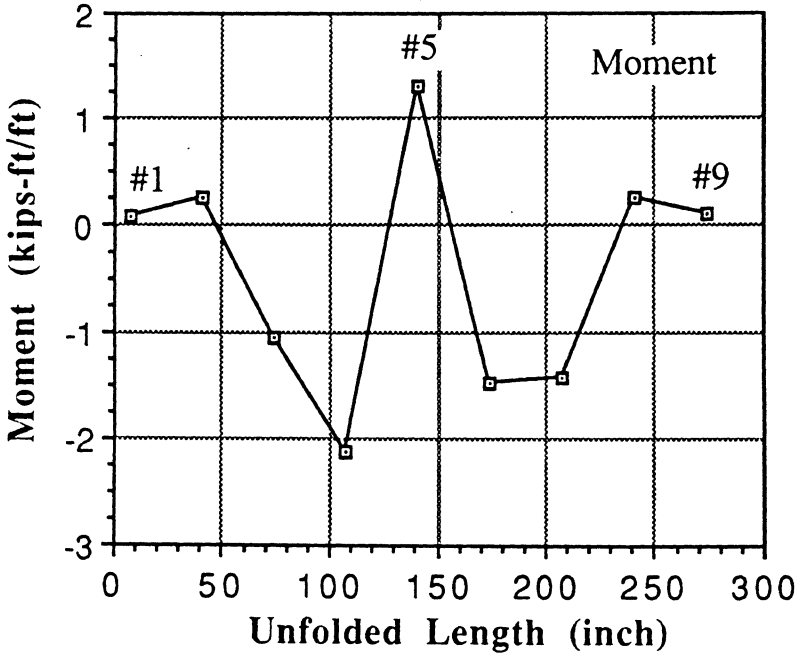

FIGURE 4.15 DISTRIBUTIONS OF THRUST AND MOMENT UNDER LOAD OF 103.91 TONS DURING SECOND LOADING SEQUENCE

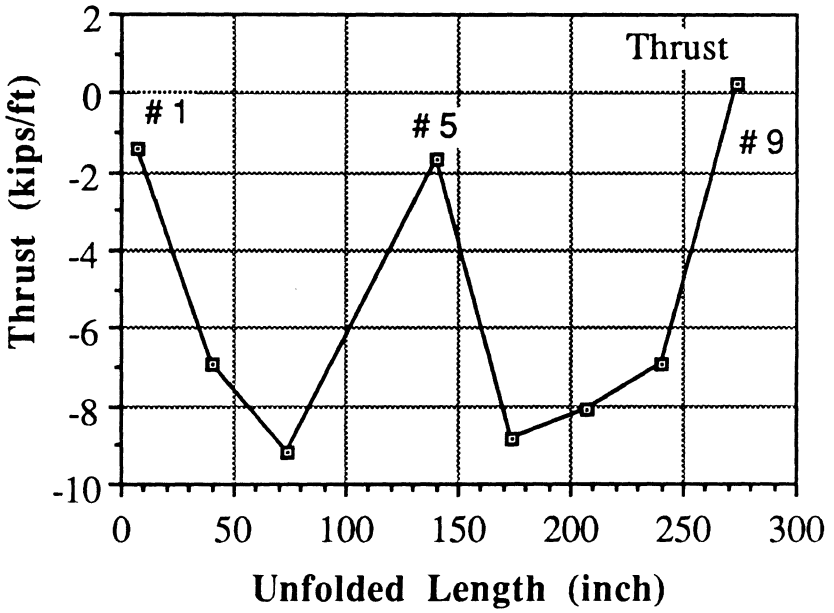

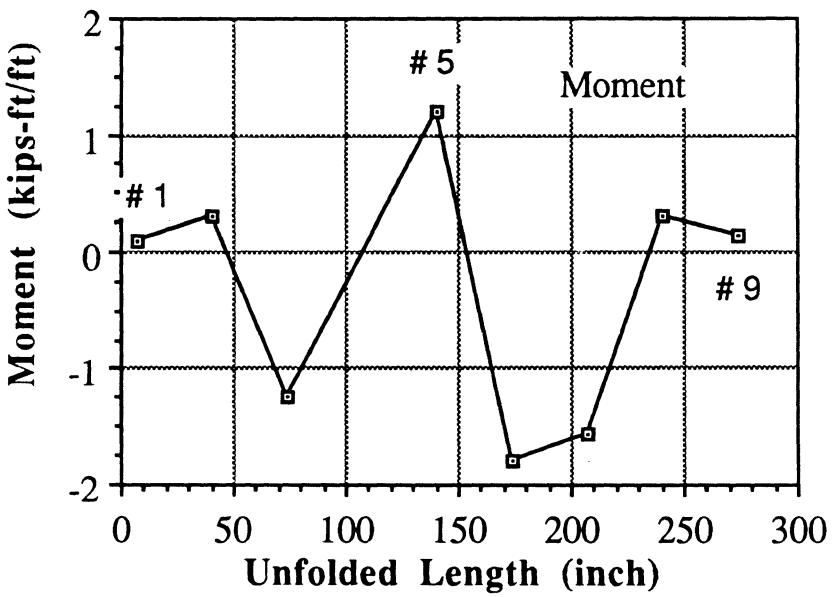

FIGURE 4.16 DISTRIBUTIONS OF THRUST AND MOMENT UNDER LOAD OF 111.6 TONS DURING SECOND LOADING SEQUENCE

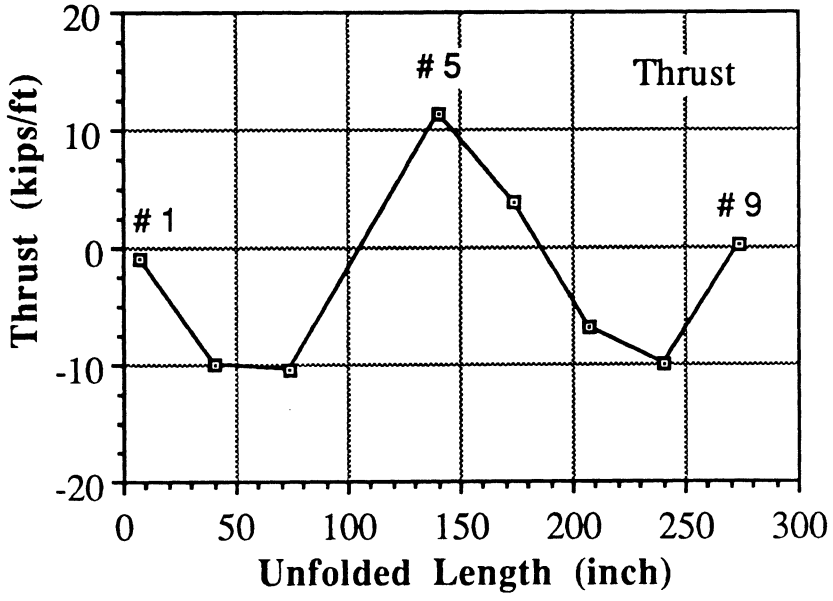

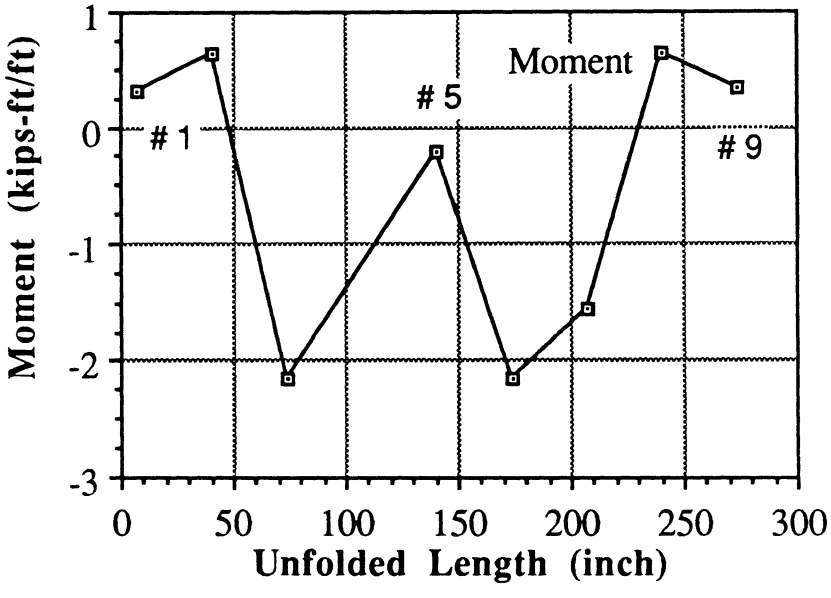

FIGURE 4.17 DISTRIBUTIONS OF THRUST AND MOMENT UNDER LOAD OF 113.9 TONS DURING SECOND LOADING SEQUENCE

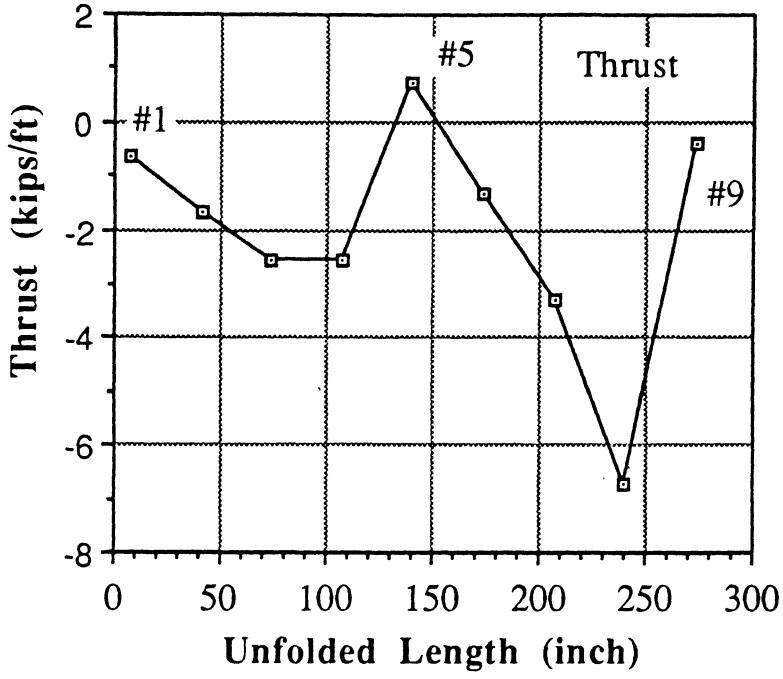

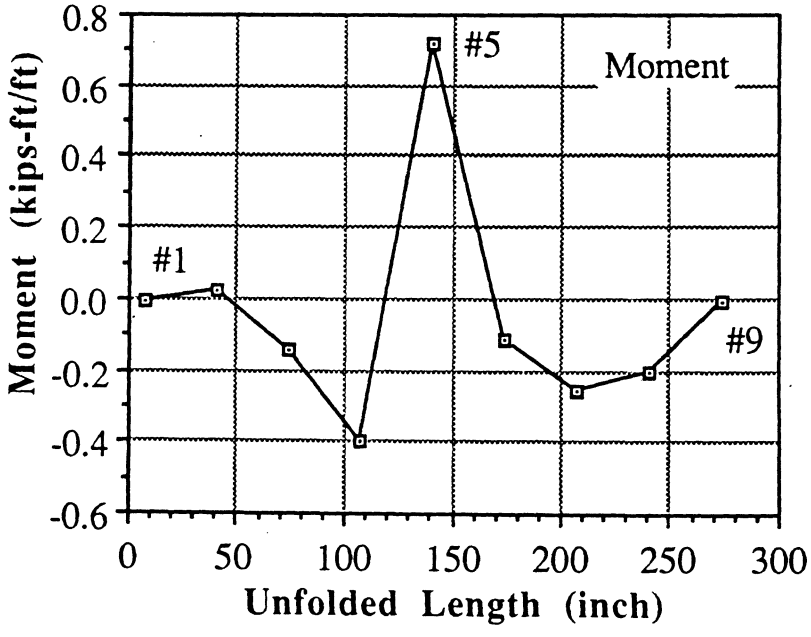

FIGURE 4.18 DISTRIBUTIONS OF THRUST AND MOMENT UNDER LOAD OF 50.03 TONS DURING THIRD LOADING SEQUENCE

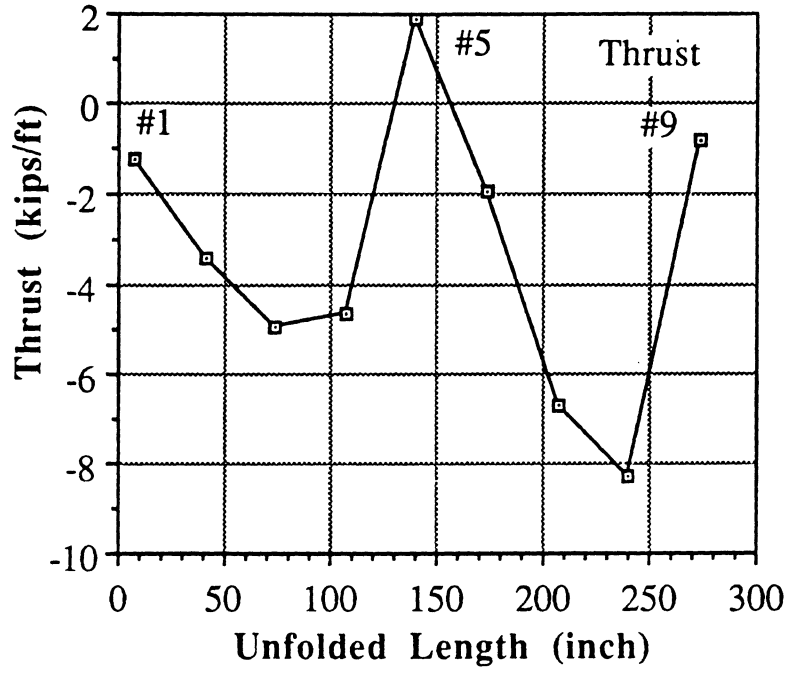

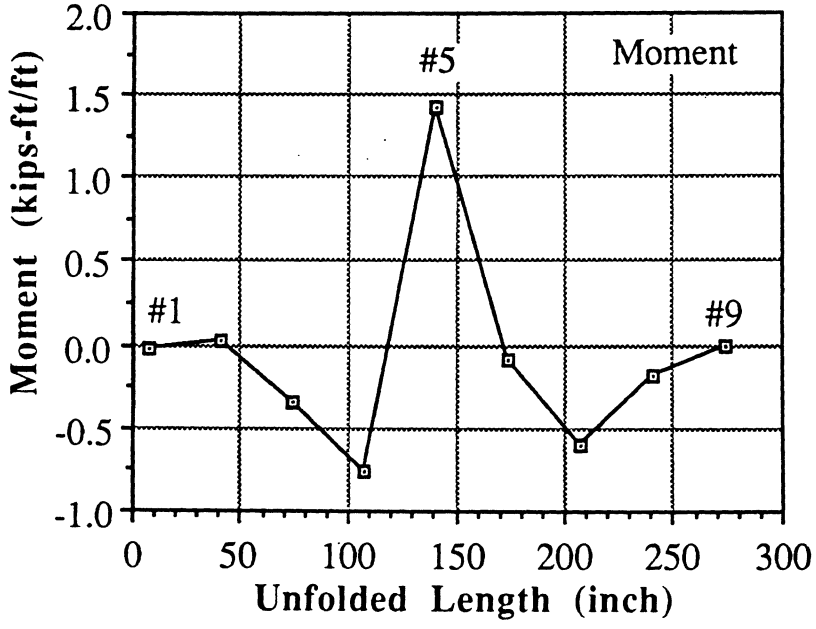

FIGURE 4.19 DISTRIBUTIONS OF THRUST AND MOMENT UNDER LOAD OF 57.73 TONS DURING THIRD LOADING SEQUENCE.

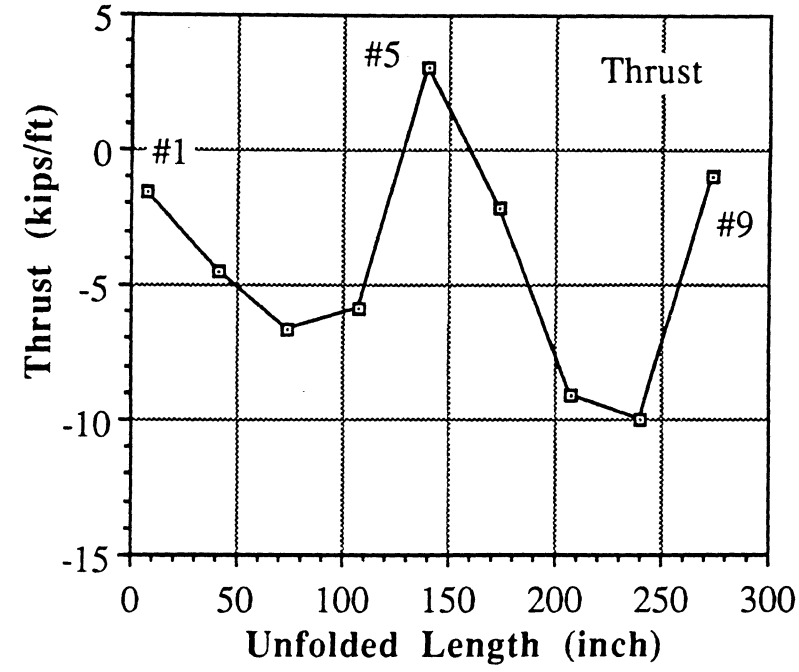

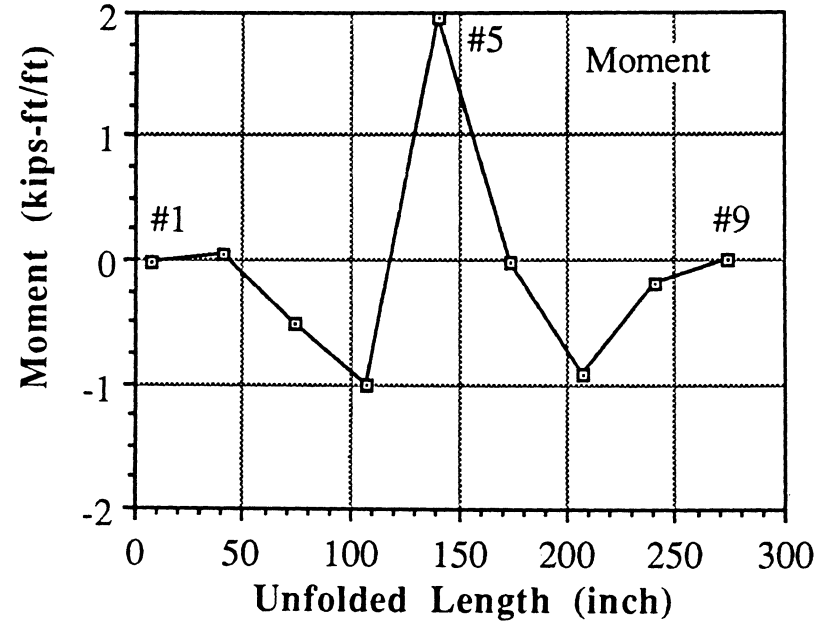

FIGURE 4.20 DISTRIBUTIONS OF THRUST AND MOMENT UNDER LOAD OF 80.81 TONS DURING THIRD LOADING SEQUENCE

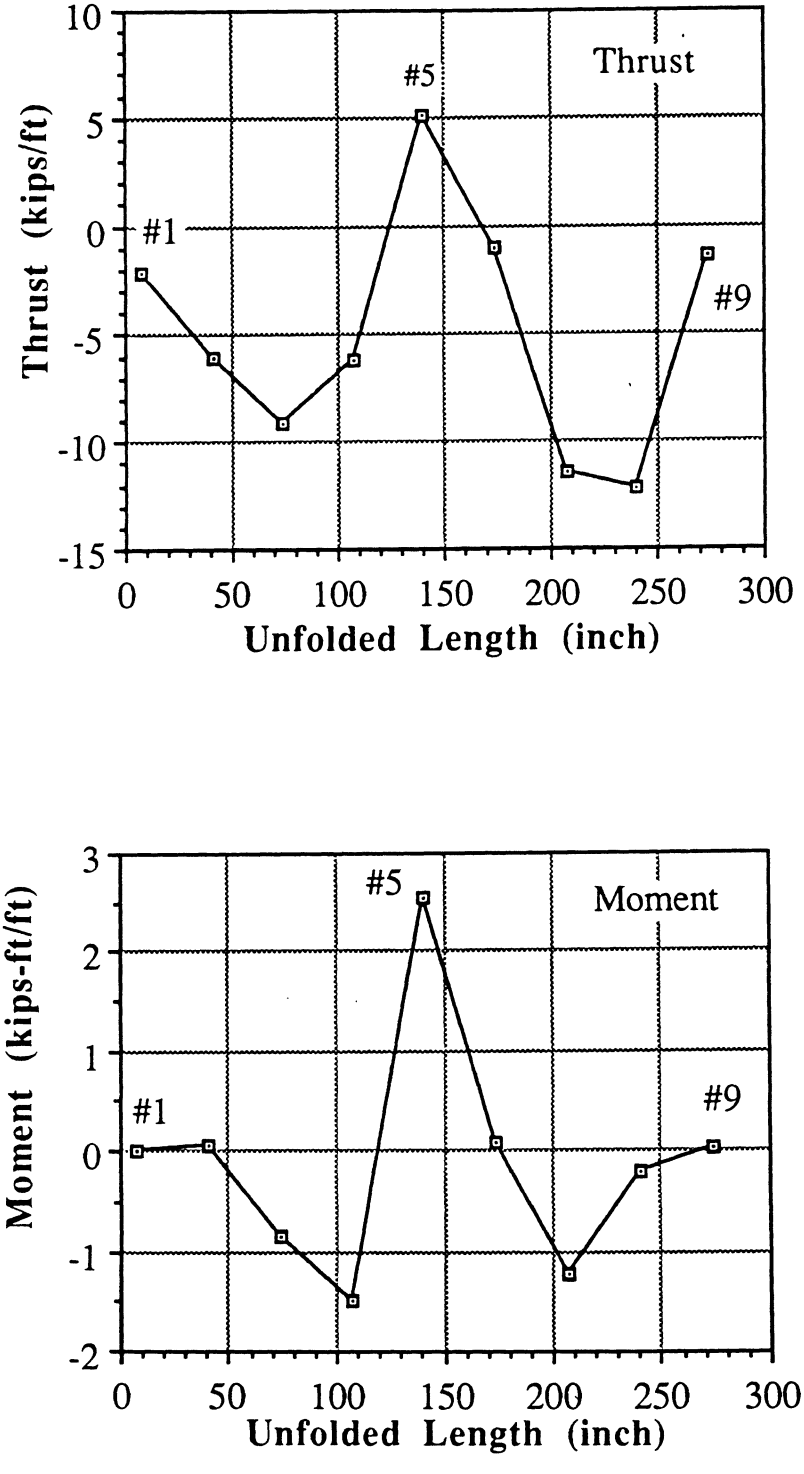

FIGURE 4.21 DISTRIBUTIONS OF THRUST AND MOMENT UNDER LOAD OF 100.1 TONS DURING THIRD LOADING SEQUENCE

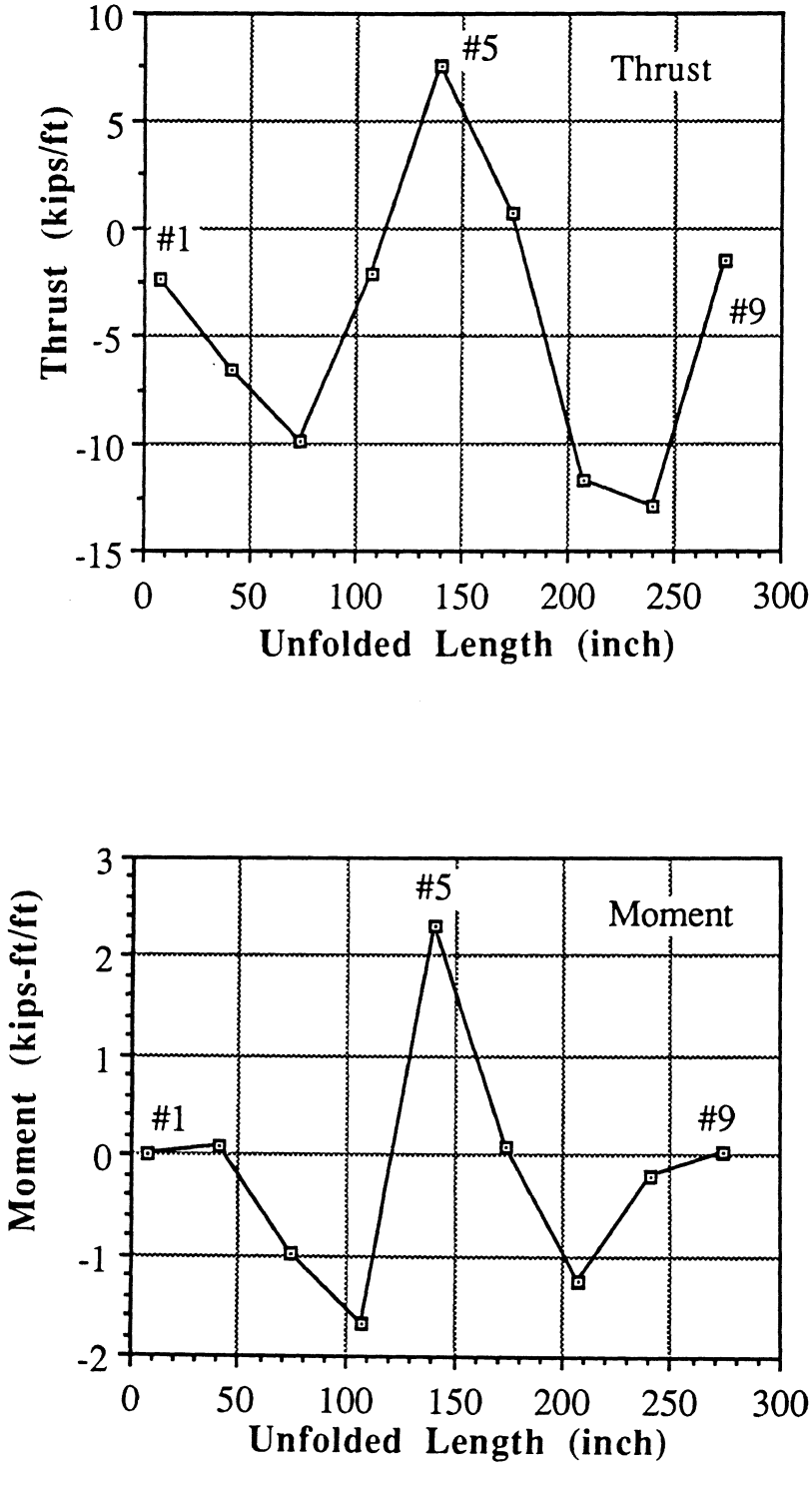

FIGURE 4.22 DISTRIBUTIONS OF THRUST AND MOMENT UNDER LOAD OF 107.8 TONS DURING THIRD LOADING SEQUENCE

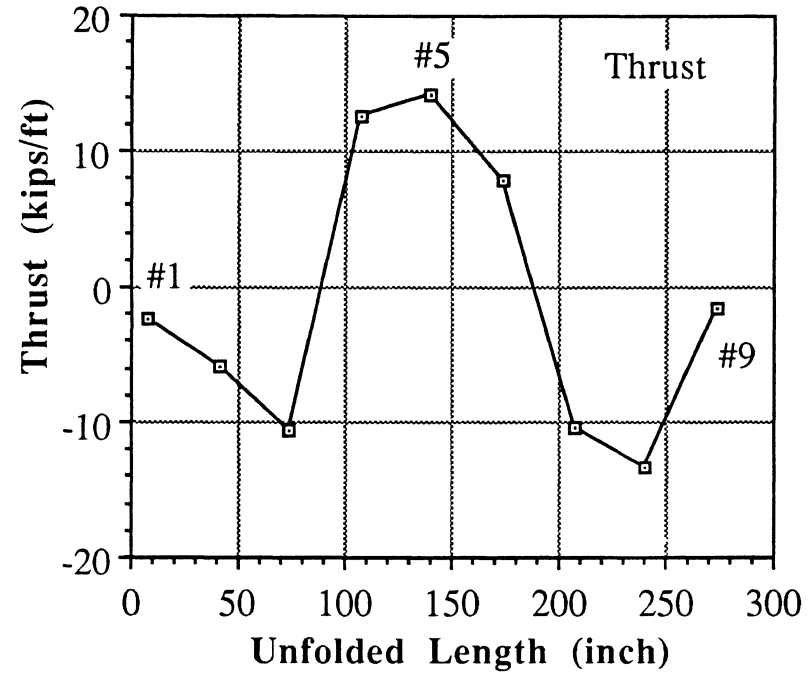

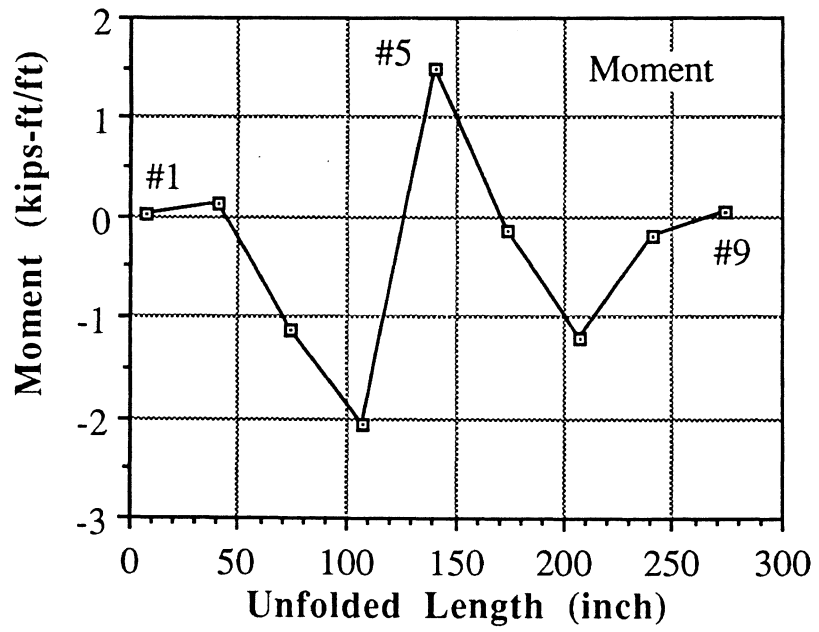

FIGURE 4.23 DISTRIBUTIONS OF THRUST AND MOMENT UNDER LOAD OF 115.5 TONS DURING THIRD LOADING SEQUENCE

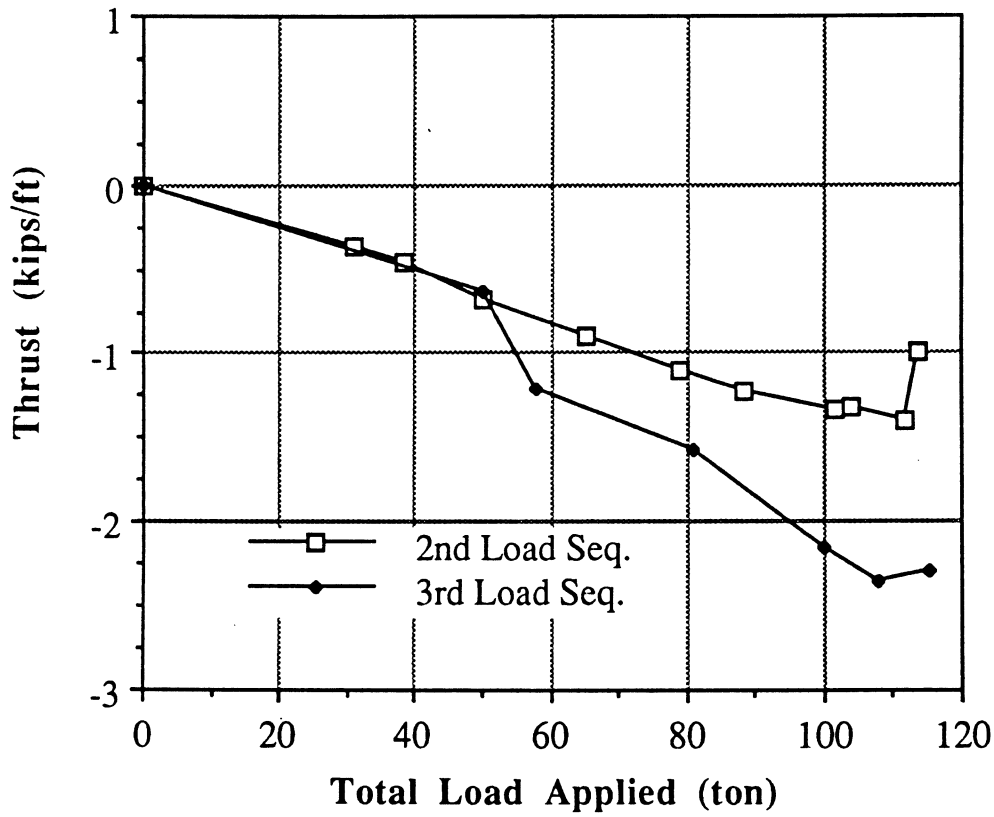

FIGURE 4.24 THRUST VS LOAD PLOTS FOR SECOND AND THIRD LOADING SEQUENCES AT SPRINGLINE (POINT #1)

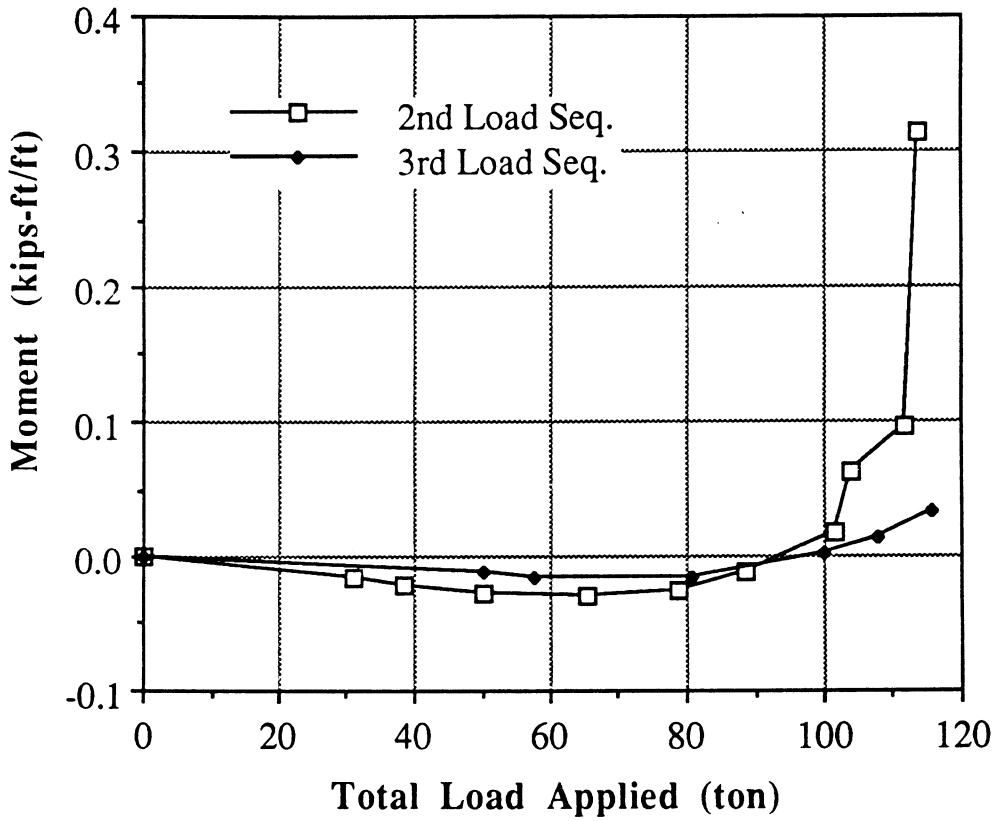

FIGURE 4.25 MOMENT VS LOAD PLOTS FOR SECOND AND THIRD LOADING SEQUENCES AT SPRINGLINE (POINT #1)

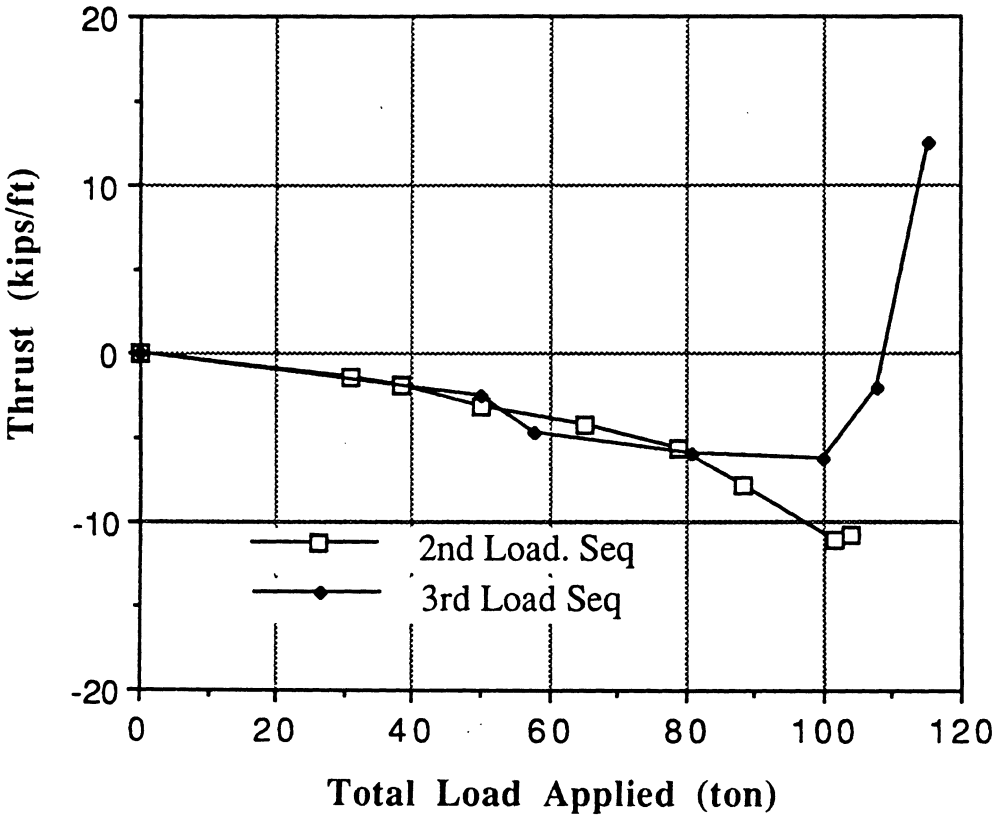

FIGURE 4.26 THRUST VS LOAD PLOTS FOR SECOND AND THIRD LOADING SEQUENCES AT SECTION #4

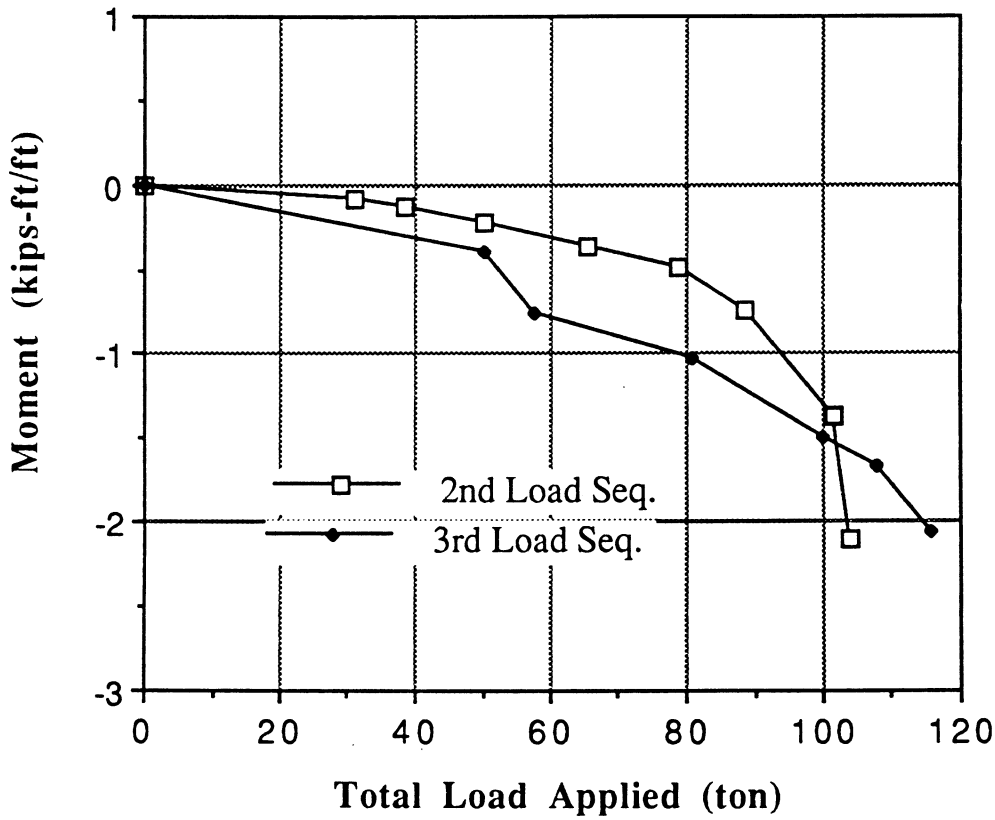

FIGURE 4.27 MOMENT VS LOAD PLOTS FOR SECOND AND THIRD LOADING SEQUENCES AT SECTION #4

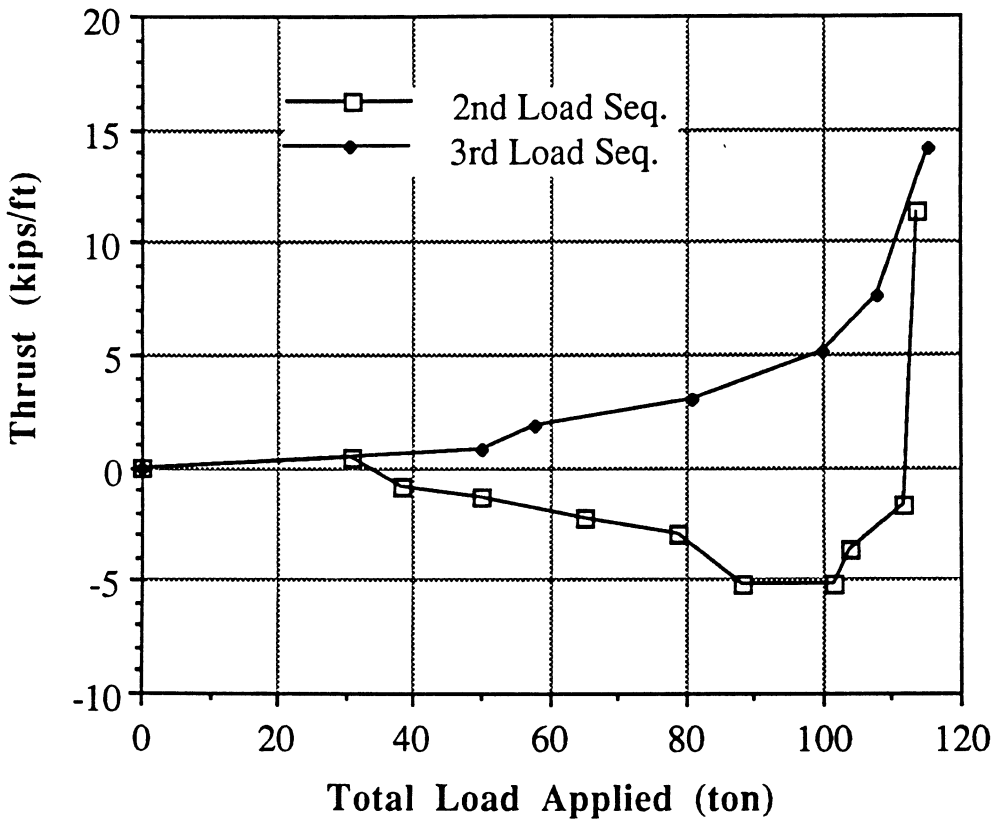

FIGURE 4.28 THRUST VS LOAD PLOTS FOR SECOND AND THIRD LOADING SEQUENCES AT CROWN (POINT #5)

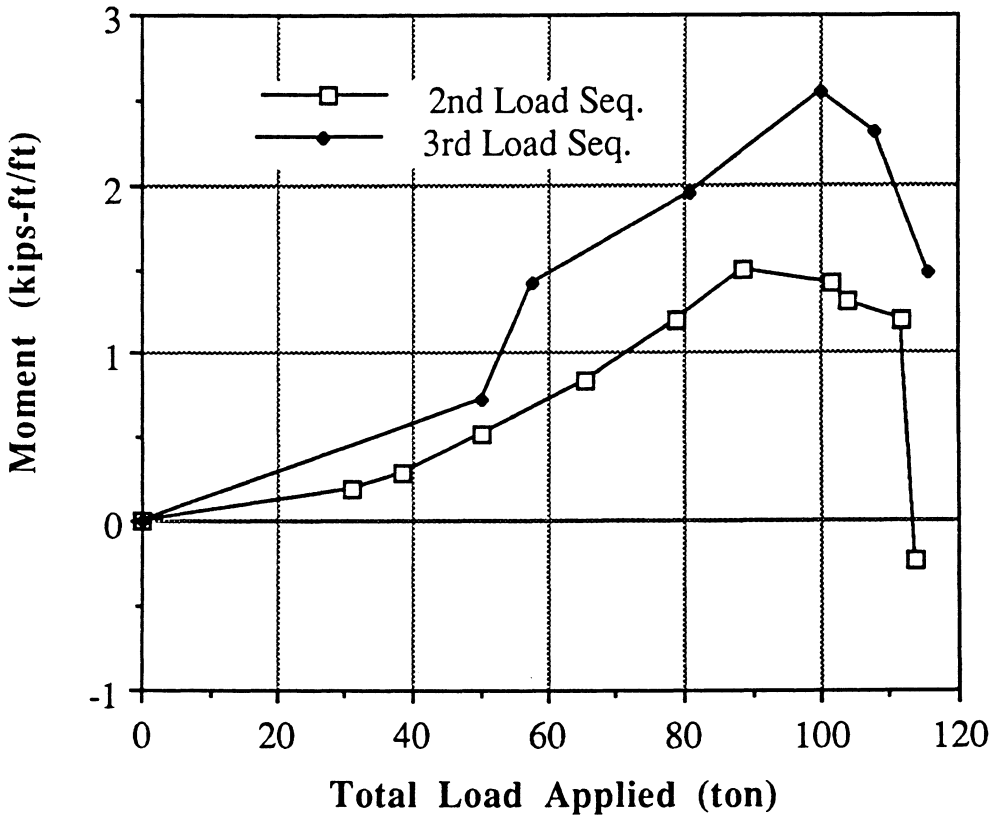

FIGURE 4.29 MOMENT VS LOAD PLOTS FOR SECOND AND THIRD LOADING SEQUENCES AT CROWN (POINT #5)

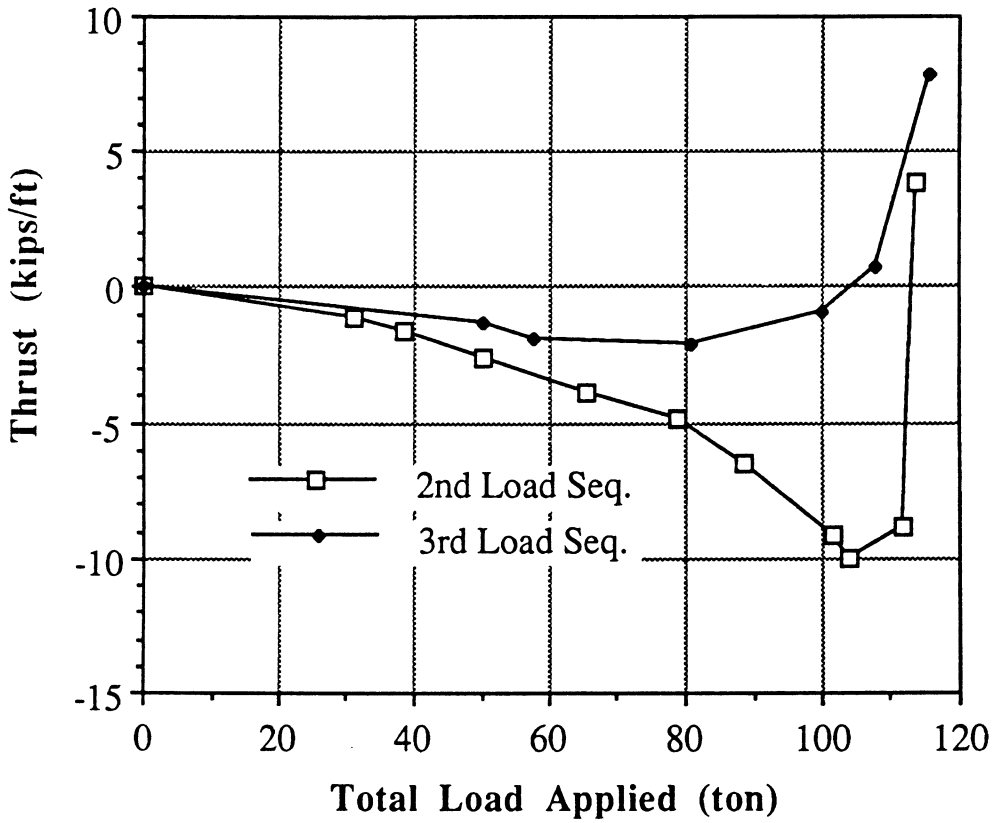

FIGURE 4.30 THRUST VS LOAD PLOTS FOR SECOND AND THIRD LOADING SEQUENCES AT SECTION #6

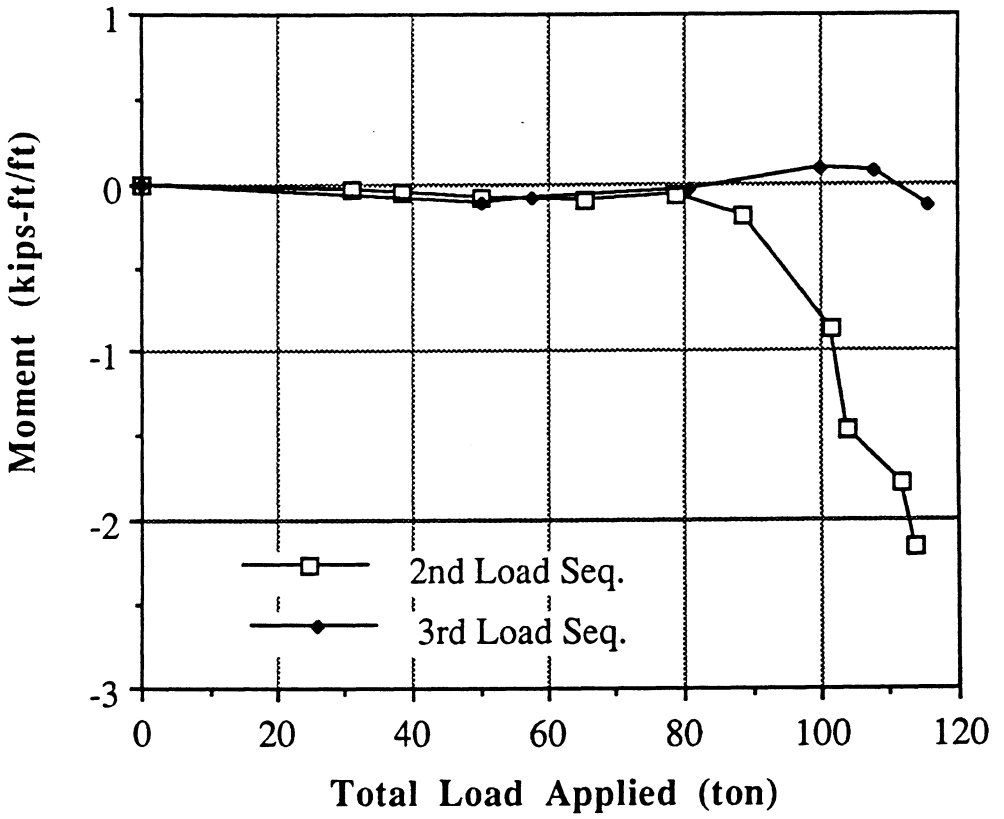

FIGURE 4.31 MOMENT VS LOAD PLOTS FOR SECOND AND THIRD LOADING SEQUENCES AT SECTION #6

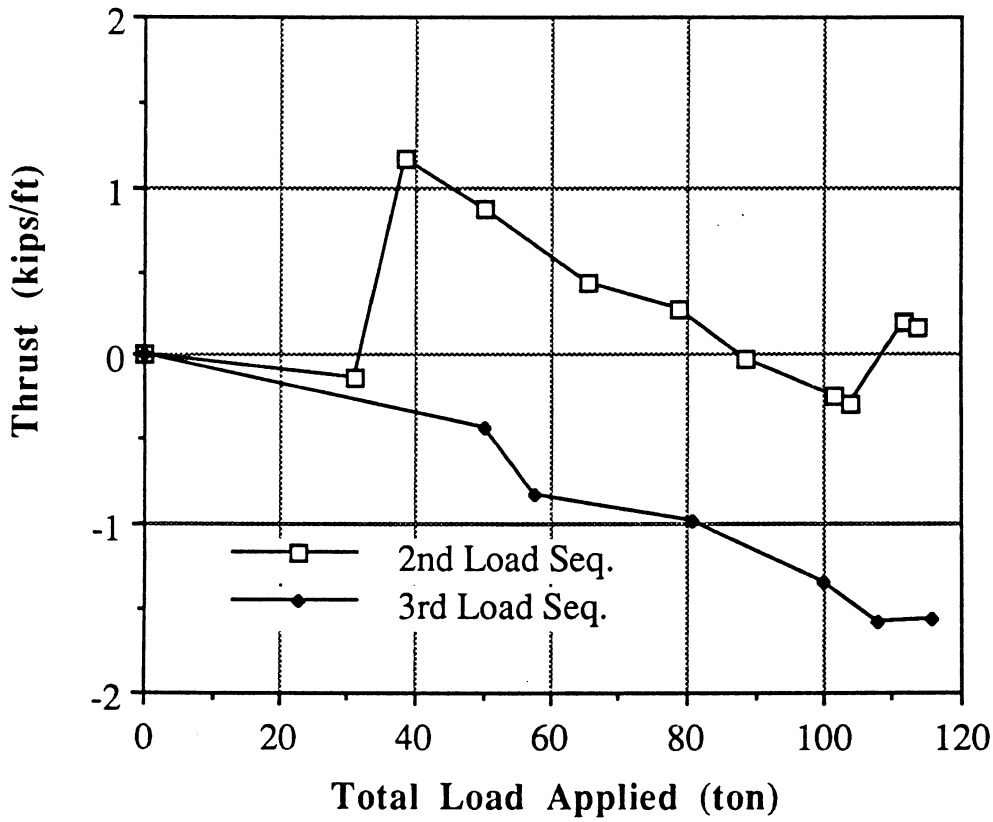

FIGURE 4.32 THRUST VS LOAD PLOTS FOR SECOND AND THIRD LOADING SEQUENCES AT SPRINGLINE (POINT #9)

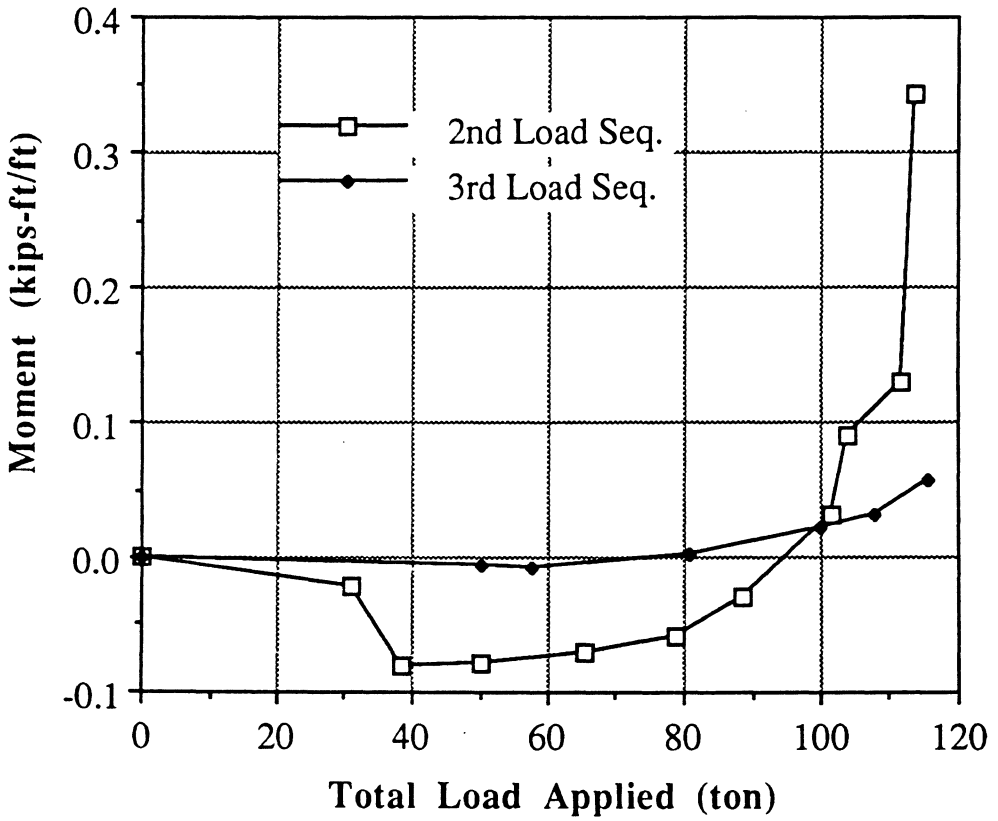

FIGURE 4.33 MOMENT VS LOAD PLOTS FOR SECOND AND THIRD LOADING SEQUENCES AT SPRINGLINE (POINT #9)

positive indicating the inward movement of the culvert. Small value of moment agrees well with small deflection data at these locations. In general, the magnitude of the thrust and the moment in the springline region was much smaller than those in the shoulder or in the crown region and agreed well with the deflection data.

Sections #2 and #8 responded similarly. Bending moment is positive in both the sections and both were in compression. Values of bending moment and the thrust were increased with increase of loading. Response at sections #3 and #7 which were at the haunch region also responded similar to each other indicating the symmetric conditions prevailed at the field. Moments at these two sections were negative indicating the outward movement of the culvert at these locations. Thrust values are in compression and increased with the load.

During the second loading sequence, the magnitude of the moment increased as the load increased at point #5 where the magnitude of the moment decreased when the load reached approximately 100 tons. The moment and thrust decreased when additional load increments were applied. At the load of 113.9 tons, the moment changed its sign and became insignificant and the thrust changed from compression to a large tension magnitude. Moment values at sections #4 and #6 were negative but not equal. Moment value at section #4 is more than the plastic moment capacity of this type of structural plate indicating the formation of plastic hinge at that location. Moments at section #5 and #6 were close to it's plastic moment capacity. Visual inspection showed us the formation of hinges at those locations also. This may be due to the fact that corrosion might have reduced the stiffness of the culvert plate since it was exposed to adverse field conditions for the past fifty years. Thrust value at these sections were in compression and increasing with the load until 101.6 tons load was on. After the eighth load (103.9 tons) step thrust value started decreasing and changed to tension at the last step of loading of the second sequence of loading.

During the early stage of second loading cycle, the system acted as a composite beam. The moment and thrust distribution increased in magnitude as applied load increased. These distribution pattern were symmetrical about the crown point upto the eighth load increment. Beyond this loading step circumferential stress at the section #4 reached the yield stress. Moment value at this section became higher than that at point #6 therefore, disturbing the symmetric nature of the distribution.

Figure 4.34 explains the nature and exact location of the slippage occured near the instrumented plane, where the crown seam was the weakest. After the slippage occured at the bolted joints that section didn't behave like a composite beam rather the system responded as a truss. Strain gages then gave localized responses.

Fig.4.28 and 4.29 gives the thrust and moment values obtained for section #5 with increments of the load. Moment values didn't change much after the 88.51 tons in the first cycle; instead it reduced little and turned negative during the last step of the second cycle and the whole of the third cycle. Thrust also behaved in the same way. It decreased after 101.6 tons of load and had sudden drastic increase at the last step of the second cycle of loading. Axial thrust was in compression until the last step of the first cycle and changed into tension during the last step of loading and remained in tension throughout the third cycle of loading. After the slippage occured at the bolted joints that section didn't behave like a composite beam.

Although the load was removed after the second loading sequence, the culvert, as indicated by the measured deflections, did not recover its original shape. Outside the crown region, the thrust response did not differ much between the second and the third loading sequence, and the moment response was smaller during the third loading sequence. The responses at points #4, #5, and #6 showed some difference between the last two loading sequences. The moment at point #5 responded slightly more but the thrust remained in tension. Yield was reached in the longitudinal direction at the crown under 115.5 ton load

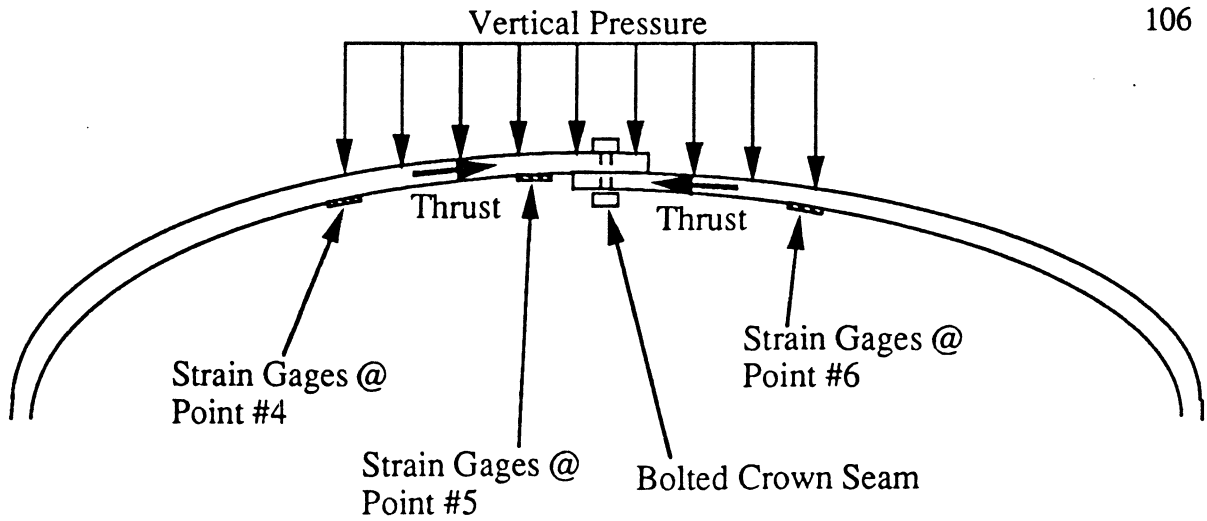

(a) Initial Stage

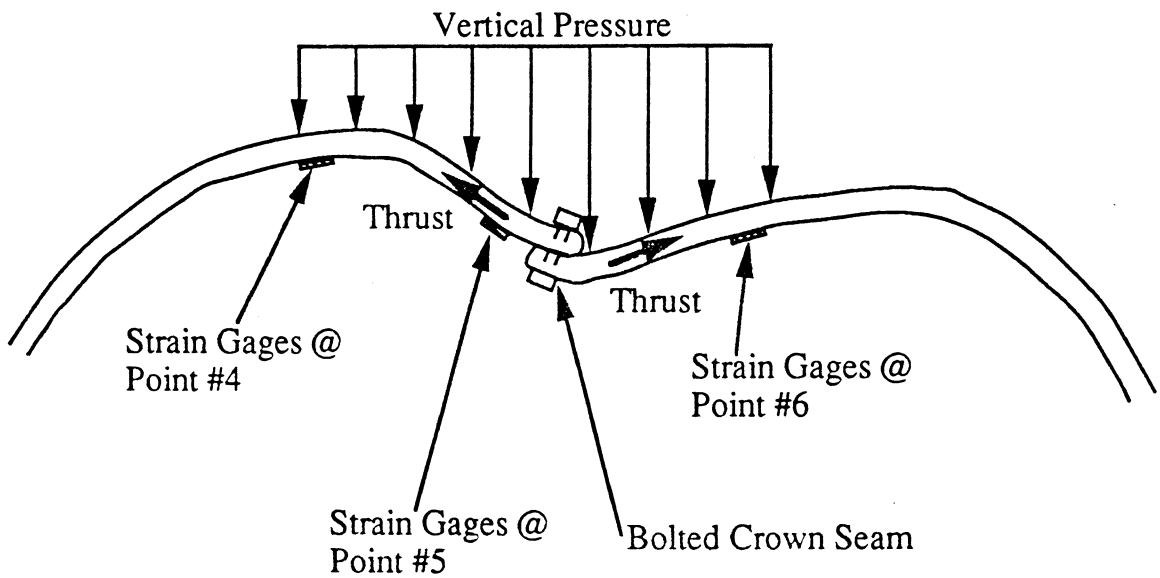

(b) Final Stage

FIGURE 4.34 FAILURE MODE OF BOLTED CROWN PLATES UNDER LOAD

during the third loading sequence.

4.4 PLASTIC MOMENT CAPACITY

The determination of the plastic moment capacity is obviously of great importance because it is the limiting or maximum moment for the corrugated steel plate. Increasing the bending moment above the yield moment will cause the strains at the extreme fibers to increase and the maximum strain will exceed the yield strain ε_y . However, because of perfectly plastic yielding, the maximum stresses will remain constant and equal to σ_y.

The plastic moment capacity of the tested corrugated steel culvert is equal to 3.745 kips-ft/ft, using ultimate yield stress of 30 ksi. Here, it must be noted that the above definition of the plastic moment doesn't take into account the axial forces. The value of 3.745 kips-ft/ft represents an upper limit. Actual moment capacity will be slightly reduced when axial forces are considered.

4.5 FORMATION OF PLASTIC HINGES AND CREASES

When M_{max} becomes equal to M_p, the cross-section at the center of the beam is completely plastic. The curvature at the center of the beam is completely plastic. The curvature at the center of the corrugation then becomes extremely large and unrestrained plastic flow may take place. No further increase in the maximum moment can occur, and the load on the beam is at its maximum value. The corrugation fails by excessive rotations that occur at the middle cross-section, while the two halves of the corrugation remain comparatively rigid. Thus, corrugation behaves like two rigid bars linked by a plastic hinge that permits the two bars to rotate relative to each other under the action of a constant moment M_p.

Available data from this test indicates that a plastic hinge is formed only at section #4, at the load of 113 tons of the second cycle of loading. Moment at points #5 and #6 became close to the upper bound plastic moment capacity. After the test, plastic hinge formation was also observed at these locations. Figure 4.35 shows the formation of plastic hinges. All the other sections are under their plastic moment capacity. According to Dessouki. A.K. and Monforton. G.R, "the formation of plastic hinges in the conduit doesn't constitute complete failure but rather affects the load carrying capacity". Duncan. J.M. in his study [8] considering both the axial force and the bending moment has concluded that:

1) Formation of a single plastic hinge will not result in formation of a failure mechanism, even in an arch structure pinned at the footings. Additional plastic hinges would have to form before the structure collapses.

2) Even after sufficient hinges have developed in the structure to form a failure mechanism, the soil will continue to restrain the deformations of the structure.

3) Both aluminum and steel harden when deformed plastically. Therefore, the use of the value of M_p based on minimum values of yield stress provides a conservative estimate of the ultimate esistance of the metal.

From the above findings we can conclude that the culvert we tested didn't develop a failure mechanism that would have caused the full failure of the culvert for the above cited reasons. Further, the maximum load that can be carried by the culvert is equal to 100 tons. Sections which reached their yield limit were tabulated in Table 4.3. This gives an idea of the critical sections of the pipe arch culvert with shallow cover.

After the testing was over close inspection of the culvert showed us the formation of creases in the plate at various location of the culvert. Table 4.4 and the Fig. 4.36 presents an idea of the location and the size of the creases. Although the formation of the creases doesn't have any significance towards this study, for the sake of completeness of this document it is presented here. Creases #1 through #9 were lined up at a distance of about

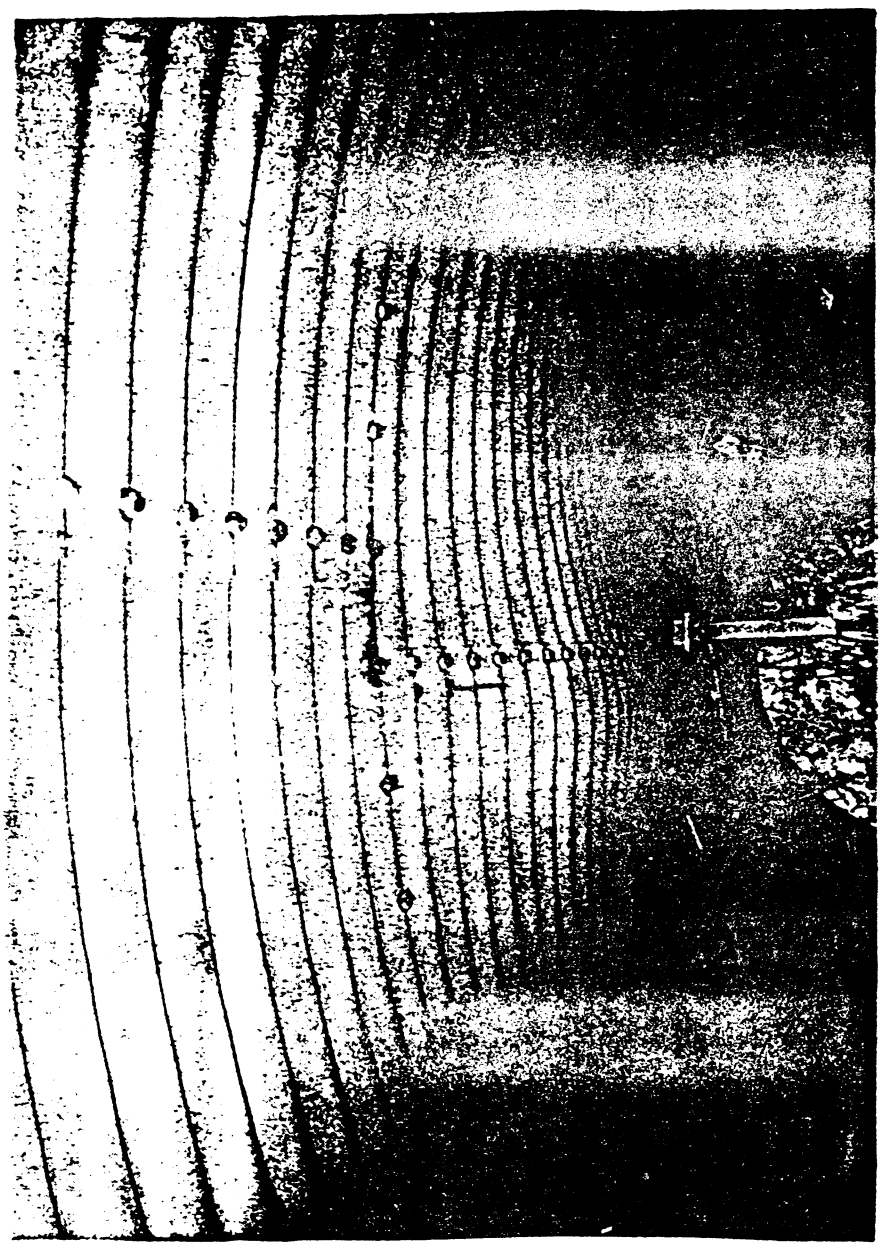

FIGURE 4.35 FIELD PICTURE OF CULVERT CROWN REGION SHOWING PLASTIC HINGE FORMATION

TABLE 4.3 YIELD STRESS REACHED DURING FAILURE TESTS

* First Sequence of Loading - Sept. 24, 1990									
Yield stress was never reached at any monitoring point during loading									
* Second Sequence of Loading - Sept. 26, 1990									
Section No.	Location	Direction	Load Increment No.						
			6	7	8	9	10	11	12
4	Crest	Circumf.	N	N	N	-Y	-Y	-Y	-Y
		Longit.	N	N	N	N	N	N	N
	Valley	Circumf.	N	N	N	N	N	+Y	+Y
		Longit.	N	N	N	N	N	N	N
5	Crest	Circumf.	N	N	N	N	N	N	N
		Longit.	N	N	N	N	N	N	N
	Valley	Circumf.	N	N	N	N	N	N	N
		Longit.	N	N	N	N	N	N	+Y
	Side	Circumf.	N	N	N	N	N	N	N
		Longit.	N	N	N	N	N	N	N
* Third Sequence of Loading - Sept. 26, 1990									
Section No.	Location	Direction	Load Increment No.						
			1	2	3	4	5	6	7
5	Crest	Circumf.	N	N	N	N	N	N	N
		Longit.	N	N	N	N	N	-Y	-Y
	Valley	Circumf.	N	N	N	N	N	N	N
		Longit.	N	N	N	N	N	+Y	+Y
	Side	Circumf.	N	N	N	N	N	N	N
		Longit.	N	N	N	N	N	N	N

(Note) N = Yield Stress Not Reached; $-Y = -\sigma_y$ Reached; $+Y = +\sigma_y$ Reached

TABLE 4.4 LOCATION AND LENGTH OF CREASES DETECTED

Crease No.	Crease Length (in.)	General Location	L_1 (in.)	L_2 (in.)
1	3/8	South Side of Crown	13-11/16	24-3/4
2	5/8	South Side of Crown	17-1/4	24-3/4
3-a	3/8	South Side of Crown	20-1/8	24-3/8
3-b	3/8	South Side of Crown	20-1/2	24-3/8
4	5/8	South Side of Crown	23-1/2	24-1/8
5	1-3/4	South Side of Crown	26-5/8	23-3/8
6	1-1/4	South Side of Crown	29-1/2	24-0
7	1/2	South Side of Crown	35-3/8	24-0
8	1-0	South Side of Crown	38-3/4	24-0
9	7/8	South Side of Crown	45-1/8	24-7/8
A	3/4	North Side of Crown	14-1/4	36-3/4
B	1-1/2	North Side of Crown	20-3/8	35-1/2
C	1-5/8	North Side of Crown	26-1/4	36-0
D	1-3/8	North Side of Crown	38-1/8	35-1/2
E	1-1/4	North Side of Crown	44-1/4	35-3/8

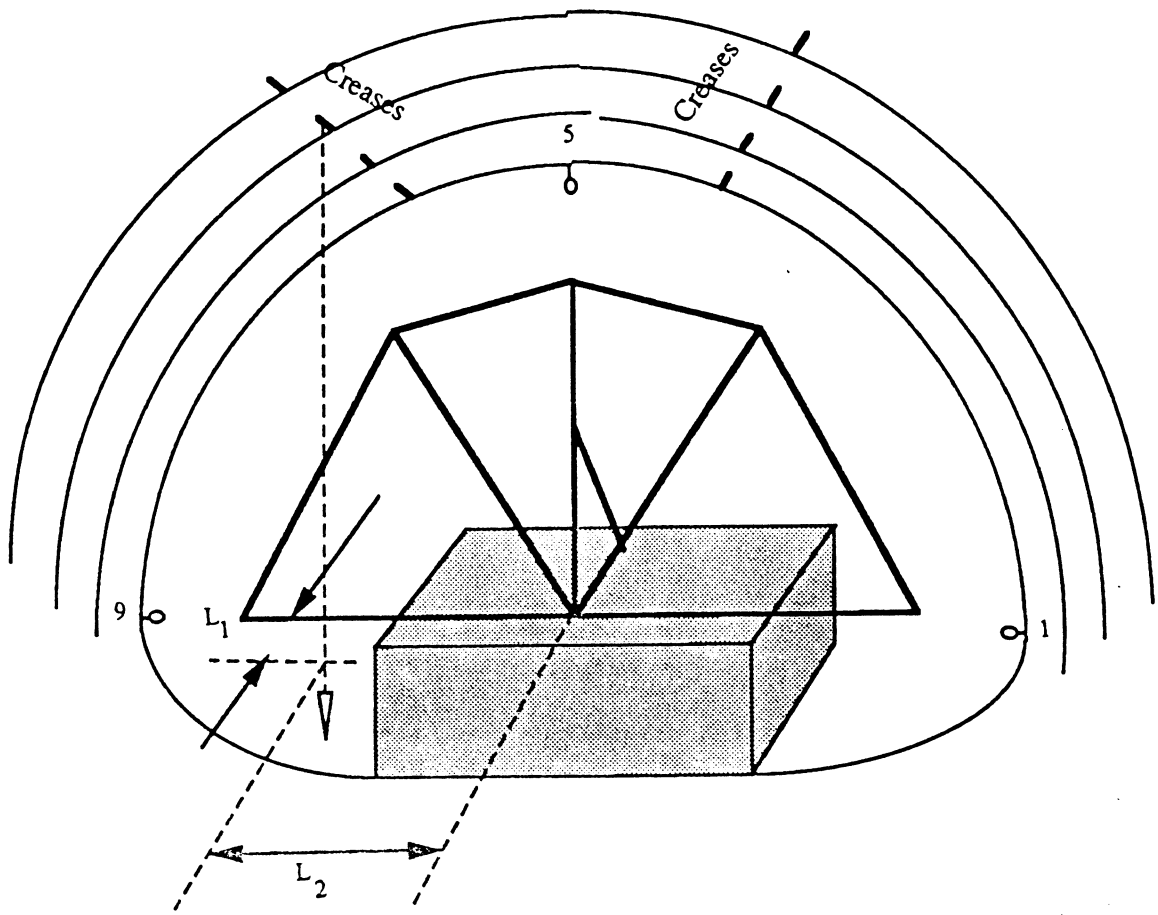

FIGURE 4.36 MEASUREMENTS TAKEN TO LOCATE CREASES

24 inches south of the crown (or at a distance of about 9.25 inches north of monitoring point #6). Creases A through E were detected at a distance of about 36 inches north of the crown (or at a distance of 2.75 inches north of monitoring point #4).

CHAPTER 5

FINITE ELEMENT ANALYSIS

5.1 INTRODUCTION

The design of corrugated metal culverts, until recently, has been largely based on empirical relations and on past experience with these types of structures. Although these methods can result in satisfactory designs, their ability to predict the behavior of the soil-culvert system is rather limited. In these methods, analysis of the structure was done by assuming a plane strain ring structure subjected to vertical loading. The soil pressure distribution on the structure is then found from the calculated pipe deflections.

Due to rapid improvements made on the computational ability in the past few decades, the finite element method has gained large popularity and wide applications. In the last two decades, the finite element method of analysis was effectively applied to culvert problems [1,2,5,8,17,]. After its successful introduction in the early 1970's, advances have been made to incorporate material nonlinearity, construction sequences, and soil-structure interface elements. In this method, both the soil and the pipe are modeled as plane-strain continuum.

Finite element method is capable of providing a more comprehensive representation of the complex soil-structure interaction problem involved. The essential requirement for a comprehensive finite element simulation are:

1) Inclusion of live load as well as dead load.
2) Adequate presentation of the true geometry and realistic boundary condition.
3) Realistic modeling of the nonlinearities in soil and structure properties.

In this investigation, numerical simulations of structural behavior of the pipe arch culvert during the failure tests were attempted with the use of the CANDE (Culvert

ANalysis and DEsign) computer program. It is capable of representing the nonlinear properties of structural and soil elements as well as the interface element. More detailed information on the CANDE program is found in References (13,14)

5.2 CANDE BACKGROUND

CANDE can be operated in a design or analysis mode. Here in this chapter only the analysis mode is briefly discussed. The assumptions common to all solution levels in CANDE are:

1) Two dimensional analysis with plain strain.

2) Small strain theory

5.2.1 SOLUTION LEVEL

There are three solution levels in CANDE. Level 1 corresponds to the elastic, closed form solution. How ever this level cannot consider such features as arch-shaped structures on footings, and the several zones of backfill material, all of which are important consideration in this study. Level 2 is finite element solution where the mesh is automatically created by CANDE whereas in level 3, which is also finite element analysis, the mesh is defined by the user.

5.2.2 PIPE TYPES

The pipe material library in CANDE includes corrugated steel, corrugated aluminum, concrete, plastic and basic pipe types. In our case corrugated steel pipe type was used. In this type uniform geometric properties of the wall section are assumed throughout the culvert periphery. Both linear and bilinear constitutive models of the pipe material are allowed under this type. In this analysis the bilinear model is used.

5.2.3 ELEMENT TYPES

There are three basic types of elements available in CANDE (1) Beam-Column element; (2) Quadrilateral element (3) Interface element. In this analysis only Beam-Column element and quadrilateral element are used. Normally Interface element is provided to allow frictional sliding, separation and rebinding of elements meeting at a common interface. Here in this analysis we avoided using this element to solve the convergence problem encountered by others.

5.2.4 SOIL MODEL

At present there are five soil models available in CANDE:

1) elastic
2) ortho-elastic
3) over-burden dependent
4) hardin model
5) Duncan model

Considering soil's non-linearity and non-homogeneity it is determined that soil can be best represented by Duncan's stress-strain hyperbola model [9,10,11]. In order to derive the Duncan's constitutive parameters several triaxial tests were conducted with the samples obtained from the test site. The main reasons for selecting this model are; (1) its availability as a part of the soil model library in the CANDE program, (2) its incorporation of the minor principal stress in defining initial and failure stresses; and (3) ease in obtaining its parameters from CTC (conventional triaxial compression) tests. Some shortcomings of this model is that it is not suitable for predicting the soil behavior where the loading conditions induced stress paths other than that of the CTC within the soil mass.

5.3 FIELD SOIL SAMPLING WORK

The backfill soil sampling work was conducted on April, 1, 1991, about six months after the completion of the field testing. The equipment utilized was a standard

truck mounted rotary drilling rig. The rig was set within the west shoulder section of the the roadway above the culvert, since the subsurface soil data was previously obtained at the location (as seen in Fig. 2.2) and a complete blockage of the local traffic posed a problem. The goal of the sampling work was to obtain a few relatively undisturbed soil samples from each of the three (crown, haunch, and springline) regions on both the east and west sides of the culvert structure. A total of six soil samples were taken by hydraulically pressing at a constant rate three inch O.D. thin-walled sampler. Upon removal of the sample tubes from the holes, their ends were double-sealed with special caps. Later, they were transported to the CGGR research laboratory in a wooden cradle.

5.4 LABORATORY SOIL TESTING METHOD

The conventional, consolidated and undrained (or CU) triaxial testing procedure was selected as a method to characterize the shear strength parameters and stress-strain characteristics of the sampled backfill soil materials. A total of 14 tests were performed using T-1500 triaxial testing device. To measure volumetric strains during the test, changes in the volume of water inside the triaxial cell were monitored with a graduated tube. For each test, a soil sample extracted from the tube was inspected to make sure that it had no defect and then trimmed down to a diameter of 2.8 inches and a height atleast twice the diameter. It was wrapped completely with a rubber membrane. Loading platens were attached with O-rings at the top and at the bottom, inside the triaxial chamber, with porous stone plates inserted between the soil specimen and the platens. To initiate the testing process, the chamber was filled with distilled water and a confining pressure ranging from 5 to 15 psi was applied to consolidate the soil. Table 5.1 presents some basic information regarding each triaxial test. Strain-controlled axial loading was exerted with a ram and the load was measured using a proving ring. To compute axial stresses during the test, the cross-sectional area of the specimen was corrected to account for Poisson's effects. The instantaneous area was computed using volumetric strain data and assuming the cross-section was equal along the length of the specimen.

TABLE 5.1 BASIC INFORMATION ON TRIAXIAL TESTS

Test No.	Boring	Sample I.D.	Sample Depth (ft.)	Zone	Confining Pressure (psi)	Moisture * Content (%)	Density * (pcf)
1	A	1P	9.1-9.6	Crown	10.0	17.44	136.74
2	A	1P	8.5-9.0	Crown	5.0	13.91	121.67
3	B	1P	7.9-8.4	Crown	15.0	18.40	NT
4	B	1P	7.4-7.9	Crown	5.0	17.60	133.39
5	A	2P	12.4-12.9	Shoulder	15.0	28.28	133.60
6	A	2P	11.9-12.4	Shoulder	10.0	32.65	133.33
7	B	2P	12.4-12.9	Shoulder	10.0	16.67	131.50
8	A	2P	10.9-11.4	Crown/Shoulder	5.0	28.13	123.10
9	B	3P	15.8-16.3	Springline	10.0	21.27	119.67
10	B	2P	11.9-12.4	Shoulder	5.0	22.84	132.48
11	B	3P	15.3-15.8	Springline	5.0	24.80	117.40
12	A	3P	15.8-16.3	Springline	15.0	29.05	120.56
13	A	3P	15.3-15.8	Springline	10.0	18.56	135.37
14	B	3P	14.8-15.3	Springline	15.0	26.71	119.05

(Note) The symbol "*" indicates initial values.

5.5 RECOMMENDED SOIL PARAMETERS

The Duncan soil model is a variable moduli (or nonlinear) model which characterizes soil behavior with tangent Young's modulus and bulk modulus. The guidelines suggested by Duncan [Duncan et al.,1980] were followed in deriving the hyperbolic model parameters.

Duncan recommends fitting the hyperbola through only two points on the stress-strain curve: 70% and 95% of the failure strength of each test. This is accomplished on the plot of transformed axes where a hyperbola plots as a straight line. The Duncan soil model contains a total of eight parameters K,n,R_f,Φ_0,$\Delta\phi$,c,K_b, and m. Derivation procedure of the two shear strength parameters c and ϕ through triaxial test results is well known. A systematic determination of the remaining six soil parameters out of triaxial test data has been presented in details by Duncan [10]. These procedures are briefly summarized in Table 5.2. Recommended values for all eight parameters were tabulated in Table 5.3.

5.6 FINITE ELEMENT SIMULATION

Half mesh is used to represent structure and backfill for our problem. This is acceptable since the structure and the loading conditions were assumed to be symmetrical. Mesh was created using both design and the measured shape of the culvert. Figure 5.1 explains the node numbering and element numbering system used for this analysis.
The boundary conditions established at the nodes are 1) nodal points along the bottom boundary were fixed in both the vertical and horizontal directions. 2) The nodes on the right and left sides of the mesh are fixed in the horizontal direction but free to move in the vertical direction.

The asphalt layer was represented by quadrilateral elements. The modulus of 1000 ksi was used to simulate the compacted form of the asphalt. The pipe material selected out of the CANDE library was corrugated steel with bilinear constitutive models. Pipe was

TABLE 5.2 DUNCAN'S HYPERBOLIC SOIL MODEL PARAMETERS

Parameters	Determination Procedure
K = Modulus Number:	From Relating Initial Modulus To Confining Pressure
n = Modulus Exponent:	From Relating Initial Modulus To Confining Pressure
R_f = Failure Ratio:	By Dividing Failure Shear Stress By Ultimate Shear Stress
c = Cohesion Intercept:	From Mohr-Coulomb Failure Criterion
ϕ_o = Friction Angle:	From Mohr-Coulomb Failure Criterion and Relating ϕ To σ_3
$\Delta\phi$ = Reduction in ϕ For 10-Fold Increases:	From Mohr-Coulomb Failure Criterion and Relating ϕ To σ_3
K_b= Bulk Modulus Number:	From Relating B To σ_3
m = Bulk Modulus Exponent:	From Relating B To σ_3

TABLE 5.3 A SUMMARY OF MATERIAL PARAMETERS

* Steel (Bilinear Elastic)

Initial Young's Modulus, $E_1 = 30 \times 10^6$ psi.
Secondary Young's Modulus, $E_2 = 1.76 \times 10^6$ psi.
Poisson's Ratio, $\upsilon = 0.3$.
Yield Stress, $\sigma_y = 33{,}000$ psi.

* Asphalt (Linear Elastic)

Young's Modulus, $E = 1 \times 10^6$ psi
Poisson's Ratio, $\upsilon = 0.41$

* Backfill Soil (Hyperbolic Model)

	Experimental	CL100	SM100
c	1.44 psi	2.78 psi	0. psi
ϕ	0.423 radians	0.524 radians	0.628 radians
$\Delta\phi$	0.	0.	0.14
R_f	0.706	0.700	0.700
K	37	150	600
n	0.217	0.450	0.250
K_b	410	140	450
m	0.49	0.20	0.

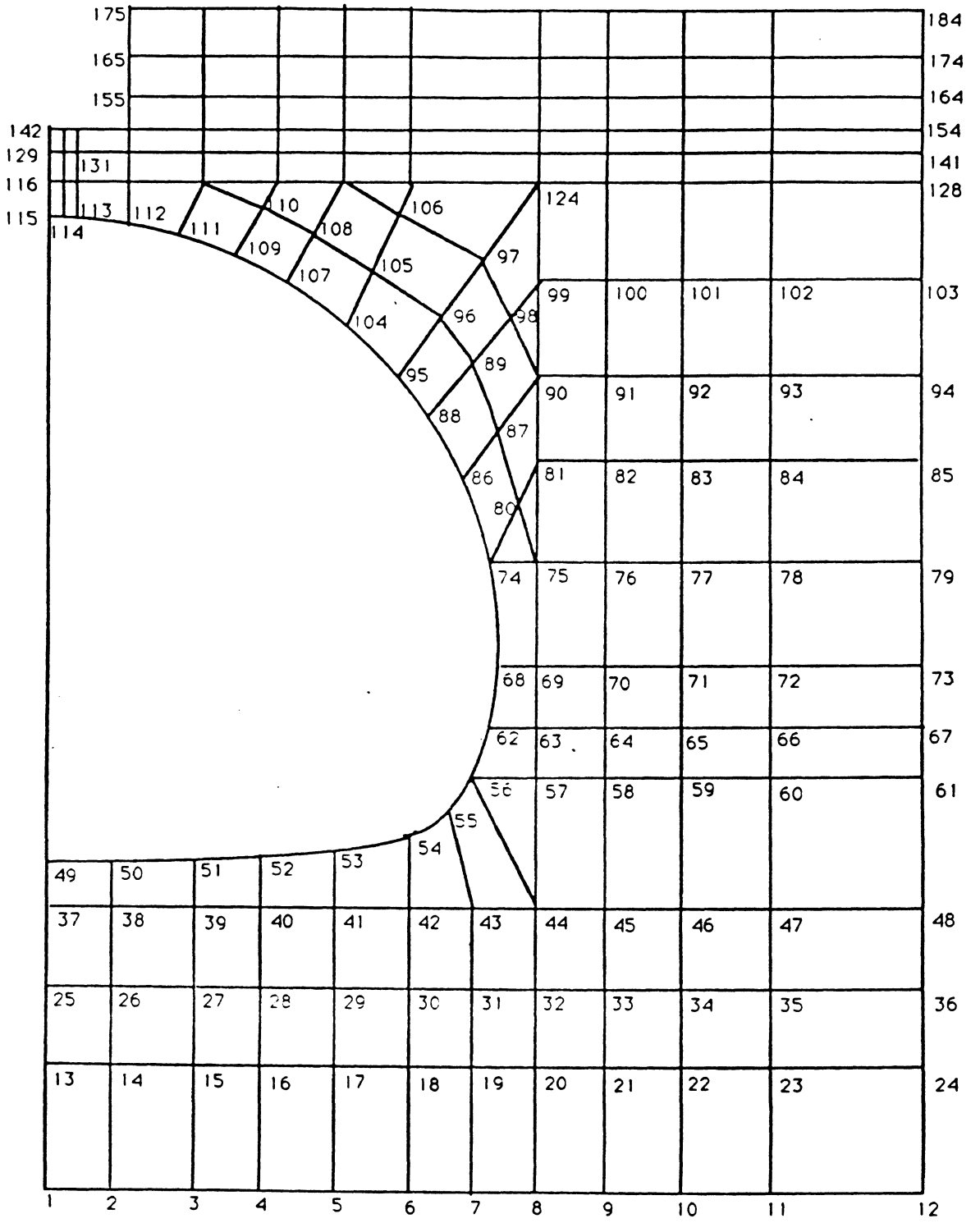

FIGURE 5.1 NODE NUMBERING SYSTEM USED FOR THE HALF MESH

represented by the beam-column elements. Interface elements between pipe and backfill material were not used inorder to avoid the convergence problems as reported by others. (Alan Rauch 1990)

Live load applied by hydraulic cylinders was converted to line load by the method proposed by Duncan and Drawsky. This method is based on load distribution in a semi-finite space. This method models an axle with several wheels by a line load which provides the same maximum vertical stress beneath the wheels on a plane at the depth of the top of the culvert crown as would the actual three-dimensional wheel loading, based on Boussinesq linear elastic vertical stress distribution analysis. This method is considered to be conservative because it provides a line load producing this peak stress along the full length of the culvert, whereas wheel loads provide this stress only beneath the wheels with stresses away from the wheel loading points. This inherent conservatism is minimized in corrugated culverts which do not have significant flexural stiffness longitudinally along the culvert and which are, therefore, vulnerable to localized overstressing directly beneath discrete wheel loads.

Duncan and Drawsky developed a simple equation and tabulated solution expressing their equivalent line load estimation procedure as

$$LL = AL / K_4$$

where LL equivalent line load (kips/ft)

AL. total axle load (kips) and

K_4 load factor (ft)

In this analysis K_4=8.7 ft was used, which is corresponding to 3 ft. cover and 4 wheels per the axle. The load factor (K_4) values, based on Boussinesq elastic analysis for various depths of soil cover and under different contact areas, are presented in Table 5.4.

No simulation of the first day test (the first load sequence) conditions was

TABLE 5.4 LOAD FACTOR (K_4) FOR VARIOUS COVER DEPTHS AND LOADING CONDITIONS

Values of Load Factor K_4 (ft.)			
Cover Depth (ft.)	Number of Wheels Per Axle		
	2	4	8
1	4.3	5.0	8.5
2	5.3	6.4	9.2
3	7.9	8.7	10.6
5	12.3	12.5	13.5
7	14.4	14.5	14.6
10	16.0	16.0	16.0

(Note) This information was obtained after Ref. [7].

attempted, since most of the deflections took place and a moderate degree of structural failure was achieved during the second and third loading sequences. The mesh consists of 184 nodes, 21 beam elements and 151 quadrilateral elements. A total of 5 types of CANDE computer program simulations were made. These simulations were done as summarized below:

Simulation #1: Experimentally derived soil parameters were input for the entire backfill soil region. (A symbol "K" is used in the graphical plots to indicate results from this simulation.)

Simulation #2: Same as simulation #1, but the parameter K value was increased to 3K. (A notation "3K" is used in the graphical plots to indicate results from this simulation)

Simulation #3: Two material types from the CANDE soil material property library (CL100 and SM100) were specified in the backfill soil region according to the boring log data. (see Figure 5.2 for locations of the two soil types. Results from this simulation were denoted by "FIELD-K" in the graphical plots.)

Simulation #4: Same as simulation #3, but the K values were magnified by a factor of 3. (Results from this simulation were denoted by "FIELD-3K" in the graphical plots.)

Simulation #5: Two material types from the CANDE soil material property library (CL100 and SM100) were specified in the backfill region, as shown in Figure 5.3. (Results from this simulation were denoted by "C100S100" in the graphical plots.)

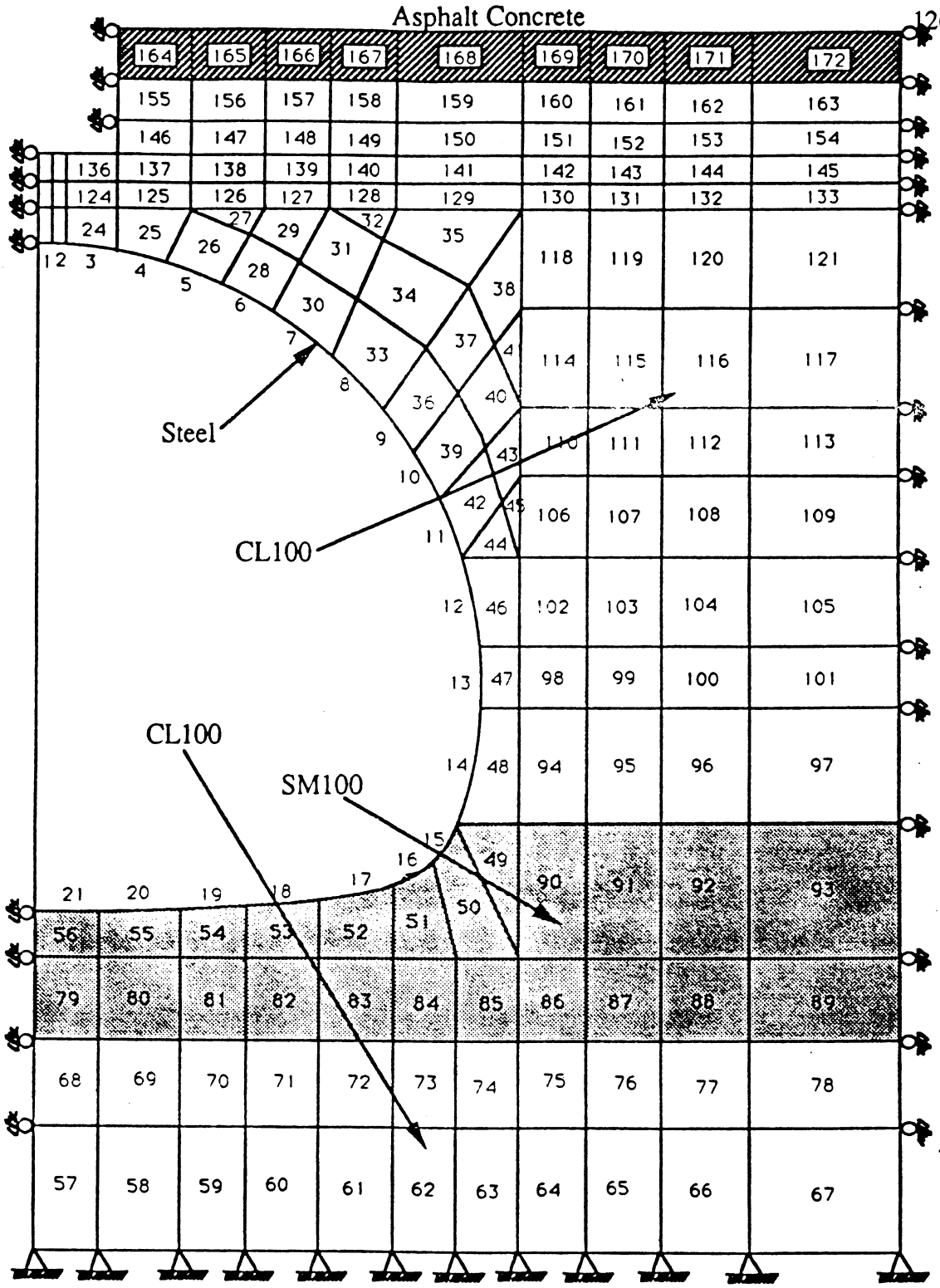

FIGURE 5.2 VARIOUS MATERIAL ZONES DEFINED FOR SIMULATION #3

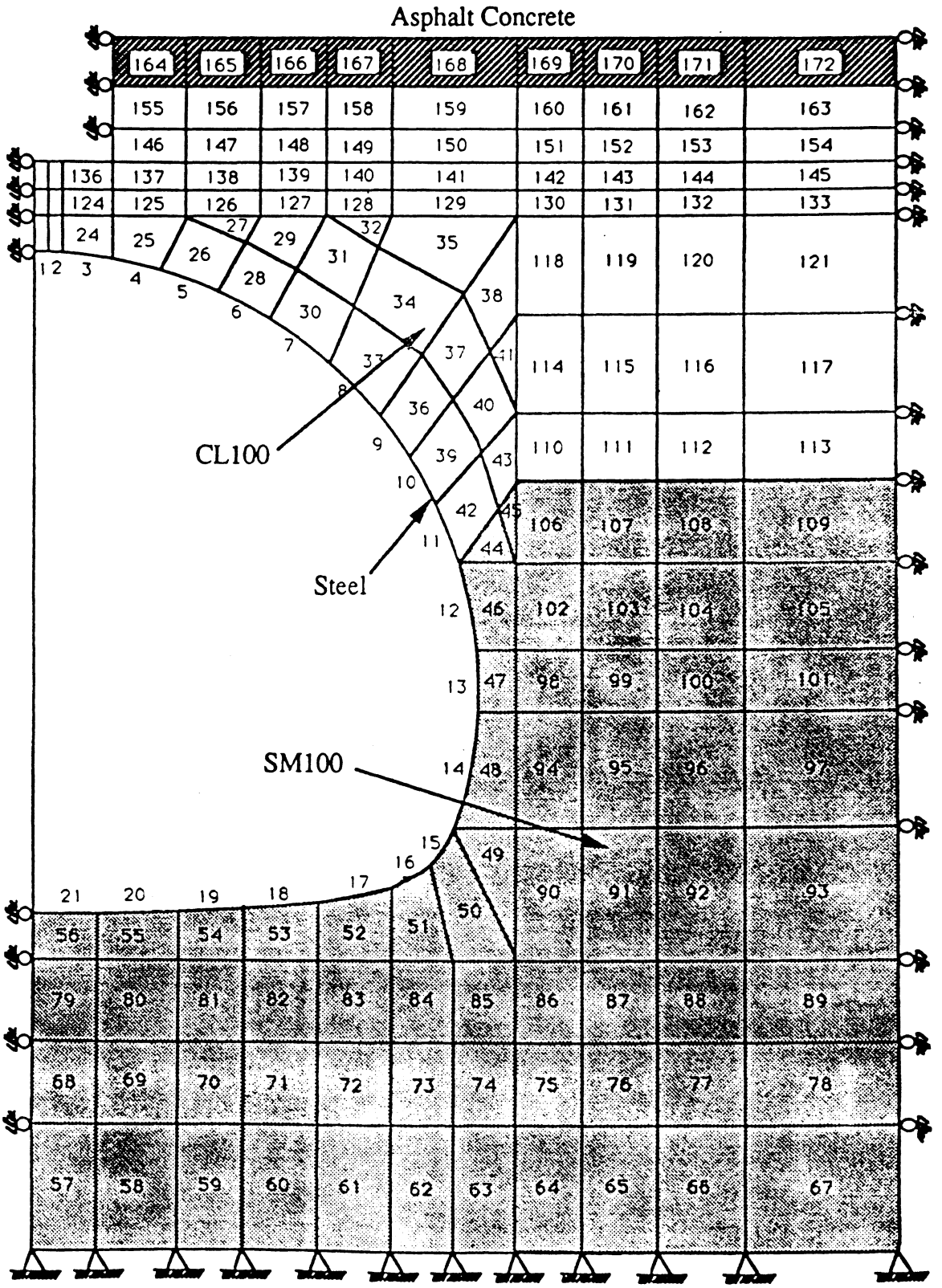

FIGURE 5.3 VARIOUS MATERIAL ZONES DEFINED FOR SIMULATION #5

5.7 CANDE PREDICTIONS AND DISCUSSION

The parameters for Duncan's soil model were obtained from the triaxial test results and from the CANDE library. Calculation of CANDE predictions were stopped whenever the stress level at any point of the structure reaches it's yield limit. Deflections predicted by CANDE were compared with the field results. Figures 5.4 through 5.8 presents the comparisons for #5 through #9. The deflections predicted by CANDE for all the points were in the conservative side. The large error in the CANDE predictions occured because of one or more of the following factors.

1. The soil samples obtained for the triaxial testing came from the shoulder part of the road section. These soil samples were relatively loose compared to the soil under the pavement section because of the compaction occured due to live loads applied over the last 37 years.

2. It is very difficult to simulate in the laboratory that the type of compaction the soil material experienced in the field.

3. The stress distribution did not distributed uniformly, after the slip took place at the bolted crown seam.

4. The maximum deflection in the field occured little away from the instrumented section. CANDE is not capable of analyzing the three dimensional problem.

The finite element simulation predictions for moment and thrust were generally higher, but the trend was similar. Figures 5.9 through 5.16 presents the moment and thrust distribution graphs. Thrust predictions agreed well in the higher loading steps. Moment predictions agreed well at points #6 and #9. variation in the magnitude of the moment is high at the crown and haunch region. The reasons for high discrepancy in the finite element predictions were may be due to the above cited reasons.

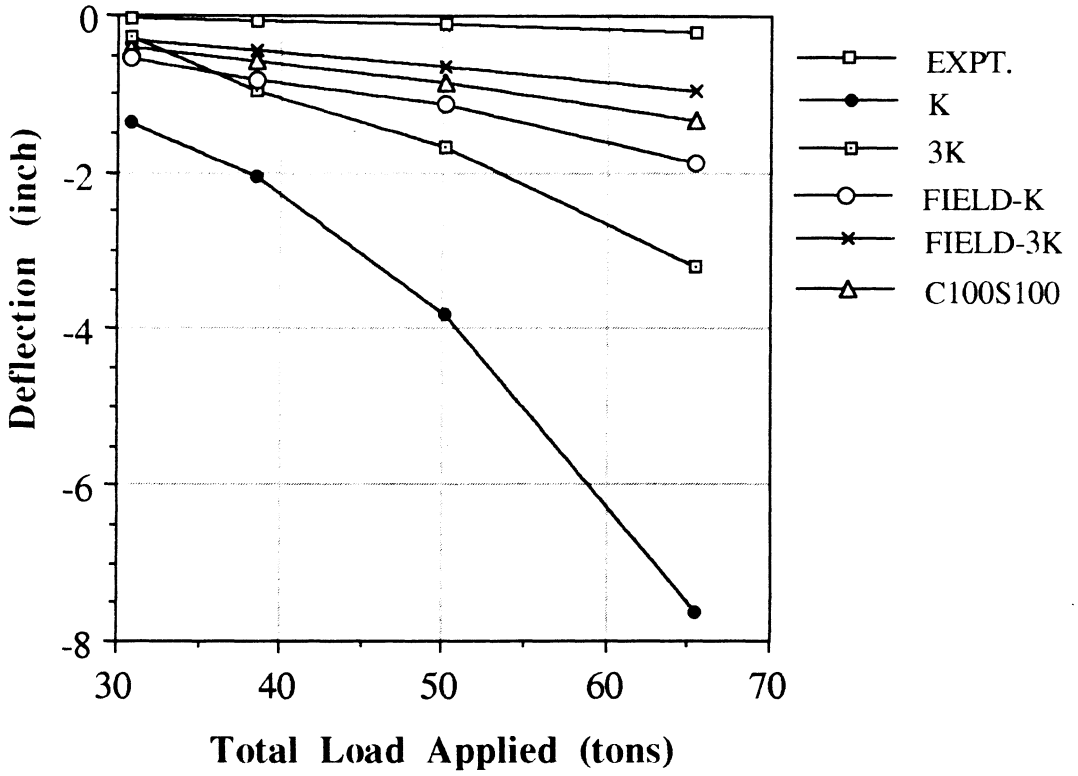

FIGURE 5.4 COMPARISON OF DEFLECTION OF MONITORING POINT #5 BETWEEN FIELD RESULTS AND VARIOUS CANDE PROGRAM SIMULATIONS

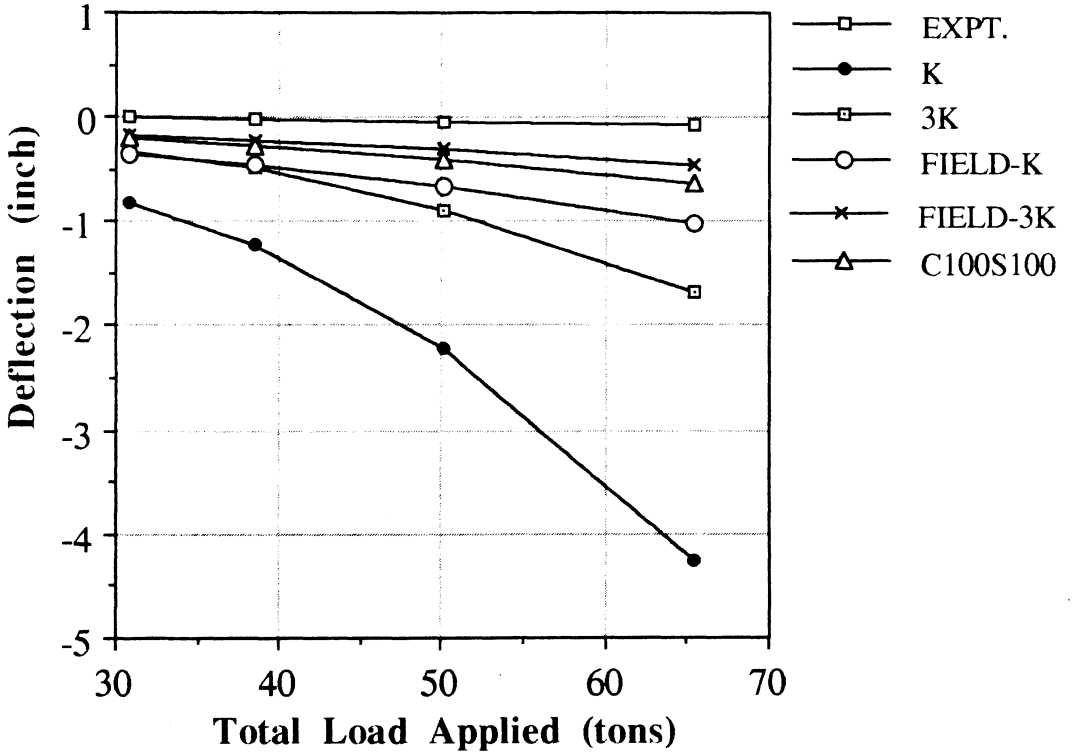

FIGURE 5.5 COMPARISON OF DEFLECTION OF MONITORING POINT #6 BETWEEN FIELD RESULTS AND VARIOUS CANDE PROGRAM SIMULATIONS

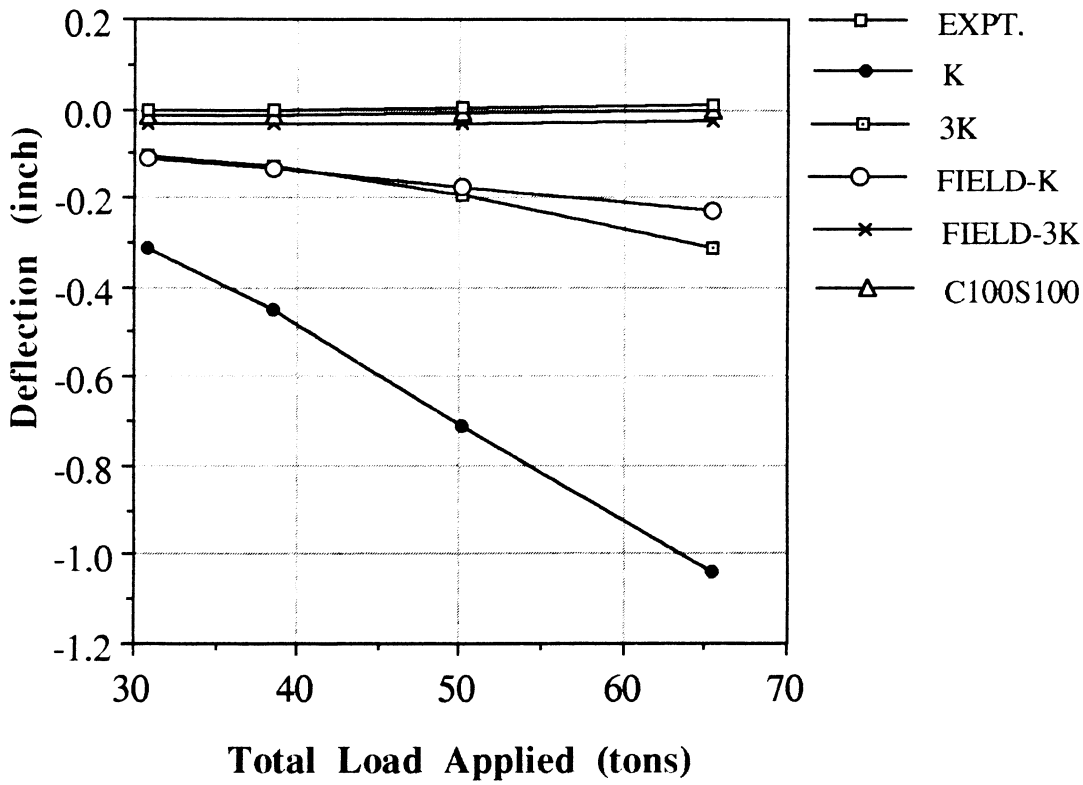

FIGURE 5.6 COMPARISON OF DEFLECTION OF MONITORING POINT #7 BETWEEN FIELD RESULTS AND VARIOUS CANDE PROGRAM SIMULATIONS

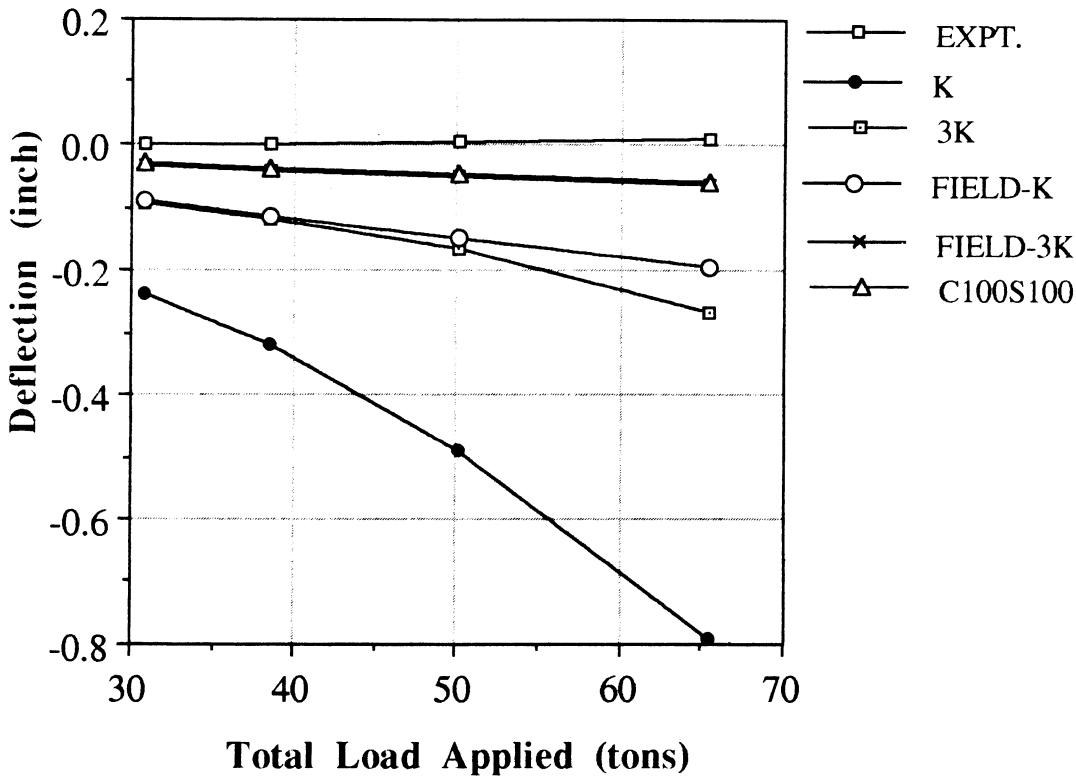

FIGURE 5.7 COMPARISON OF DEFLECTION OF MONITORING POINT #8 BETWEEN FIELD RESULTS AND VARIOUS CANDE PROGRAM SIMULATIONS

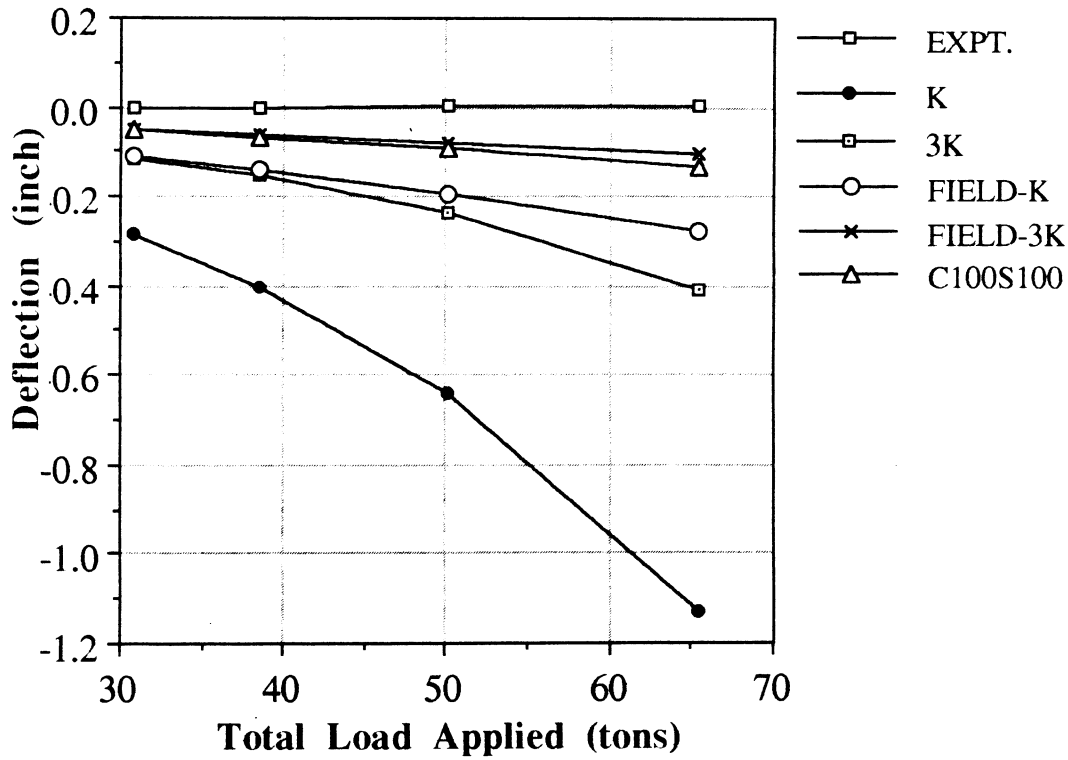

FIGURE 5.8 COMPARISON OF DEFLECTION OF MONITORING POINT #9 BETWEEN FIELD RESULTS AND VARIOUS CANDE PROGRAM SIMULATIONS

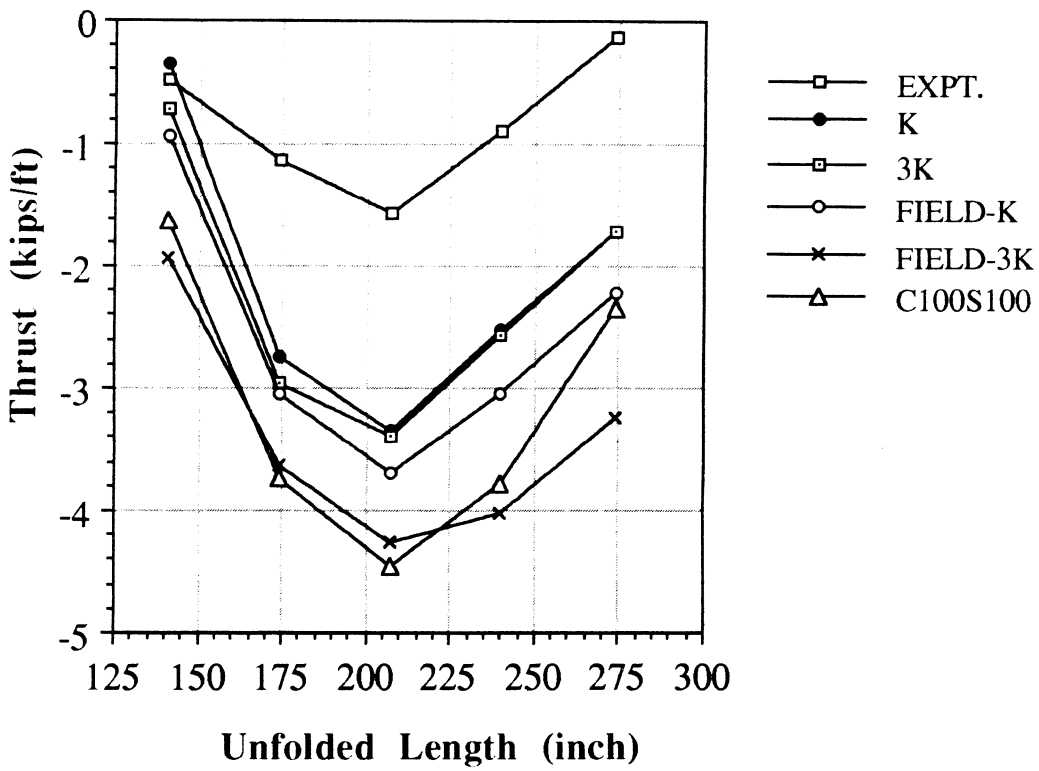

FIGURE 5.9 COMPARISON OF THRUST DUE TO 30.79 TON LOAD BETWEEN FIELD RESULT AND VARIOUS CANDE SIMULATIONS

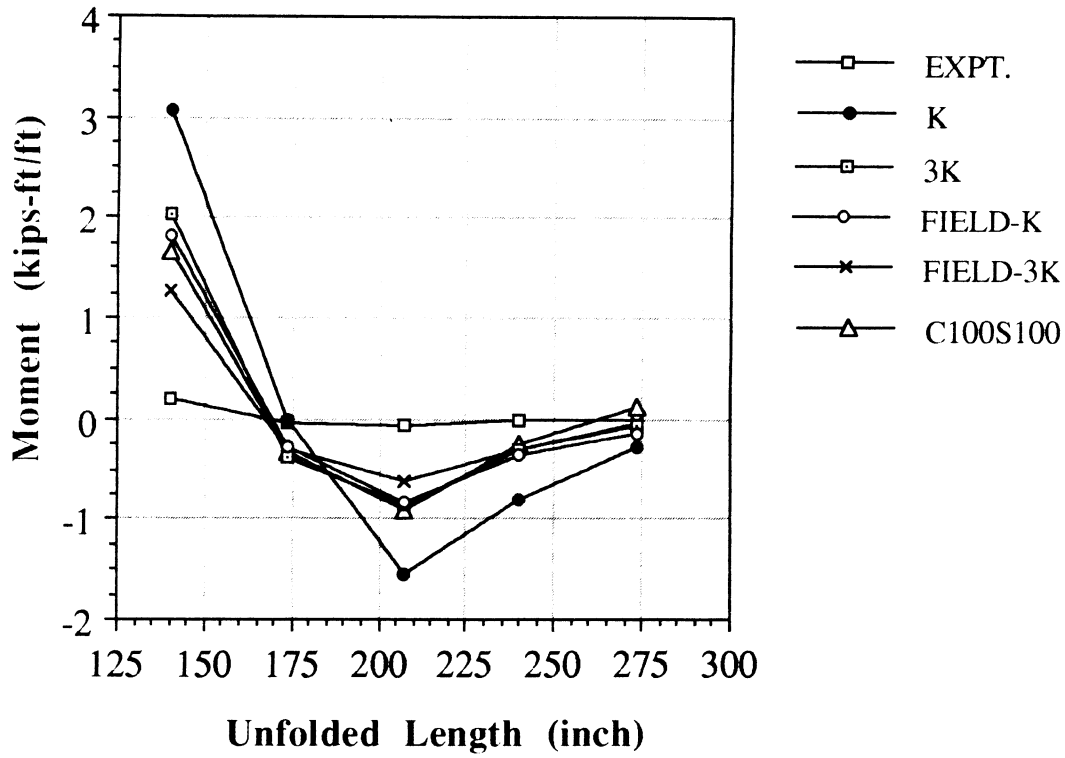

FIGURE 5.10 COMPARISON OF MOMENT DUE TO 30.79 TON LOAD BETWEEN FIELD RESULT AND VARIOUS CANDE SIMULATIONS

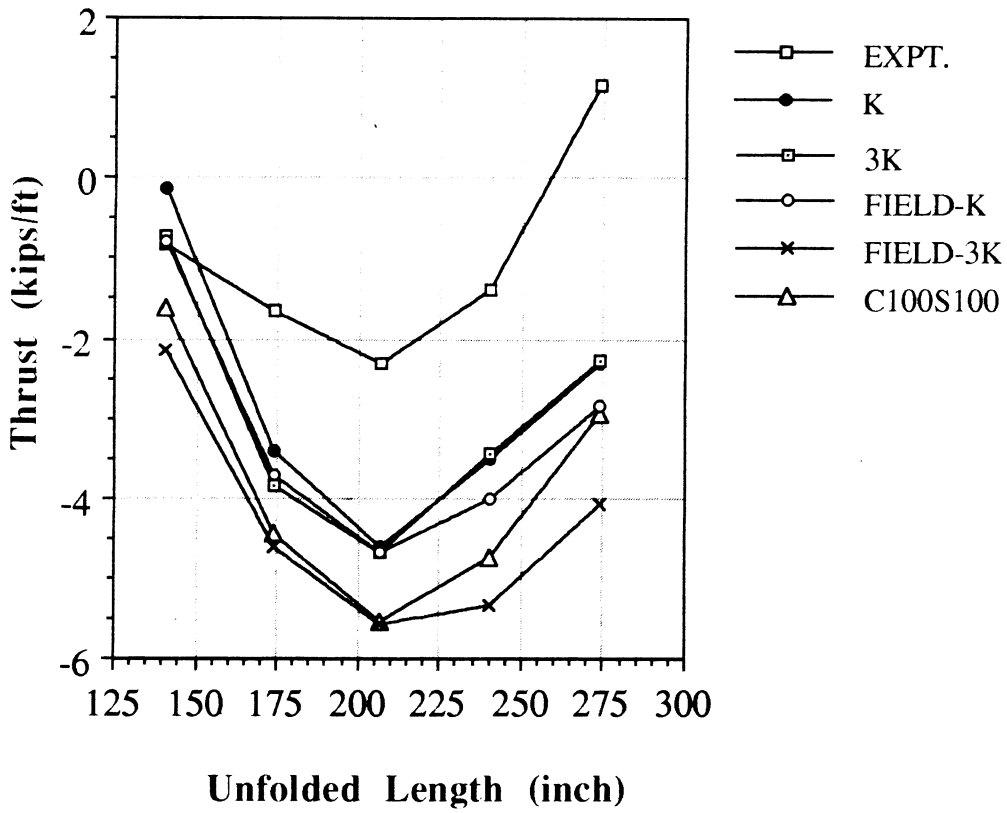

FIGURE 5.11 COMPARISON OF THRUST DUE TO 38.48 TON LOAD BETWEEN FIELD RESULT AND VARIOUS CANDE SIMULATIONS

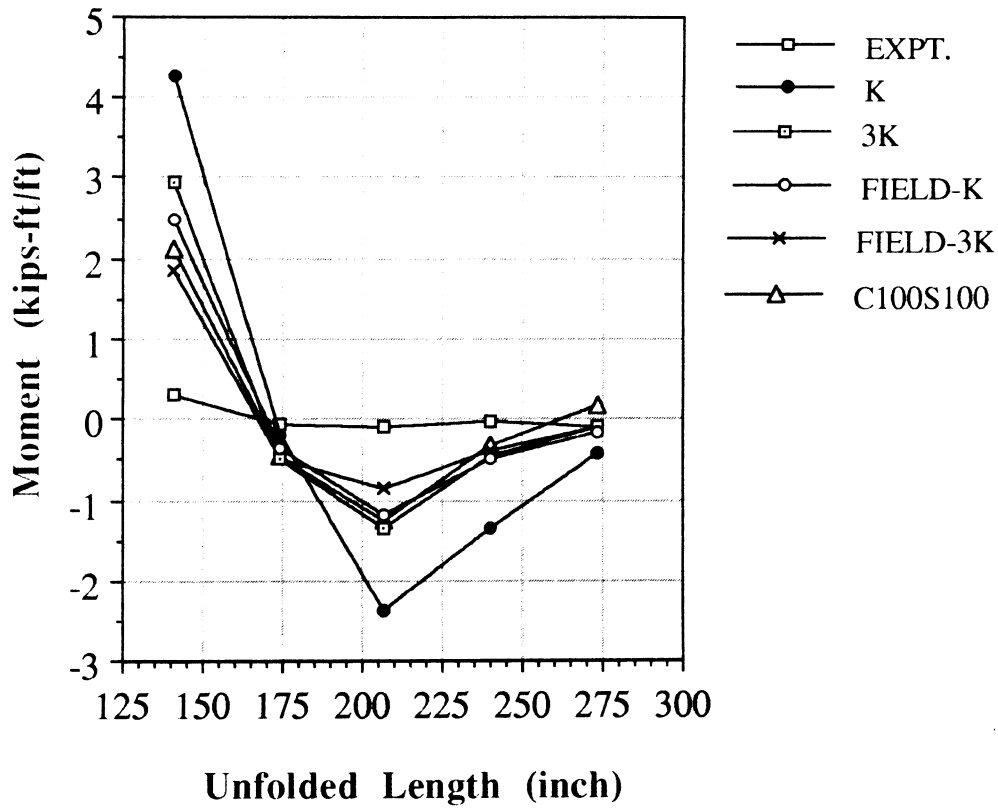

FIGURE 5.12 COMPARISON OF MOMENT DUE TO 38.48 TON LOAD BETWEEN FIELD RESULT AND VARIOUS CANDE SIMULATIONS

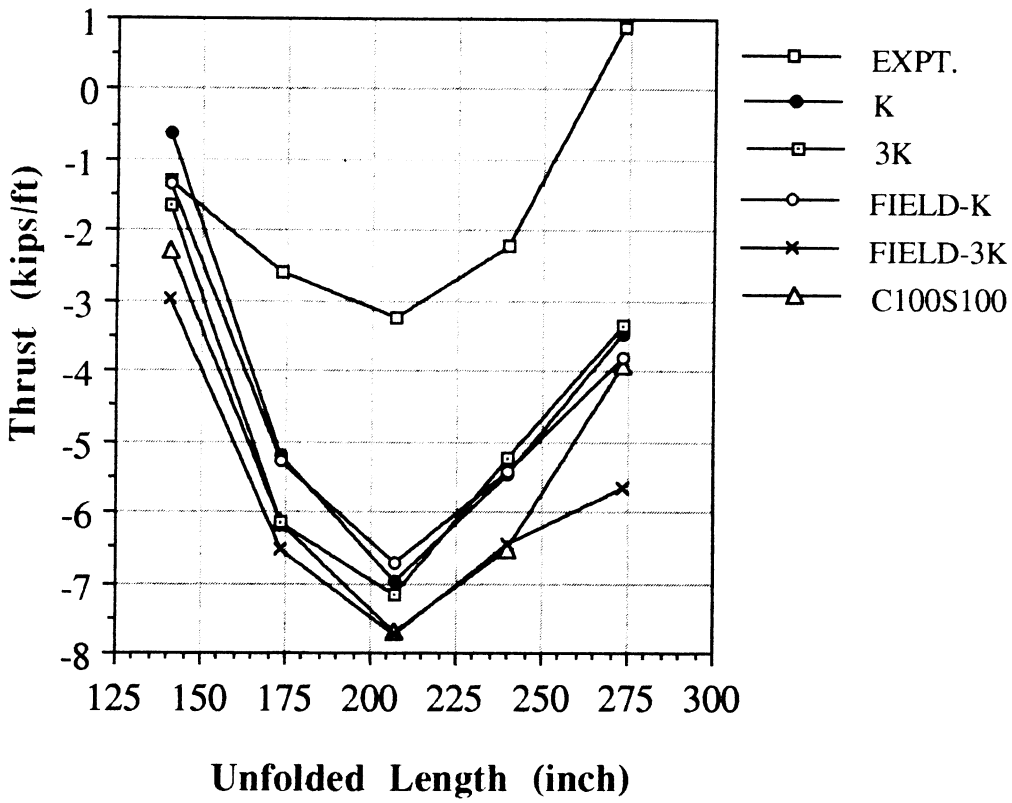

FIGURE 5.13 COMPARISON OF THRUST DUE TO 50.03 TON LOAD BETWEEN FIELD RESULT AND VARIOUS CANDE SIMULATIONS

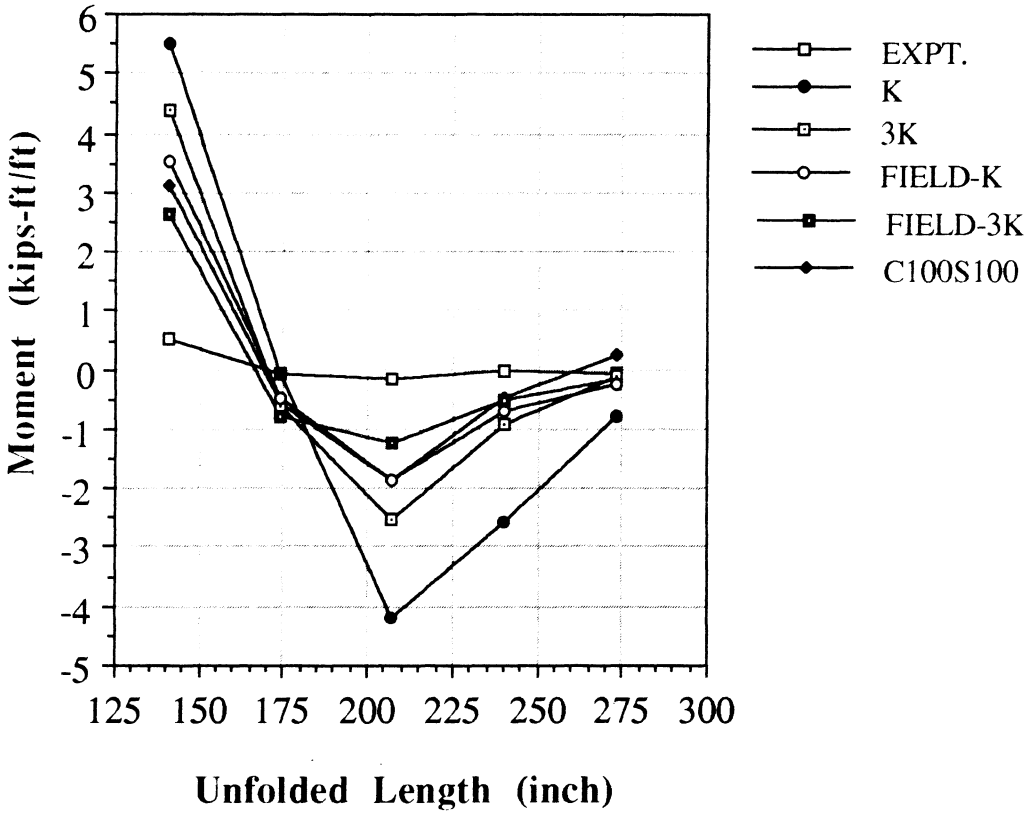

FIGURE 5.14 COMPARISON OF MOMENT DUE TO 50.03 TON LOAD BETWEEN FIELD RESULT AND VARIOUS CANDE SIMULATIONS

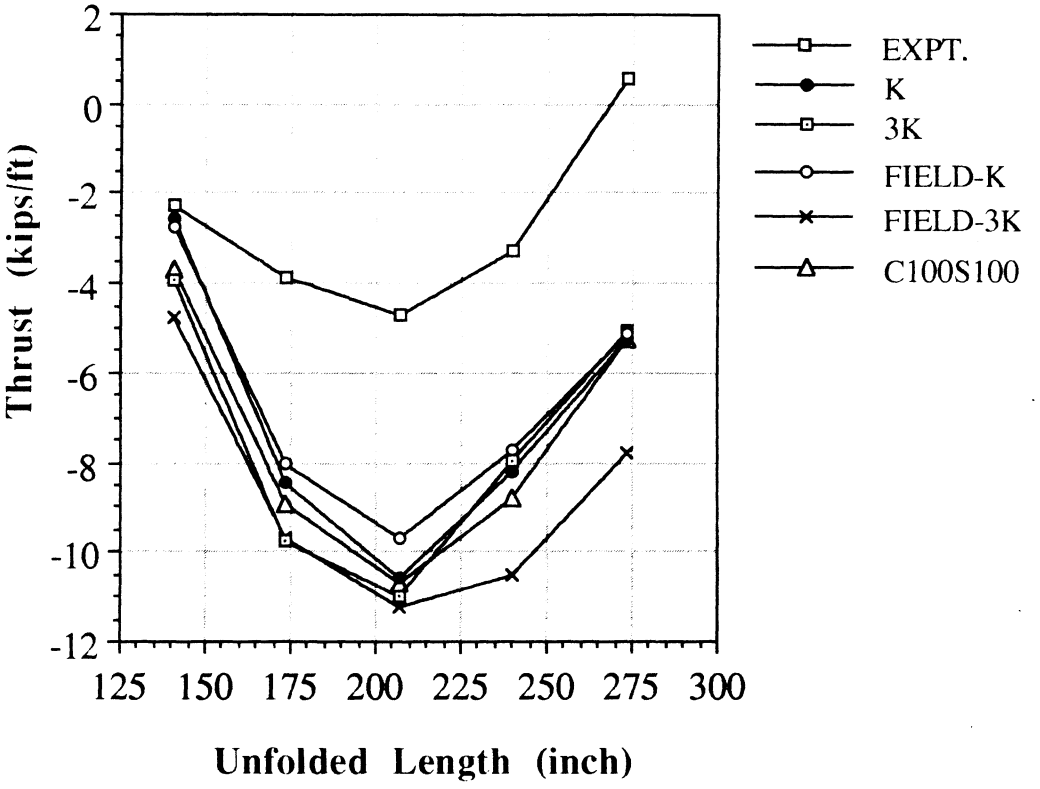

FIGURE 5.15 COMPARISON OF THRUST DUE TO 65.43 TON LOAD BETWEEN FIELD RESULT AND VARIOUS CANDE SIMULATIONS

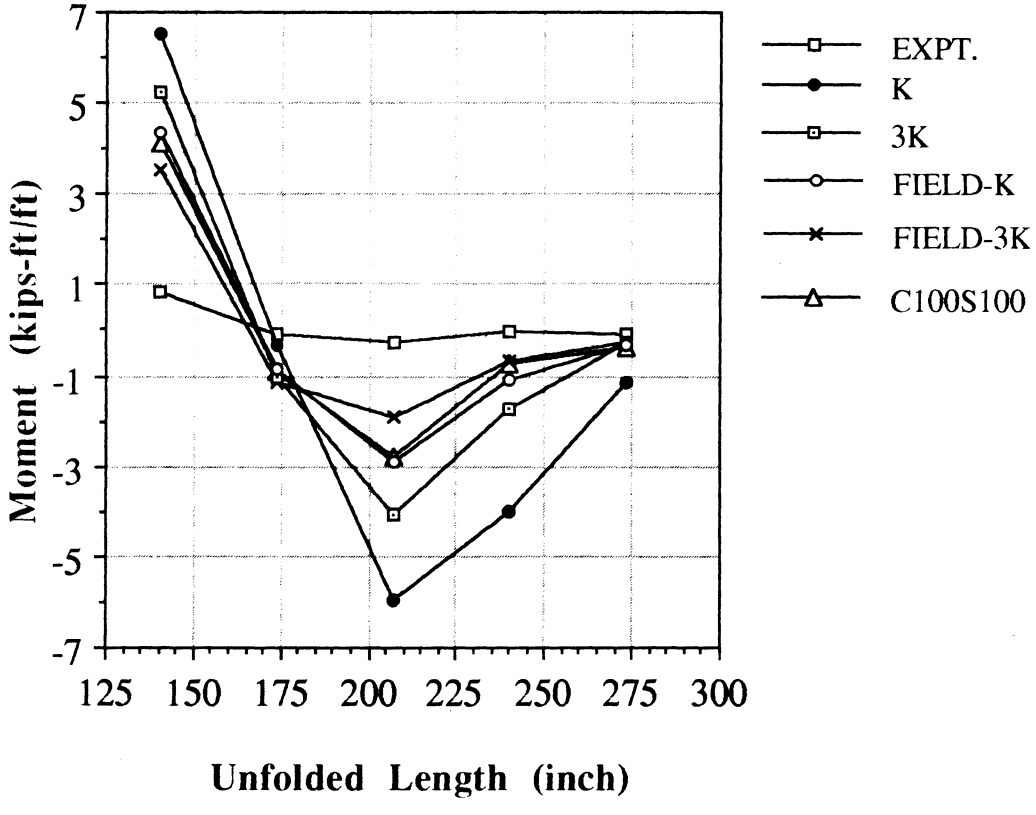

FIGURE 5.16 COMPARISON OF MOMENT DUE TO 65.43 TON LOAD BETWEEN FIELD RESULT AND VARIOUS CANDE SIMULATIONS

A parametric study was also conducted to determine the influence of the modulus number. Duncan and his co-workers have speculated, for loose soils modulus number may be increased upto three times the value of K to incorporate the loading and unloading effect. To determine this effect, we have done a simulation by increasing the value of the K by three times. Influence of the parameter changes was not significant. The value of the modulus exponent "n" is always very similar for primary loading and unloading, and in the hyperbolic relationships it is assumed to be the same.

CHAPTER 6

CONCLUSIONS AND RECOMMENDATIONS

6.1 SUMMARY AND CONCLUSIONS

A full-scale field test was conducted in a long span pipe arch culvert. An exceptional live load was applied through two hydraulic cylinders. Field data were collected and analysed for all three loading sequences. Finite element simulations were conducted using the CANDE computer code. Duncan's hyperbolic soil model was used to simulate the backfill soil. Tape extensometer was used to determine the shape of the culvert before and after the test. Although it gave fairly accurate data, collection of such data was very time consuming. Position transducers were used to collect deflection data upon each loading step. Strain gage data was also collected upon each loading step. Hp data acquisition system was used to collect data from the position transducers and strain gages. The following conclusions were made at the end of the study:

* The maximum load carrying capacity of a pipe arch culvert, with 3 feet cover of cohesive soil was determined to be approximately 100 tons.

* The maximum moment capacity of the pipe arch culvert is 3.745 kips-ft/ft (without taking axial forces into account)

* The maximum vertical crown deflection was 6.99 inches for approximately 115 tons during the third loading sequence.

* Partial failure occured due to the formation of plastic hinges.

* Severe distress occured at the crown region and a slip occured at the bolted connection. After that the culvert responded like a truss rather than a

composite beam.

* Critical sections of this type of culvert was determined to be sections four five and six. (Although section six didn't reach its yield limit, it was very close to doing so.)

* Formation of creases were observed approximately two feet away from the instrumented region on both south and north sides.

* Generaly moment and thrust distribution were as expected. Both increased till the loadwas approximately 100 tons during the second loading sequence. Severe distress occured at the crown region for the higher loading steps and the thrust at the crown increased sharply and moment became very small.

* Deflection predicted by finite element simulations always larger than the field results. Moment and thrust predictions were also very large but the trend agreed well with the field results.

* Parametric study undertaken to determine the influence of modulus number "K" gave better agreement for the deflection between the field and CANDE predictions. This parametric study didn't give good agreement for moment and thrust between field results and theoretical values.

6.2 RECOMMENDATIONS

Tape extensometer readings should be taken after each step of the loading to eliminate the error caused in the deflection calculation because of the change of angle in the the position transducer wire. Actual deflection is not two dimension as we assumed. Attempts should be made to measure the three dimensional deflection in the future research work.

Soil boring should be done exactly over the crown region to get good soil parameters for the Duncan's soil model. Using multiaxial device and different stress paths for the soil testing is recommended.

For finite element simulation of live load, a better method for converting the concentrated load to line load should be used. A simpler technique is needed to model this type of loads for plane strain analysis. Although it may be on the conservative side, it is safer to use CANDE as a design tool for these type of structures. Analysis of this type of structures using CANDE should be subjected to further research.

REFERENCES

1. Abdel-sayed, George, and Baidar Bakt (1982), "Analysis of live-load effects in soil-steel structures," Soil-structure interaction of subsurface conduits,Trans. Research Record 878, TRB, Washington, D.C., pp. 49-55.

2. Alan, F. Rauch (1990) "Experimental and numerical investigation of a deep-corrugated steel, box-type culvert," Thesis presented to Ohio University, Athens, Ohio, in partial fulfillment of the requirements for the Degree of Master of Science in Civil Engineering,June.

3. Beal, David B. (1982), "Field test of long-span aluminum culvert," Journ. of Geotechnical Eng. Div., ASCE, Vol. 108, No.GT6, June, pp. 873-890.

4. Cary, Raymond L. (1986), "Inelastic flexural stability of corrugations," Durability, strength, and analysis of culverts and tunneling machines, Trans. Research Record 1087, TRB, Washington, D.C., pp 87-91

5. Chang, Ching S., Julio M. Espinoza, and Ernest T. Selig (1980), "Computer analysis of Newton Creek culvert," Journ. of Geotechnical Eng. Div., ASCE, Vol. 106, No. GT5, May, pp.531-556.

6. Dessouki, A.K., and G.R. Monforton (1986), "Effect of soil failure on soil-steel structures," Journ. of Geotechnical Eng., ASCE, Vol.112, No.5, May, pp.522-36.

7. Duncan, James M., Seed R. B., and Drawsky, R.H (1985) "Design of Corrugated Metal Box Culverts," Trans. Research Record 1008,TRB,Washington D.C., pp 33-41.

8. Duncan, James M. (1979), "Behavior and design of long-span metal culverts," Journ. of Geotechnical Eng. Div., ASCE, Vol. 105, No GT3, March, pp. 399-418.

9. Duncan, James M. (1980), "Hyperbolic stress-strain relationships," Proc. of the Workshop on Limit Equilibrium, Plasticity, and Generalized Stress-Strain in Geotechnical Engineering, ASCE, New York, May, pp. 443-60.

10. Duncan, J.M., and C.Y.Chang (1970), "Nonlinear analysis of stress and strain in soils," Journ. of Soil Mechanics and Foundations Div.,ASCE, Vol.96, No.SM5,

September, pp. 1629-53.

11. Duncan,J.M., Byrne,P., Wong, K.S., and Mabry, P., "Strength, Stress-Strain and Bulk Modulus Parameters of Finite Element Analysis and Movements in Soil Masses", Report No.UCB/GT/80-01, University of California, Berkeley, 70pp, August 1980.

12. Ghobrial, Medhat, and George Abdel-Sayed (1985), "Inelastic buckling of soil-steel structures," Culverts: analysis of soil-culvert interaction and design, Trans. Research Record 1008, TRB, Washington, D.C., pp. 7-14.

13. Katona, M.G., and J.M.Smith (1976), "CANDE user manual," Report No. RD-77-6, Fed. Highway Admin., Washington, D.C., October.

14. Katona, M.G., J.M. Smith, R.S.Odello, and J.R. Allgood (1976), "CANDE: a modern approach for the structural design and analysis of buried culverts," Report No. FHWA-RD-77-5, Fed. Highway Admin., Washington, D.C., October.

15. Kondner, R.L. (1963), "Hyperbolic stress-strain response: cohesive soils," Jour. of the Soil Mechanics and Foundations Div., ASCE, Vol 89, No. SM1, February, pp. 115-143.

16. Meyerhof, G.G., and Baikie, L.D., "Strength of steel culvert sheets bearing against compacted sand backfill."

17. Seed, R.B., and J.R.Raines (1988), "Failure of flexible long-span culverts under exceptional live loads," Presented at 67th Annual Meeting of the TRB, Washington, D.C.,pp. 37-45.

18. Selig, Ernest T., and Samuel C.Musser (1985), "Performance evaluation of a rib-reinforced culvert," Culverts: analysis of soil-culvert interaction and design, Trans. Research Record 1008, TRB, Washington, D.C., pp. 117-122.

19. Wong, K.S., and J.M. Duncan (1974), "Hyperbolic stress-strain parameters for nonlinear finite element analyses of stresses and movement in soil masses," Report No. TE 74-3, University of California, Berkeley, July.